EXPERIMENTAL STUDY ON THERMAL AND STRUCTURAL ANALYSIS OF TOOL & CUTTER GRINDING OPERATION USING FINITE ELEMENT METHOD

A dissertation

Submitted In partial fulfillment of the requirement for the award of

Degree of

MASTER OF ENGINEERING

IN

CAD/CAM & ROBOTICS

Submitted By

Vinod Dhull

800881023

Under the guidance of

Dr. S.K. Mohapatra
Professor & Head
Mechanical Engg. Department
Thapar University, Patiala

Dr. V. K. Singla
Assistant Professor
Mechanical Engg. Department
Thapar University, Patiala

Mechanical Engineering Department

Thapar University

Patiala-147004 (INDIA)

CERTIFICATE

I hereby declare that the work which is being presented in the dissertation work entitled, "**Experimental study on thermal and structural analysis of tool & cutter grinding operation using finite element method**", in partial fulfillment of the requirements for the award of degree of **Master of Engineering in Mechanical Engineering in CAD/CAM & ROBOTICS** submitted in Mechanical Engineering Department, Thapar University, Patiala, is an authentic record of my own work carried out under the supervision of **Dr. S. K. mohapatra and Dr.V.K.Singla** refers other researchers work which are duly listed in the reference section.

The matter embodied in this thesis has not been submitted for the award of any other degree of this or any other university.

Date: - 15 July'2010
Place: - Patiala

(VINOD DHULL)

....

This is to certify that the above statement made by the candidate is correct and true to the best of our knowledge.

Dr. V. K. Singla
Assistant Professor
Mechanical Engg. Department
Thapar University, Patiala

Dr. S.K. Mohapatra
Professor & Head
Mechanical Engg. Department
Thapar University, Patiala

15/7/10

Countersigned by

(Dr. S.K.MOHAPATRA)
Professor and Head
Mechanical Engineering Department
Thapar University, Patiala

(Dr. R.K.SHARMA)
Dean
Academic Affairs
Thapar University, Patiala

13.8.10

ACKNOWLEDGEMENT

I would like to express a deep sense of gratitude and thank profusely to my guides **Dr. S. K. Mohapatra and Dr. V. K. Singla** for their sincere & invaluable guidance, suggestions and attitude, which inspired me to submit the thesis report in the present form. Their dynamism and diligent enthusiasm have been highly instrumental in keeping my spirits high. Their flawless and forthright suggestions blended with an innate intelligent application have crowned my task with success.

I am also thankful to **Dr. S. K. Mohapatra,** Professor & Head, Department of Mechanical Engineering for his encouragement and inspiration for execution of the thesis work. I am also thankful to **Mr. Anirban bhattacharya, Assistant** Professor, Department of Mechanical Engineering for his encouragement and inspiration for execution of the thesis work.

I am deeply indebted to my parents for their inspiration and ever encouraging moral support, which enabled me to pursue my studies.

I am also very thankful to the entire faculty and staff especially Mr. Sukhbir Singh of Mechanical Engineering Department for their intellectual support and cooperation.

Dated: 15-07-2010

VINOD DHULL

Roll No. 800881023

ABSTRACT

Grinding machines remove material from the work piece by abrasion, which can generate substantial amounts of heat. Currently finite element method approach is used by researchers to evaluate results for almost every problem to observe the variation in data in experimental results and simulated results.

Finite element approach has made work in different fields like grinding, turning, milling, etc, highly accurate and precise. Tool & Cutter grinders are used to sharpen various cutting tools used on the lathes and milling machines, debur, or used to remove surface imperfections and to work on extremely hard materials. In the present work an attempt has been made to work on thermal and structural analysis of different work pieces using tool & cutter grinder and its analysis following finite element method approach.

Finite Element Method (FEM) approach is defined as a computer aided mathematical technique for obtaining approximate numerical solutions to the abstract equation of calculus that predict the response of physical system subjected to external influence.

In the present study the comparison has been made between data for experimental study and software study comparing the data for variation of stresses in ABAQUS software and variation of temperature in ANSYS software. Different types of materials like mild steel, high chromium steel and stainless steel are used for further carrying out the study of thermal and structural analysis for the same and to compare the results obtained for experimental studies and simulated studies.

Machining operations have been performed using the above mentioned grinder as a machine tool and by varying the different machining parameters such as depth of cut, feed, cutting speed of wheel, the force and temperature which will affect the thermal and structural properties of the work piece will be obtained.

LIST OF FIGURES & TABLE

Table No.

CONTENTS

CHAPTER 1

INTRODUCTION

1.1 GRINDING

The grinding machine consists of a power driven grinding wheel spinning at the required speed (which is determined by the wheel's diameter and manufacturer's rating, usually by a formula) and a bed with a fixture to guide and hold the work-piece. The grinding head can be controlled to travel across a fixed work piece or the work piece can be moved whilst the grind head stays in a fixed position. Very fine control of the grinding head or tables position is possible use in a vernier calibrated hand wheel, or using the features of NC or CNC controls.

Grinding machines remove material from the work piece by abrasion, which can generate substantial amounts of heat. They therefore incorporate a coolant to cool the work piece so that it does not overheat and go outside its tolerance. The coolant also benefits the machinist as the heat generated may cause burns in some cases. In very high-precision grinding machines (most tool & cutter and surface grinders) the final grinding stages are usually set up so that they remove about 200nm (less than 1/100000 in) per pass - this generates so little heat that even with no coolant, the temperature rise is negligible.

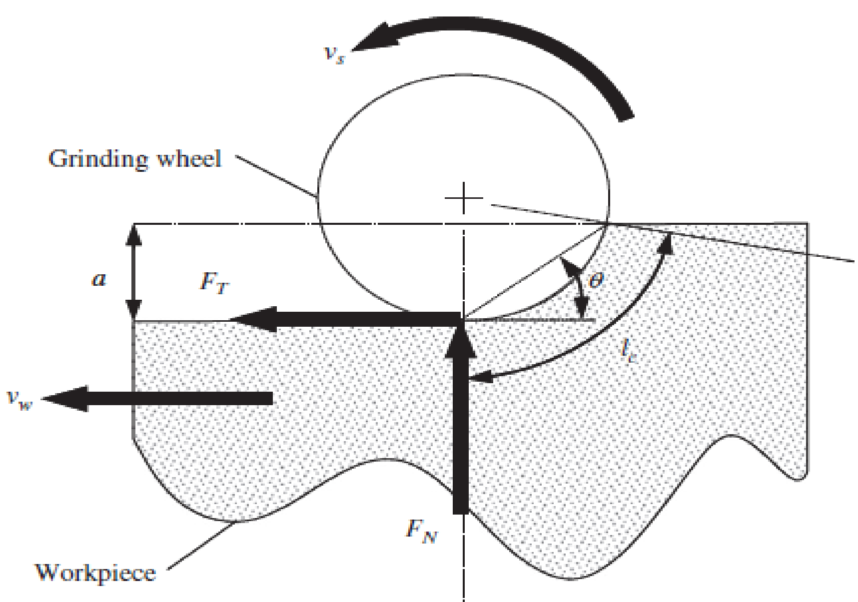

Fig.1 **Process Parameters Used in Grinding [14]**

1.2 TYPES OF GRINDERS

Belt Grinder

Belt grinder is that type of grinder that is usually used as a machining method to process metals and other materials, with the aid of coated abrasives. Sanding is the machining of wood; grinding is the common name for machining metals. Belt grinding is a versatile process suitable for all kind of applications like finishing, deburring, and stock removal.

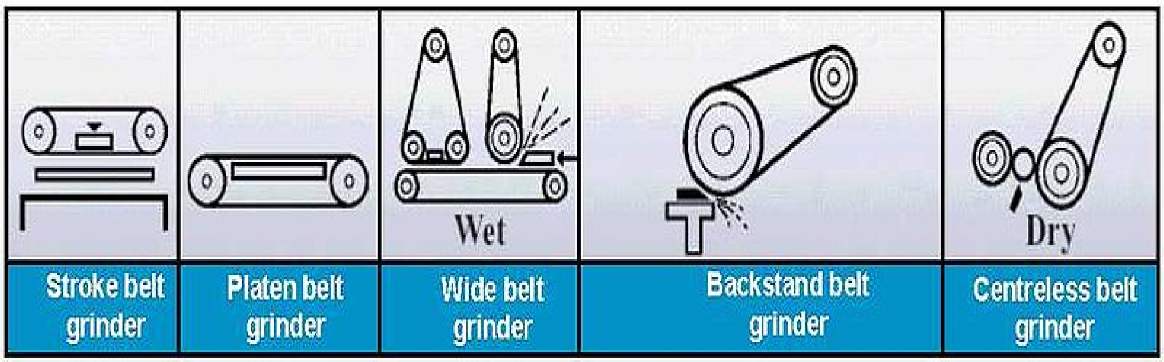

Fig.1.1 **Belt Grinder**

Bench Grinder

Bench grinder is usually has two wheels of different grain sizes for roughing and finishing operations and is secured to a workbench. It is used for shaping tool bits or various tools that need to be made or repaired. Bench grinders are manually operated.

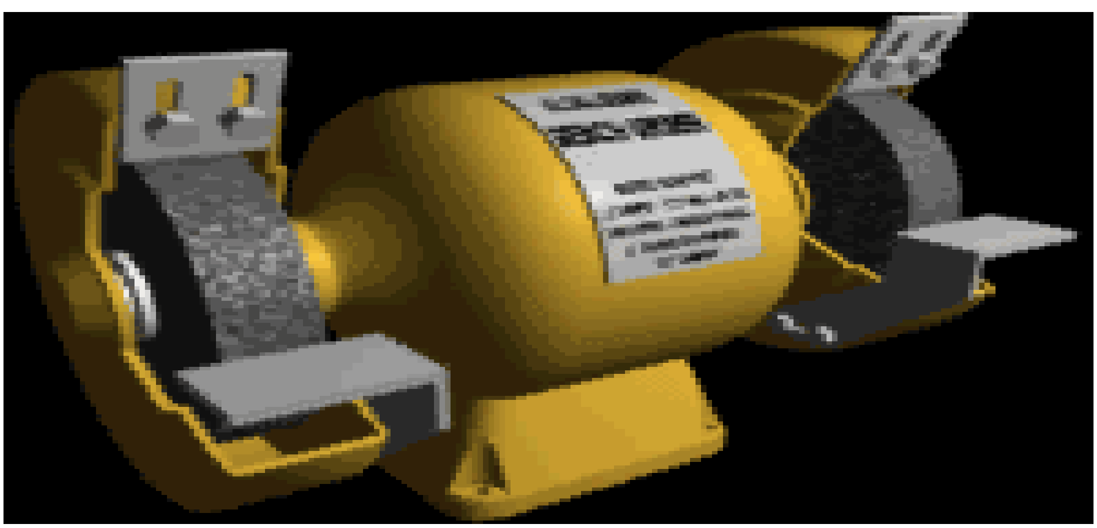

Fig1.2 **Bench Grinder**

Cylindrical Grinder

A cylindrical grinder may have multiple grinding wheels. The work piece is rotated and fed past the wheels to form a cylinder. It is used to make precision rods.

Fig 1.3 **Cylindrical Grinder**

Surface Grinder

A surface grinder has a "head" which is lowered, and the work piece is moved back and forth past the grinding wheel on a table that has a permanent magnet for use with magnetic stock. Surface grinders can be manually operated or have CNC controls.

Fig 1.4 **Surface Grinder**

Tool and Cutter Grinder

These usually can perform the minor function of the **drill bit** grinder, or other specialist tool room grinding operations. The table moves longitudinally and laterally, the head can swivel as well as being adjustable in the horizontal plane. This flexibility in the head allows the critical clearance angles required by the various cutters to be achieved.

Fig.1.5 **Tool and Cutter Grinder**

Jig Grinder

Jig grinder as the name implies, has a variety of uses when finishing jigs, dies and fixtures. Its primary function is in the realm of grinding holes and pins. It can also be used for complex surface grinding to finish work started on a mill. The machine operates by a high speed air spindle rotating a grinding bit. The air spindles are removable and interchangeable to achieve varying surface speeds. Some spindles are fixed speed (60000 rpm), others are adjustable (30000-50000 rpm), and still others are very high speed (175000 rpm). The machines have a standard X-Y table with the notable exception of knee travel. All axes are indexed to .0001" via a vernier scale on the hand wheels, with higher accuracy available with the use of measuring bars. A well-kept jig grinder will reliably position work to a higher degree of accuracy than is possible with hand wheels alone.

These features are all critical in positioning a hole and peg system a precise distance from a reference surface or edge.

Pedestal Grinder

This study guide will cover the major working parts, functions, and machining techniques that can be found used on most Pedestal Grinders. This study guide has been designed to directly represent the questions that will be found on the open book written assessment and as an aid for the hands-on usability assessment. Both assessments will also include questions related to standard machine shop safety and APS internal user safety guidelines. Answering the questions found at the end of the study guide will enable the user to successfully pass the hands-on usability and written assessments. Study guide practice test and answers can be found at the end of the guide. Grinding is the process of removing material by the cutting action of the countless hard and sharp abrasive particles of a revolving grinding wheel as they come in contact with the surface to be ground.

The grinding wheels are held between two flanged disks. A roughing or coarse-grained wheel is usually mounted on one end of the spindle and a fine wheel on the other. There can also be a wire wheel mounted on one side for special applications. A tool rest is provided for each wheel so that tools may be held or steadied while being ground.

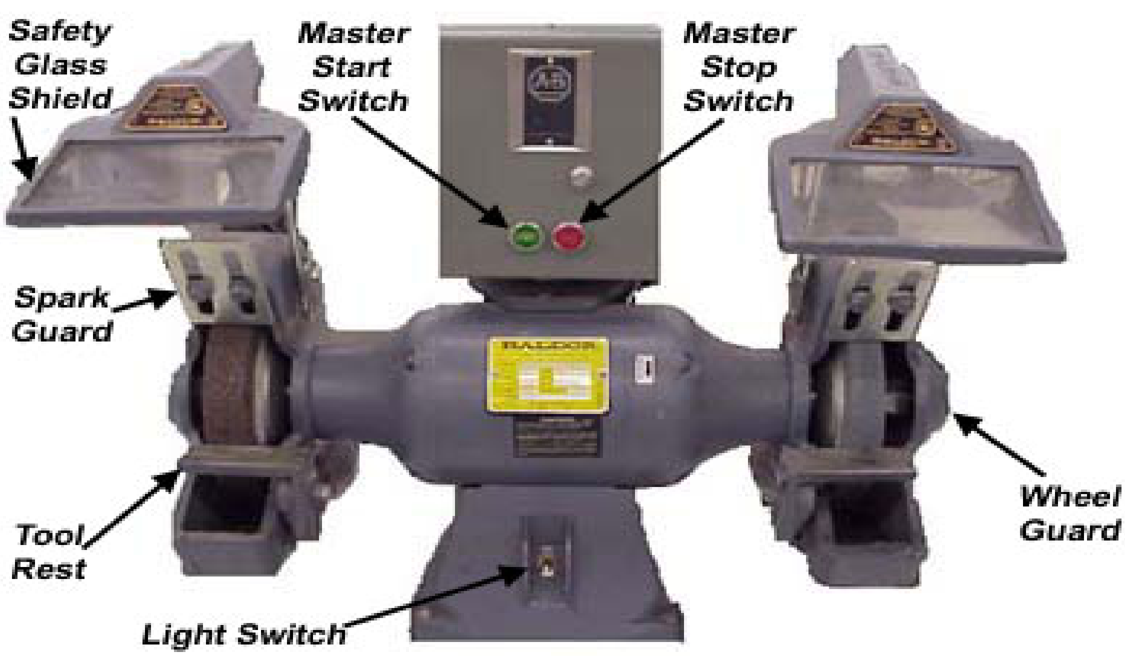

Fig. 1.6 **Main Parts of a Pedestal Grinder**

1.3 THERMAL ASPECTS IN GRINDING

Grinding is an expensive operation because the specific energy consumed is considerably higher than in other cutting processes [Boothroyd and Winston, 1989, Kalpakjian, 1997], to a degree exceeding the melting energy of materials [Malkin, 1984]. As a consequent result of high power consumption, the process control to prevent the detrimental effects resulting from such high degrees of energy requires a great effort. In grinding, energy is not only expended on the formation of chips, but other mechanisms are also involved, such as plowing and rubbing which respectively are associated with the plastic deformation to the sides of the main grinding groove and the sliding friction on worn areas of the abrasive grains sliding against the work piece surface.

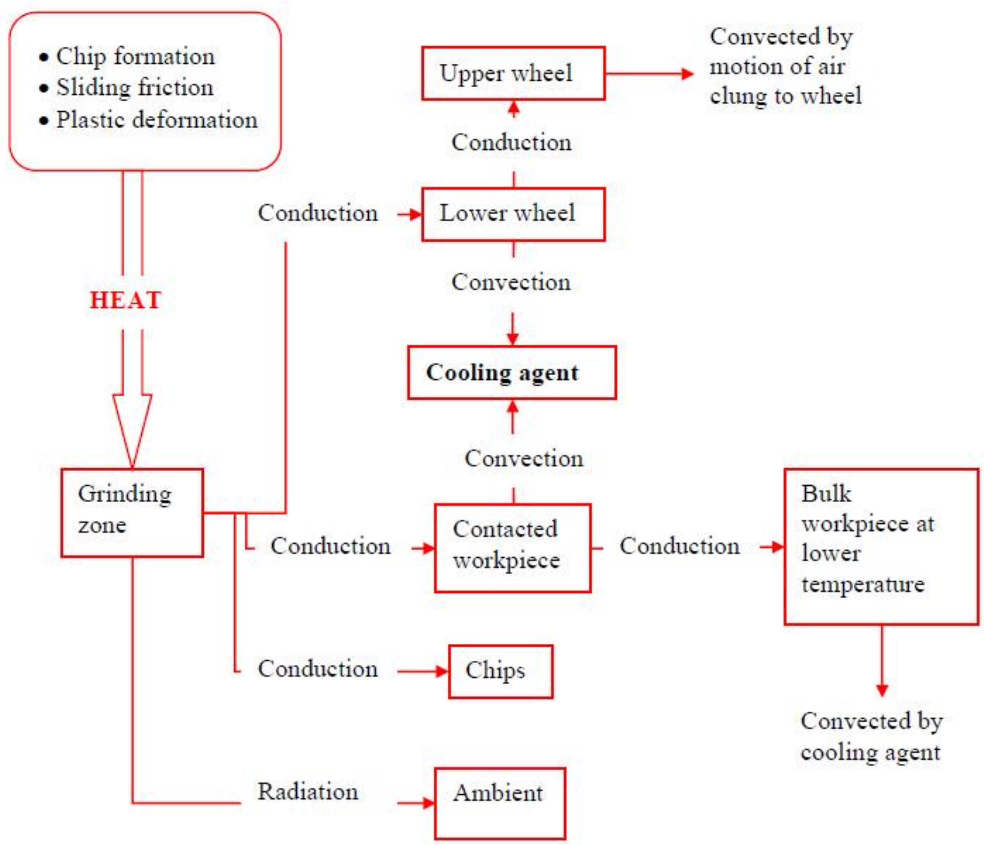

Fig. 1.7 **Diagram of Heat Flow during Grinding**

1.4 GRINDING PROCESS

1.4.1 Abrasive Machining

In all the cutting processes the tool is made of a certain material and has a clearly define geometry. The cutting process is carried out by chip removal, the mechanics of which are reasonably well understood. There are many situations in manufacturing, however, where the work piece material is either too hard or its shape is difficult to produce with sufficient accuracy by any of the cutting methods, one of the best methods for producing such parts is to use abrasives. An abrasive is a small, hard particle that has sharp edges and irregular shape, unlike the cutting tools. Abrasives are capable of removing small amount of material from the surface by a cutting process that produces tiny chips.

In abrasive machining process, material removal involves the interaction of abrasive grits with the work piece at high speeds and shallow penetration depths and the chips that are formed by other machining processes. Abrasive machining is the oldest of the basic machining processes. The results that can be obtained by abrasive machining range from the finest and smoothest surfaces produced by any machining process, in which very little material is removed, to rough, coarse surfaces that accompany high material removal rates. The abrasive particles may be free and mounted on a resin on a belt (called the coated product). Closed packed into wheels or stones, with abrasive held together by bonding material (called bonded product or a grinding wheel)

The metal removal process is basically same in all abrasive machining processes but the important differences due to spacing of active grains (grains in contact with the work) and the rigidity and degree of fixation of the grains. Abrasive machining process has two unique characteristics. First, cutting edge very small, and many of these edges can cut simultaneously. When suitable machines are employed, very fine cuts are possible and fine surfaces and close dimensional control can be obtained. Second, because extremely hard abrasive grits can be produced, very hard materials such as hardened steels, carbides, hard non metallic materials like glass, ceramics can readily be machined. As a result, abrasive machining processes are not only important as manufacturing processes, they are indeed essential. These processes, however, are not necessarily confined to fine or small-scale material removal. They are also used for large scale removal operations and can indeed compete economically with some machining processes, such as milling and turning. Many of aircraft could not be manufactured without these processes.

1.4.2 Abrasive Materials

An abrasive is a hard material that can cut or abrade other substances. Natural abrasives have existed from the earliest times. For example, sand stone was used by ancient peoples to sharpen tools and weapons. Early grinding wheels were cut from slabs of sandstone but because they were not uniform in structure throughout, they wore unevenly and did not produce consistent results. Emery, a mixture of alumina (Al_2O_3) and magnetite (Fe_3O_4), is a natural abrasive used on coated paper and cloth corundum (natural Al_2O_3) and diamonds are other naturally occurring abrasive materials.

The abrasives commonly used in manufacturing are as follows:

1. Conventional abrasives
    a) Aluminium oxide
    b) Silicon carbide
2. Super abrasives
    a) Cubic boron nitride
    b) Diamond

Hardness, the ability to resist penetration, is the key property of an abrasive. The particle must be able to decompose at elevated temperatures. Two other properties that are significant in abrasive grits: attrition and friability. Attrition refers to the abrasive wear action of the grits, resulting in dulled edges, grit flattening, and wheel glazing. Friability, that is, the ability of the abrasive grains to fracture (break down) into smaller pieces: this property gives abrasives self-sharpening characteristics, which are important in maintaining the sharpness of the abrasives in their use exposing the new sharp edges. High friability indicates low strength or low fracture resistance of the abrasive; thus , a high friable abrasive grain fragments more rapidly under grinding forces than an abrasive grain with low friability. Aluminium oxide has lower friability than silicon carbide, hence it has tendency to fragment.

The shape and size of the abrasive grain also affects its friability; blocky grains for example, which may be analogous to negative rake angle cutters, are less friable than plate like grains.

Aluminium oxide: Synthetic aluminium oxide (Al_2O_3), first made in 1983, is obtained by fusing bauxite, iron filings and coke, it contains aluminium hydroxide, ferric oxide, silica and other impurities. The mass of aluminium oxide that is formed is crushed, and the particles are graded to size. Although aluminium oxide is softer than silicon carbide, it is considerably tougher. Consequently, it is a better general purpose abrasive, grains are quite chemically stable and best suited for Fe-based metals and alloys (steels) which are hard, strong and diffusive. Aluminium oxides are divided into two groups.

a) ***Fused:*** fused aluminium oxides are categorized as white (very friable), dark (less friable), and microcrystalline.

b) ***Unfused:*** unfused alumina also known as ceramic aluminium oxides, can be harder than fused alumina. The purest form of fused alumina is seeded gel. First introduced in 1987, seeded gel has a particle size on the order of 0.2 μm (0.8μin), which is much smaller than that of commonly used abrasive grains. These particles are sintered to form larger sizes. Because of their hardness and relatively higher friability, seeded gels maintain their sharpness and are therefore used for difficult to-grind materials.

Silicon Carbide (SiC): It is first discovered in 1891, and made by charging an electric furnace with silica sand, petroleum coke, salt and saw dust. By passing large amount of current through the charge, a temperature of over 4000^0F is maintained for several hours, and a solid mass of silicon carbide crystal results. After the furnace has cooled, the mass of the crystal is removed, crushed and graded (sorted) into various desired sizes. The resulting grits or grains are irregular in shape, with cutting edges having every possible rake angle. Silicon carbide crystals are very hard, friable and rather brittle. This limits their use. Silicon carbide is sold under the trade names carborundum and Crystolon. The grains are less chemically stable and these are generally used for non ferrous and softer metals and alloys as well as tungsten carbides. Silicon carbides are divided into *green* (more friable) and *black* (less friable) types and generally have higher friability than aluminium oxide; hence, they have higher tendency to fracture and remain sharp, hence used for relatively harder work materials.

Cubic Boron Nitride (CBN): Cubic Boron Nitride is not found in nature. It is produced by combination of intensive heat and pressure of catalyst. CBN is extremely hard, registering at 4700 on the knoop scale. It is the second hardest substance created by nature or manufactured and is often referred to, along with diamonds, as a super abrasive. CBN surpasses diamond in the important characteristic of thermal resistance. At temperature of 650^0C, at which diamond may begin to revert to plain carbon dioxide, CBN continues to maintain its hardness and chemical integrity. When the temperature of 1400^0C is reached, cBN changes from its cubic form to a hexagonal form and loses its hardness. CBN can be used successfully in grinding iron, steel and iron alloys, Ni-based alloys, and other materials. CBN works very effectively on hardened materials (R_c 50 or higher). It can also be used for soft steel under selected situations. CBN does well at conventional grinding speeds (6000 to 12000 ft/min), resulting in lower total grinding cost /piece in conventional equipment. CBN can also perform well a high grinding speeds (12000ft/min and higher) and will enhance the benefits from future machine tools. CBN can also solve difficult-to-grind jobs, but it also generates cost benefits in many production grinding operations despite its higher cost.

Diamond: diamonds are hardest of all materials. Those that are used for abrasives are either natural, off-colour stones (called granets) that are not suitable for gems or small, synthetic stones that are produced specially for abrasives purpose. Manufactured stones appear to be somewhat more friable and thus tend to cut faster and cooler. They do not perform as satisfactorily in metal bonded wheels. Diamonds abrasives wheels are used extensively for sharpening carbide and ceramic cutting tools. Diamonds are also used for truing and dressing other types of abrasive wheels. Diamonds are usually used only when cheaper abrasives will not produce the desired results. Garnets are used primarily in the form of very finely crushed and graded powders for fine polishing.

1.4.3 Abrasive Grain Size

As used in manufacturing process, abrasives are generally very small compared with the size of the cutting tools and inserts. Also, abrasives have sharp edges, thus allowing the removal of very small quantities of material from the work piece surface. Consequently, very fine surface finish and dimensional accuracy can be obtained. The size of an abrasive grain is identified by the grit number, which is a function of sieve size. The smaller the sieve size, the larger is the grit number.

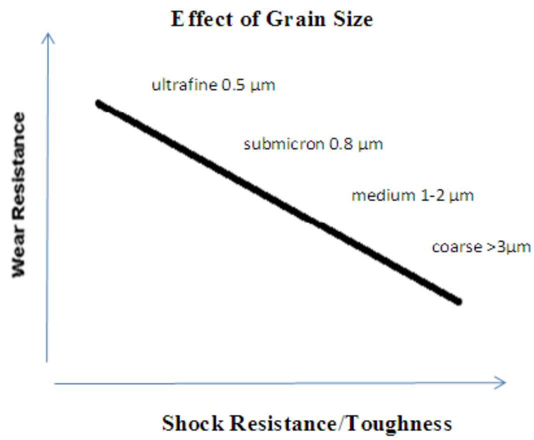

Fig 1.8 **Effect of grain size of wear [12]**

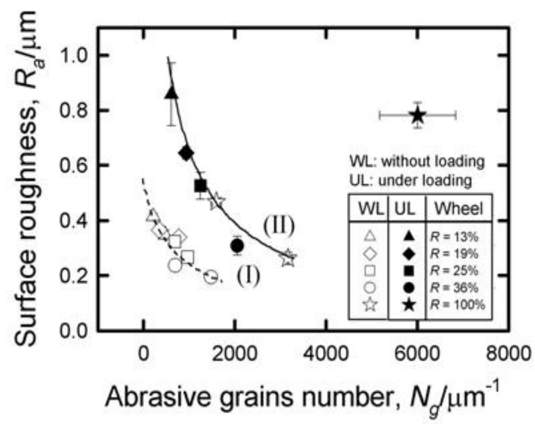

Fig 1.9 **Effect of abrasive grain number on surface roughness**

1.4.4 Bonded Abrasives

Because each abrasive grain usually removes only a very small amount of material at a time, high rates of material removal can be obtained if larger number of these grains acts together; this is accomplished by using bonded abrasives, typically in the form of grinding wheel. The abrasive grains are held together by a bonding material, which acts as supporting posts or braces between the grains. Some porosity is essential in bonded wheels to provide clearance for the minute chips being produced and to provide cooling; otherwise the chips would interfere with the grinding process. It is thus impossible to use a grinding wheel that is fully dense and solid with no porosity. Porosity can easily be observed simply by looking at the surface of any grinding wheel.

1.5 WORKPIECE MATERIAL

a) **Stainless Steel**

b) **Mild Steel**

c) **High Chromium Steel**

Material Properties

a) **Stainless Steel**

Mechanical Properties

The mechanical properties of stainless steels are almost always requirements of the product specifications used to purchase the product. For flat rolled products the properties usually specified are tensile strength, yield stress (or proof stress), elongation and Brinell or Rockwell hardness. Much less frequently there are requirements for impact resistance. Bar, tube, pipe, fittings etc. also usually require at least tensile strength and yield stress. These properties give a guarantee that the material in question has been correctly produced, and are also used by engineers to calculate the working loads or pressures that the product can safely carry in service.

Figure 1.10 Stainless steel work piece

➢ Different Grades of Stainless Steel

- 200 —austenitic chromium-nickel-manganese alloys
  - 201—austenitic that is hardenable through cold working
  - 202—austenitic general purpose stainless steel

Table 3.1 Material composition of stainless steel checked by spectrometer (composition testing machine)

Analysis

Start | New | Print | Del | Exit

Sample:

Element	Burn 1	Burn 2	Burn 3	Burn 4	Average
Fe %	35.3	70.1	71.3		58.9
C %	H 1.01	L 0.0058	L 0.0085		L 0.343
Si %	H 12.2	0.189	0.194		H 4.19
Mn %	L 5.00	L 9.47	L 9.27		L 7.91
P %	H 0.567	< 0.0100	< 0.0100		H 0.189
S %	H 0.194	< 0.0100	< 0.0100		H 0.0647
Cr %	L 3.83	L 17.7	L 17.2		L 12.9
Mo %	H 1.34	L 0.0000	L 0.0000		L 0.449
Ni %	H 3.29	0.674	0.476		1.48
Al %	> 1.20	< 0.0050	< 0.0050		0.448
Co %	2.67	0.0319	0.0334		0.913
Cu %	> 8.50	1.71	1.44		> 8.50
Nb %	L 0.777	L 0.0000	L 0.0000		L 0.259
Ti %	0.169	< 0.0010	< 0.0010		0.0565
V %	L 0.276	L 0.0063	L 0.0000		L 0.0944
W %	H 6.54	L 0.0000	L 0.0000		H 2.18
Pb %	> 0.350	< 0.0500	< 0.0500		> 0.350

Yield Strength

An unusual feature of annealed austenitic stainless steels is that the yield strength is a very low proportion of the tensile strength, typically only 40-45%. The comparable figure for mild steel is about 65-70%. As indicated above a small amount of cold work greatly increases the yield (much more so than the tensile strength), so the yield also increases to a higher proportion of tensile. Only a few % of cold work will increase the yield by 200 or 300MPa, and in severely cold worked material like spring temper wire or strip, the yield is usually about 80-95% of the tensile strength.

As engineering design calculations are frequently made on yield criterion the low yield strength of austenitic stainless steels may well mean that their design load cannot be higher than that of mild steel, despite the tensile strength being substantially higher. Design stresses for various grades and temperatures are given in Australian Standard AS1210 "Unfired Pressure Vessels".

Ductility

The other mechanical property of note is the ductility, usually measured by % elongation during a tensile test. This shows the amount of deformation a piece of metal will withstand before it fractures. Austenitic stainless steels have exceptionally high elongations, usually about 60-70% for annealed products, as shown in figure 2. It is the combination of high work hardening rate and high elongation that permits the severe fabrication operations which are routinely carried out, such as deep drawing of kitchen sinks and laundry troughs.

Hardness

Hardness (measured by Rockwell hardness machine) is another value for the strength of a material. Hardness is usually defined as resistance to penetration, so these test machines measure the depth to which a very hard indenter is forced into a material under the action of a known force. Each machine has a different shaped indenter and a different force application system, so conversion between hardness scales is not generally very accurate. Although conversion tables have been produced these conversions are only approximate, and should not be used to determine conformance to standards. It is also sometimes convenient to do a hardness test and then convert the result to tensile strength. Although the conversions for carbon and low alloy steels are fairly reliable, those for stainless steels are much less so.

- **Hardenss Testing of Stainless Steel**

Sr. NO	**Rockwell Hardness Testing on Scale C**
1	53
2	54
3	54
Average	**53.66**

b) **Mild Steel**

Mild steel is the most common form of steel because its price is relatively low while it provides material properties that are acceptable for many applications. Low carbon steel contains approximately 0.05–0.15% carbon and mild steel contains 0.16–0.29% carbon, therefore it is neither brittle nor ductile. Mild steel has a relatively low tensile strength, but it is cheap and malleable; surface hardness can be increased through carburizing

It is often used when large quantities of steel are needed, for example as structural steel. The density of mild steel is approximately 7.85 g/cm^3 (0.284 lb/in^3) and the Young's modulus is 210,000 MPa (30,000,000 psi).

Low carbon steels suffer from *yield-point run out* where the material has two yield points. The first yield point (or upper yield point) is higher than the second and the yield drops dramatically after the upper yield point. If a low carbon steel is only stressed to some point between the upper and lower yield point then the surface may develop Lüder bands

Mild Steel Properties

This article is aimed at explaining what is mild steel and discuss some facts related to it. Keep reading to know about various mild steel properties and understand the role it plays in manufacture of metal items.

- **Hardenss Testing of Mild Steel**

Sr. NO	**Rockwell Hardness Testing on Scale C**
1	43
2	44
3	44
Average	**43.6**

Mild steel is the type of steel, which is used in 85% of all steel applications in the United States of America. This article will talk about mild steel properties and enlighten you about why exactly is it called 'mild and what it really means.

Table 3.2 Material composition of Mild steel checked by spectrometer (composition testing machine)

Analysis

Start | New | Print | Exit

Sample: ms

Element	Burn 1	Burn 2	Burn 3	Average
Fe %	98.7	98.7	98.7	98.7
C %	0.165	0.168	0.163	0.165
Si %	0.216	0.212	0.220	0.216
Mn %	0.500	0.504	0.499	0.501
P %	0.0475	0.0474	0.0489	0.0479
S %	0.0438	0.0401	0.0380	0.0406
Cr %	0.0581	0.0504	0.0525	0.0536
Mo %	< 0.0050	0.0067	0.0086	0.0067
Ni %	0.0407	0.0320	0.0344	0.0357
Al %	< 0.0010	< 0.0010	< 0.0010	< 0.0010
Co %	0.0070	0.0072	0.0071	0.0071
Cu %	0.118	0.110	0.123	0.117
Nb %	0.0047	0.0054	0.0040	0.0047
Ti %	< 0.0020	< 0.0020	< 0.0020	< 0.0020
V %	< 0.0020	< 0.0020	< 0.0020	< 0.0020
W %	< 0.0150	< 0.0150	< 0.0150	< 0.0150
Pb %	< 0.0250	< 0.0250	< 0.0250	< 0.0250
Sn %	0.0099	0.0098	0.0105	0.0101
B %	0.0013	0.0013	0.0014	0.0013
Ca %	0.0002	0.0002	0.0002	0.0002
Zr %	< 0.0020	< 0.0020	< 0.0020	< 0.0020
As %	< 0.0050	< 0.0050	0.0053	< 0.0050

Steel is any alloy of iron, consisting of 0.2% to 2.1% of carbon, as a hardening agent. Besides carbon, there are many metal elements that are a part of steel alloys. The elements other than iron and carbon, used in steel are chromium, manganese, tungsten and vanadium. All these elements along with carbon, act as hardening agents. That is, they prevent dislocations from occurring inside the iron crystals and prevent the lattice layers from sliding past each other. This is what makes steel harder than iron.

Figure 1.11 Mild steel work piece

Varying the amounts of these hardening agents, creates different grades of steel. The ductility, hardness and mild steel tensile strength is a function of the amount of carbon and other hardening agents, present in the alloy. The amount of carbon is a deciding factor, which decides hardness of the steel alloy. A steel alloy with a high carbon content is mild steel, which is in fact much harder and stronger than iron. Though, increased carbon content increases the hardness of the steel alloy, it causes a decrease in its ductility. Read more on 'Physical Properties of Steel. Mild steel can also be described as steel which is not stainless steel. Mild steel differs from stainless steel in its chromium content.

Mild Steel Properties and Uses

Here is a compilation of mild steel properties and its uses in various fields of technology.

- Let us see, what makes the mild steel composition. Other than maximum limit of 2 % carbon in the manufacture of carbon steel, the proportions of manganese (1.65%), copper (0.6%) and silicon (0.6%) are fixed, while the proportions of cobalt, chromium, niobium, molybdenum, titanium, nickel, tungsten, vanadium and zirconium are not.
- A high amount of carbon makes mild steel different from other types of steel. Carbon makes mild steel stronger and stiffer than other type of steel. However, the hardness comes at the price of a decrease in the ductility of this alloy.

Carbon atoms get affixed in the interstitial sites of the iron lattice and make it stronger.

- What is called as mildest grade of carbon steel or 'mild steel' is typically carbon steel, with a comparatively mild amount of carbon (0.16% to 0.19%). It has ferromagnetic properties, which make it ideal for manufacture of electrical devices and motors.
- The calculated average industry grade mild steel density is 7.85 gm/cm^3. Its Young's modulus, which is a measure of its stiffness is around 210,000 Mpa.
- Mild steel is the cheapest and most versatile form of steel and serves every application which requires a bulk amount of steel.
- The high amount of carbon, also makes mild steel vulnerable to rust. Naturally, people prefer stainless steel over mild steel, when they want a rust free technology. Mild steel is also used in construction as structural steel. It is also widely used in the car manufacturing industry.

c) High chromium steel

High Chromium irons to be used in the early finishing stands of hot strip mill. The microstructure of these materials is given by a tempered martensitic matrix surrounded by an interconnected network of primary and eutectic carbides. In this paper a closer look into the properties of high speed steels is proposed. A wide range of micro structural conditions was obtained by changing the chemical composition and even by tempering the steels at different temperatures, in order to obtain different matrix micro hardness. The wear behaviour can be explained on the basis of the operating mechanism, given by the combination of abrasion, triboxidation and by adhesion.

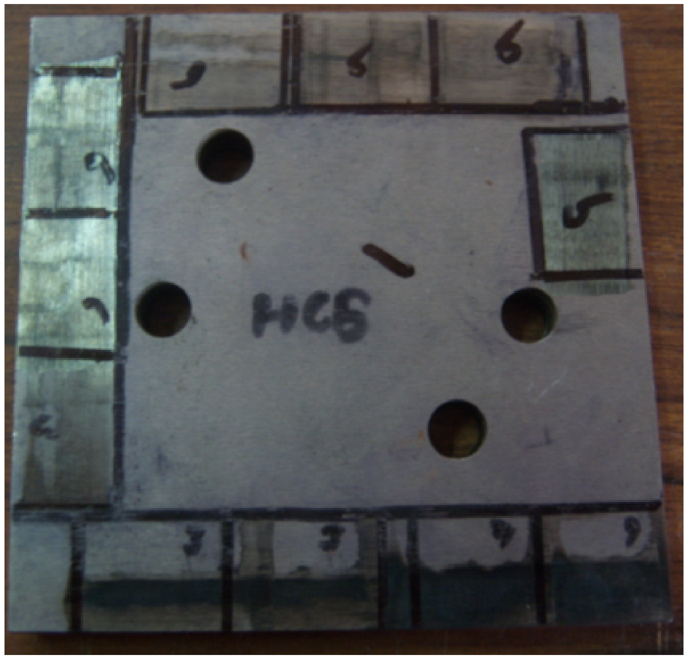

Figure 1.12 High Chromium steel work piece

While abrasion rules the tribological behaviour of HSS, triboxidation becomes more and more decisive in controlling the behaviour of HiCr irons. Strong demand for improving thermal efficiency of power generation plants promoted the use of **high-chromium steels**, which have high creep strength and corrosion resistance. Aiming at cost reduction for future nuclear power plants, these materials are also regarded as candidates for structural materials, being favoured for lower thermal expansion rate compared with austenitic stainless steels. In structural design and life management of these plants, failure due to the combination of fatigue and creep damages has been considered as an important phenomenon to be evaluated, in addition to simple creep failure under sustained loading such as inner pressure.

- **Hardenss Testing of High Chromium Steel**

Sr. NO	**Rockwell Hardness Testing on Scale C**
1	55
2	55
3	54
Average	**54.66**

Table 3.3 Material composition of High Chromium steel checked by spectrometer (composition testing machine)

Analysis

Start | New | Print | Del | Store | Exit

Sample:

Element	Burn 1	Burn 2	Burn 3	Burn 4	Burn 5	Average
Fe %	69.2	69.5	69.5	69.7		69.5
C %	0.0769	0.0897	0.0179	0.0353		0.0550
Si %	0.511	0.516	0.485	0.497		0.502
Mn %	1.58	1.55	1.60	1.56		1.57
P %	0.0172	0.0091	0.0367	0.0291		0.0230
S %	< 0.0050	< 0.0050	0.0068	0.0088		< 0.0050
Cr %	19.4	19.3	19.5	18.9		19.3
Mo %	0.300	0.298	0.296	0.294		0.297
Ni %	8.05	7.96	7.73	8.12		7.97
Al %	< 0.0010	0.0329	< 0.0010	0.0025		0.0088
Co %	0.107	0.108	0.106	0.106		0.107
Cu %	0.488	0.495	0.507	0.509		0.500
Nb %	0.0057	0.0065	0.0072	0.0087		0.0070
Ti %	0.0158	0.0182	0.0152	0.0153		0.0161
V %	0.0399	0.0378	0.0402	0.0396		0.0394
W %	< 0.0200	< 0.0200	0.0354	0.0308		< 0.0200

The author has been conducting a series of creep-fatigue tests for three types of **high-chromium steels** used in fossil power plants and the applicability of life prediction methods has been studied. It was found that the time fraction rule gives a relatively small amount of creep damage and overpredicts the failure life, whereas a simple ductility exhaustion method provides very large creep damage which leads to too conservative prediction of failure lives. A modified ductility exhaustion method developed on the re-definition of creep damage as a ductility consumer gave a moderate amount of creep damage and provided reasonable life predictability. Moreover, an empirical formula was derived which can represent the life reduction in compressive hold tests as a function of pure fatigue life and hold time.

CHAPTER 2

LITERATURE REVIEW

W.B. Rowe et al.[1](1999) studied the critical factors for the control of thermal damage in grinding at conventional work speeds have been established with reference to experimental and previously published work. For ferrous materials, significant damage occurs above a maximum work piece background temperature of 475°C. It is also known that the energy entering the work piece is reduced due to conduction into the grinding wheel. It has been found that the partitioning of energy between the grinding wheel and the work piece remains approximately constant. However, the overall partition ratio to the work piece, which takes account of energy transfer to the chips as well as energy transfer to the wheel, is variable. The effective thermal properties of the grinding wheel may be established by correlating theory with grinding experiments. An effective coefficient for the temperature equation can be obtained corresponding to the use of the geometric contact length in the equation. Using these conclusions, a simplified approach has been developed for control of thermal damage.

An efficient finite element procedure has been developed to calculate the temperatures and stresses arising due to a moving source of heat formulated by **S. Chandrasekar** et al. [2](2001) . The procedure is applied to calculate the thermal stresses produced in hardened steels during grinding. The thermal load during grinding is modeled as a uniformly or triangularly distributed, 2D heat source moving across the surface of a half-space. The grinding of elastic and elastic–plastic work piece materials has been simulated. The calculated transient stresses and temperatures in an elastic solid are found to be in good agreement with prior analytical and numerical results. In an elastic–plastic work piece material, for which no analytical solution is available for the residual stress distributions, the finite element calculations show that the near surface residual stress is predominantly tensile and that the magnitude of this stress increases with increasing heat flux values. Based on an analysis of the effects of work piece velocity, heat flux magnitude and convective cooling, on the residual stress distributions in an elastic–plastic solid, it was seen that the calculated thermal stress distributions are consistent with experimentally measured residual stresses on ground surfaces. Furthermore, the results explain often cited observations pertaining to thermally induced grinding stresses in metals.

T. Jin et al. [3](2001) discussed that thermal model is presented for deep grinding with particular relevance to the HEDG process. HEDG is defined as deep grinding at high work speeds and very high removal rates. The contact between the work piece and wheel is represented as a circular surface. It is found that the contact angle and also the Peclet number (widely used in heat transfer and defined below) have strong effects on the grinding zone temperatures. Experiments were carried out to demonstrate the high removal rates achievable and to measure the resulting contact temperature. It was found that high removal rates and absence of thermal damage could be achieved as predicted. The new model is shown to provide a good estimation of contact temperatures. It is also confirmed that HEDG can achieve low specific grinding energy compared with shallow grinding and creep grinding. The chips take away a substantial proportion of the heat generated in the grinding process. As in creep grinding, burn-out of the coolant causes a steep rise in contact temperature of the work piece.

Fritz Klocke et al. [4](2002) worked on technological and economical pressure in production engineering requires an optimization of existing production processes. The finite element method (FEM) is an appropriate tool to gain the necessary knowledge of these processes. This paper will present some examples of the application of FEM in different branches of manufacturing technology: cutting with a geometrically defined and an undefined cutting edge; electro-erosion technology; metal forming processes; tribology. After the presentation of the problem, the simulation set-up for each example will be discussed and the results will be presented. Thus, this paper will provide an overview of the current possibilities for the application of FEM in manufacturing technology.

H. H. Tsai et al. [5](2002) reported that grinding is required for high surface quality and precise dimensional and geometrical accuracy. Among the technical problems in grinding, the geometrical inaccuracy of the work piece due to thermal deformation is of particular concern in precision grinding. Especially, mould steel of low thermal conductivity will deform to become convex during grinding due to the accumulated heat in the work piece, which induces a concave surface profile of the work piece after grinding, called over-grinding. This seriously affects the geometrical accuracy and decreases the yield rate. The present study contributes to the calculation of the three-dimensional transient temperature by the finite difference method, and the model construction of the thermal bending moment, stress and deformation of the work piece using beam theory. The proposed models are discretized by the numerical multi-integral method for solution of the induced deformation of the work piece. The clamped models predict the concave deformation fairly well. They can be used as the upper and lower bounds of the thermal deformation in surface grinding.

Athanasios G. Mamalis et al. [6](2003) discussed that finite element model is proposed for the simulation of grinding of hardened steels with aluminum oxide wheels. For this task the implicit FEM code MARC is used. The proposed model is a transient state, non-linear problem that can calculate the maximum temperature and the temperature fields on the ground work piece. The input data required for the analysis are provided through a series of grinding experiments. From the numerical results obtained from the analysis it is possible to predict the size of the heat affected zones of the work piece.

Hédi Hamdi et al [7](2004) proposed grinding induces residual stresses, which can play an important role on the fatigue and wear resistance of the component. It is generally expected that conventional grinding leads to tensile residual stresses, while compressive stresses are obtained with high speed grinding (HSG). In this paper, a finite element thermo mechanical model for the calculation of residual stresses induced by a surface grinding process on a steel work piece (AISI 52100) is presented. A model giving the energy conducted as heat in the work piece as a function of the grinding wheel speed, the work piece speed, and the cutting depth is proposed. This model is available for conventional grinding for wheel speeds less than 120 $m\ s^{-1}$. It is shown that, for such grinding conditions, the simulation leads to tensile residual stresses. Moreover, the computation shows that the temperature in the grinding area increases when the peripheral wheel speed increases too. So it is expected that for wheel speeds corresponding to HSG (>120 $m\ s^{-1}$), the surface temperature can reach values leading to an austenitic transformation and therefore, during cooling, the work piece can be subjected to a superficial quenching leading to compressive residual stresses. Finally, the present paper shows that the metallurgical phenomena in the grinding area must be surrounded and must be taken into account in future models.

Y.B. Guo et al. [8](2004) solved a problem in Chip types and stated in machining effects are determined by the combined effects of work piece material properties, cutting speed, and tool geometry. The understanding of chip formation plays an important role in machining process optimization and surface integrity. Discontinuous chips, one of the major chip types, are usually formed in hard machining at high speeds. In this study, a new method has been presented to simulate discontinuous chips in high-speed machining AISI 4340 (32 HRc). The work piece material properties have been modeled using the Johnson–Cook (JC) plasticity model, and material crack formation and propagation simulated using the Johnson–Cook damage model. It has been shown that discontinuous chip is due to the internal crack initiation and propagation in front of the tool and above the cutting edge, rather than from the free surface. The simulated chip morphology correlated well with the experimental results.

The Abrasive Engineering Society [9](2004) stated that thermal damage is usually the limiting factor to grinding operations, controlling heat is important to good grinding practices. The effects of excess heat in a work piece appear in many different ways ranging from obvious work piece burn, to changes in hardness, to changes in compressive stresses, to changes in metallurgical structure and composition. Controlling thermal damage can include changes in process parameters such as feed rate, wheel characteristics such as bond structure and type of abrasive grain, dressing techniques, fluid types or fluid delivery. There are many variables that affect the flow of energy that creates undesirable metallurgical changes in the work piece.

Fundamental modeling of chatter vibrations in metal cutting and grinding processes was analyzed by **Y. Altintas** et al. [10](2004) the avoidance of chatter vibrations in industry is also presented. The fundamentals of orthogonal chatter stability law and lobes are reviewed for single point machining operations where the process is one dimensional and time invariant. The application of orthogonal stability to turning and boring operations is presented while discussing the process nonlinearities that make the solution difficult in frequency domain. Various stability models are compared against experimentally validated time domain simulation model results. The dynamic time domain model of transverse and plunge grinding operations is presented with experimental results. Off-line and real-time chatter suppression techniques are summarized along with their practical applications and limitations in industry.

D.J. Stephenson et al. [11](2004) studied in the 3D Finite Element simulations have been carried out to investigate transient heat transfer under high efficiency deep grinding (HEDG) conditions. The results have been compared to those obtained from 2D analytical models and experimental measurements. It has been found that the steady-state heat transfer condition can be readily obtained in HEDG after the maximum contact length is achieved and that side wall convective cooling has little effect on the grinding temperatures for thin steel plates. The temperature distribution on the work piece across the grinding width in cylindrical grinding shows obvious slopes and film boiling of grinding fluid may occur at the trailing edge of grinding width. Good agreement has been found between the FE results and experimental observations. 3D FE simulation and 2D analytical modeling predict quite similar values for the maximum temperatures on the finished surface of the work piece.

J. C. Aurich et al. [12](2005) studied an overview of current simulation methods describing the interaction of grinding process and grinding machine structure, e.g., vibrations, deflections, or thermal deformations. Innovative process models which describe the effects of the grinding wheel–workpiece interaction inside the contact zone are shown in detail. Furthermore, simulation models representing the static and dynamic behavior of a grinding machine and its components are discussed. Machine tool components with a high influence on the process results are modeled more detailed than those with low influence. The key issue of the paper is the coupling of process and machine tool models for predicting the interactions of process and machine. Several coupling methods are introduced and the improvements of the simulation results are documented. On the basis of the presented simulation approaches, grinding processes and machines can be designed more effectively resulting in higher workpiece quality and process stability.

Martin Baker [13](2005) proposed a finite element model of a two-dimensional, orthogonal metal-cutting process was used to study the influence of the cutting speed on the cutting force and the chip formation process. The model uses a generic flow stress law. Friction is neglected as its speed dependence is only poorly known. It is shown that the experimentally observed decrease of the cutting force with the cutting speed and the plateau at high cutting speeds are reproduced by the simulation. The decrease is mainly caused by a change in the shear angle due to thermal softening. At large cutting speeds, segmented chips are produced. It is also shown by an analytical calculation that segmented chips at large cutting speeds are energetically more favorable than continuous chips.

D.A. Doman et al. [14](2006) presented a review of two-dimensional (2D) and three-dimensional (3D) finite element models. The scale of the modeling approaches either macro- or micro-scale. Macro-scale models consider the overall wheel–work piece interaction while micro-scale models focus on the individual grain– work piece interactions. Each model was discussed and the relevant boundary conditions, material constitutive treatments, and load inputs were compared. Macro-scale models are intended to capture the aggregate effects of the abrasive wheel on the work piece. Thermal (T) models can predict the temperature distribution within the work- piece whereas structural (S) models can determine the mechanical deformations and resulting stresses. Thermal–structural (TS) models, or coupled models, can determine the resulting total stress from both thermal and mechanical loads. Ceramic (C) models are treated in that work as a separate category from the thermal or structural analyses because of their fundamental difference in material removal mechanisms.

J. Kopac and P. Krajnik [15](2006) proposed the high-performance that grinding is essential to achieve high dimensional accuracy and surface integrity of ground components at optimum cost efficiency. at increased wheel speeds with highly efficient abrasives. They have emphasized that an increased grinding cutting speed is the most important factor in achieving improved quality, tool life and productivity. In this way the advantages of HSG (High Speed Grinding) refer to a reduction in the grinding forces, the grinding wheel wear, and work piece surface roughness .An increase in temperature in the grinding zone that in turn can cause thermal subsurface damage.

Martin Baker [16](2006) presented a finite element model of a two-dimensional orthogonal high-speed cutting process was used to perform parameter variations of a generic flow stress law with strain hardening, thermal softening, and rate-dependent hardening. The influence of the material parameters on cutting forces and on the chip formation process was discussed. It was shown that the strength of chip segmentation can be understood qualitatively by adiabatic flow stress curves, with the maximum of the curve determining the onset of segmentation and the subsequent decrease in the flow stress determining its strength. The results were used to study the stages of the segmentation process. A qualitative comparison with experimental results was also performed.

D. Zhang et al. [17](2006) discussed the three degree of freedom numerically controlled micro-positioning table has been developed, optimized for applications such as improving the machining precision of precision grinders. The table consists of a moving platform, coupled to a base, three piezoelectric actuators and three capacitive sensors. An elastic structure with three notch-type flexure hinges both guides the platform and generates a preload for the piezoelectric actuators. The dimensions of the platform and flexure hinges and the position of flexure hinges are designed with the aid of finite element modeling to provide good stiffness with little bending deformation of the platform. The inverse model of the table is developed for numerical control. Experimental results are compared to the model predictions. The table has a natural frequency of 584 Hz, a resolution of 6 nm, an open loop control stiffness of 104 N/μm at the center of the moving platform and a closed loop control stiffness of 650 N/μm across the working area of the table.

A. Lefebvre et al. [18](2006) proposed that the high temperatures generated in grinding are the main factor responsible for thermal damage on the ground surface. The energy partition ratio is often investigated experimentally in order to predict this temperature. The method of the foil/work piece thermocouple is frequently used. The disruptions of this measurement technique have been studied numerically on a global scale of the wheel by a 2D finite element method taking into account the mica sheets and the constantan foil. The longitudinal thermal inertia of the thermocouple has been determined for various junction thicknesses. The simulations show that the systematic error on the maximum temperature rise (MTR) measurement cannot be neglected and is dependent on grinding conditions such as the work piece velocity and the arc contact length. Moreover, the junction thickness and the assumed heat flux conducted into the electrode also have an influence on this error. However, the sensor is always accurate during the cooling time outside the foil/wheel contact zone.

In the last decade the relevance of modeling and simulation of grinding processes was presented by **E. Brinks Meier** et al. [19](2006) It has significantly risen which is caused by industrial needs and is indicated by the number of publications and research activities in this area. This keynote paper results from a collaborative work within the STC G and gives an overview of the current state of the art in modeling and simulation of grinding processes: Physical process models (analytical and numerical models) and empirical process models (regression analysis, artificial neural net models) as well as heuristic process models (rule based models) are taken into account, and outlined with respect to their achievements in this paper. The models are characterized by the process parameters such as grinding force, grinding temperature, etc. as well as work results including surface topography and surface integrity.

M.A. Davies et al. [20](2007) proposed that performance of material removal processes and resultant work piece quality, the measurement of temperature during material removal is done extensively. In this review several widely used temperature measurement methods and show they can be applied to temperature monitoring during material removal. Since there is little documentation on measurement uncertainties as relates to material removal, this paper outlines the physics of each method, detailing the sources and evaluation of uncertainty. Finally, using criteria critical in measuring material removal, methods are compared, and the results presented in guide-format for participants in this field of work.

S. Malkin, C. Guo [21](2007) analyzed that thermal damage is one of the main limitations of the grinding process, so it is important to understand the factors which affect grinding temperatures. It's studied the analytical methods to calculate grinding temperatures and their effect on thermal damage. The general analytical approach consists of modeling the grinding zone as a heat source which moves along the work piece surface. A critical factor for calculating grinding temperatures is the energy partition, which is the fraction of the grinding energy transported as heat to the work piece at the grinding zone. For shallow cut grinding with conventional abrasive wheels, the energy partition is typically 60%–85%. For High Efficiency Deep Grinding (HEDG) using CBN wheels with large depths of cut and fast work speeds, preheated material ahead of the grinding zone is removed together with the chips, thereby lowering the temperature on the finished surface.

K. Salonitis et al. [22](2008) discussed that grind-hardening process is based on the utilization of the generated heat in the grinding zone for inducing a metallurgical transformation on the surface of the ground workpiece. The workpiece surface is locally heated above the austenitization temperature and subsequently is quenched to increase surface hardness. A theoretical model was developed for the prediction of the heat-generation rate as a function of the process parameters and the grinding wheel characteristics. The model combined with a database of relationships among the heat entering the workpiece, the process parameters, and the hardness penetration depth (HPD), which was presented by the authors in an earlier publication, allows the assessment of the grinding wheel effect characteristics on the hardening output of the process. The experimental results have verified the predictions of the theoretical model and served for its calibration.

A. Brosse et al. [23](2008) discussed the grinding process is commonly used to produce high-quality parts. The experience on this subject has shown that the main effects on ground surface are residual stresses or metallurgical change, which are directly linked with the temperature and the power absorbed during the process. Numerical simulations is a good mean to predict these effects in relation with the process parameters but the numerical models need input data such as the value and shape of the heat flux entering the work piece. In order to estimate heat flux, the temperature measurement was necessary but had shown its limits. Nowadays, a new method given by thermo graphy seems promising for determination of temperature fields under the ground surface. This measurement combined with an inverse method allows the identification of the shape and value of the heat flux. This paper presented a new method for measuring the temperatures in grinding by means of thermo graphy. The principle of measurement is proposed in combination with first results obtained from numerical simulations in order to obtain a new model of the heat flux entering the work piece during the grinding process.

Hyung Wook et al [24](2008) presented a study in which the new predictive model for the micro-grinding process was developed by consolidating mechanical and thermal effects within the single grit interaction model at micro scale material removal. The size effect of micro-machining was also included in the proposed model. In order to assess thermal effects, the heat partition ratio was experimentally calibrated and compared with the prediction of the Hahn model. Then, on the basis of this predictive model, a comparison between experimental data and analytical predictions was conducted in view of the overall micro-grinding forces in the x and y directions. Although there are deviations in the predicted micro-grinding forces at low depths of cut, these differences are reduced as the depth of cut increases. On the other hand, the optimization of micro machine tools was performed on the basis of the proposed design strategy. Individual mathematical modeling of key parameters such as volumetric error, machine working space, and static, thermal, and dynamic stiffness were conducted and supplemented with experimental analysis using a hammer impact test.

A. Chandra et al. [25](2008) discussed and compared various machining processes and stated grinding is a high energy process that generates significant heat. A number of researchers have investigated thermal aspects of grinding and other machining processes. Of particular interest are the total heat generated and its partitioning between the work piece and elsewhere (chips, coolant, wheel). Vibration assisted grinding experiments at relatively modest frequencies as well as ultrasonic frequency indicates that modulation reduces cutting force and temperature. Modulation at 3 kHz and 7.5 m amplitude reduced the force by 15% and peak temperature rise by 34% over the unmodulated case. Modulation at 40 kHz and 2.8 m amplitude reduces the cutting force by 31% and the peak temperature rise by 28% over the unmodulated case.

The random nature of grit distribution was proposed **Huang-Cheng Chang** et al. [26](2008) this paper presents a closed form expression for the stochastic grinding force as a function of the grinding conditions and grit distribution. The stochastic grit density function is introduced to describe the random grit distribution of the rotating wheel. The dynamic grinding force is formulated as the convolution of a single-grit force and the grit density function. The single-grit force is obtained from analysis of the grinding geometry and treated as a deterministic impulse response of the grinding process. The spectrum characteristics of the grinding force are investigated in the frequency domain, where the power spectrum density (PSD) of the total grinding force can be expressed as a product of the energy spectrum density of the single-grit force and the PSD of the grit density function. The analytical nature of the PSD expression of the grinding force allows the identification of the PSD of the grit density function and the mechanistic grinding coefficients, and facilitates the analysis of the effects of the grit distribution and grinding conditions upon the grinding force. The results show that predictions drawn from the theoretical model are substantiated by the PSD, variance, and time domain signal of the experimentally measured grinding forces under various grinding conditions.

H. Sudermann et al. [27](2009) studied increasing industrial requirements on the precision of edge geometry lead to the investigation of burr formation, particularly in finishing operations such as grinding. The objective of the presented research is to understand the mechanisms of burr formation in grinding following a description of previous research and existing approaches to understand burr formation in grinding, experimental investigations in flat surface grinding of tempered steel are described.

FINITE ELEMENT MODELING

3.1 HISTORY

The FEM is one of the most important developments in computational methods to occur in the 20th century. In just a few decades, the method has evolved from one with applications in structural engineering to a widely utilized and richly varied computational approach for many scientific and technological areas.

3.2 FINITE ELEMENT METHOD

The finite element method has become a powerful tool for the numerical solution of a wide range of engineering problems. With the advances in computer technology and CAD systems, complex problems can be tried out on a computer before the first prototype is built. Finite element method (FEM) is defined as a computer aided mathematical technique for obtaining approximate numerical solutions to the abstract equation of calculus that predict the response of physical system subjected to external influence.

3.3. STEPS OF FINITE ELEMENT METHOD

Finite element method can be divided into several distinctive steps. Theoretical approach to the method and its different steps are as:-

3.3.1. Discrimination

Discrimination is the process of dividing domain of problem into small regions or sub domains known as elements. Corner points of elements are called nodes. Here are the most usual elements:

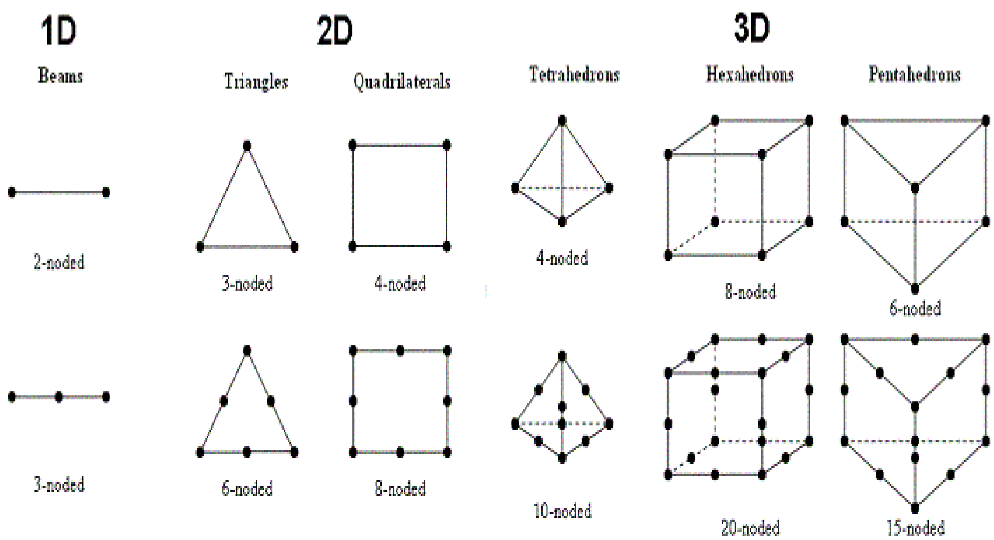

Fig. 3.1 Presentation of Different Types of Elements

All elements and nodes must be numbered so that we can set up a matrix of connectivity. The picture below shows discrimination of a transverse frame into beam elements and discrimination of a plane stress problem into quadrilateral elements.

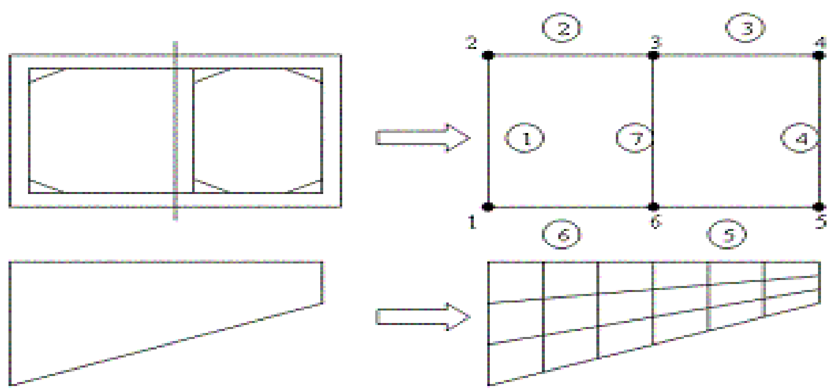

Fig. 3.2 Discrimination of Frame and Plane Stress Problems

3.3.2. Element analysis / Element stiffness matrix

The element analysis has two key components, expressing the variable within the elements, and maintaining equilibrium of the elements. The governing equation is converted to algebraic form which is represented in matrix form and is called element equation or element stiffness matrix. This enables solution by computer.

Element stiffness matrix represents the response of elements according to its property in the system for the parameters. Same matrix can be used for all elements. For conversion of governing equation (differential or integral) into algebraic form we are required to follow following steps:-

1. **Construction of Trial Solution**

It is a cyclic process by hit trial. The equation with certain Degree of freedom (DOF) is taken, which is solved by applying boundary condition at the starting for manual processing or after formulation of system stiffness matrix for solution through computer.

2. **Application of Optimization Criteria**

Optimization criteria are used to find the values of trial function. Two methods for optimization are

a) Method of weighted residual MWR. (Differential equation)

b) Collocation method.

c) Sub domain method.

d) Least square method.

e) Galerkin method

f) Ritz variation method

3.3.3. Estimation of Accuracy

Accuracy of solution is checked for closeness to exact solution. Also accuracy can be checked by checking the reducing difference of the consecutive solutions obtained by increasing degree of freedom known as property of convergence. Sources of error in FEM are as follows:-

1. **Domain Error**

Disrcitization of domain is approximate. Discretization error results from transforming the physical system (continuum) into a finite element model, and can be related to modeling the boundary shape, the boundary conditions, etc.

Discretization error due to poor geometry representation.

Discretization error effectively eliminated

Fig: 3.3 Discretization Error

2. **Computational Error**

Integration and differentiation induce error. Computational error results from the use of elements that don't precisely describe the behavior of the physical problem. Elements which are used to model physical problems for which they are not suited are sometimes referred to as ill-conditioned or mathematically unsuitable elements. For example a particular finite element might be formulated on the assumption that displacements vary in a linear manner over the domain. Such an element will produce no formulation error when it is used to model a linearly varying physical problem (linear varying displacement field in this example), but would create a significant formulation error if it used to represent a quadratic or cubic varying displacement field.

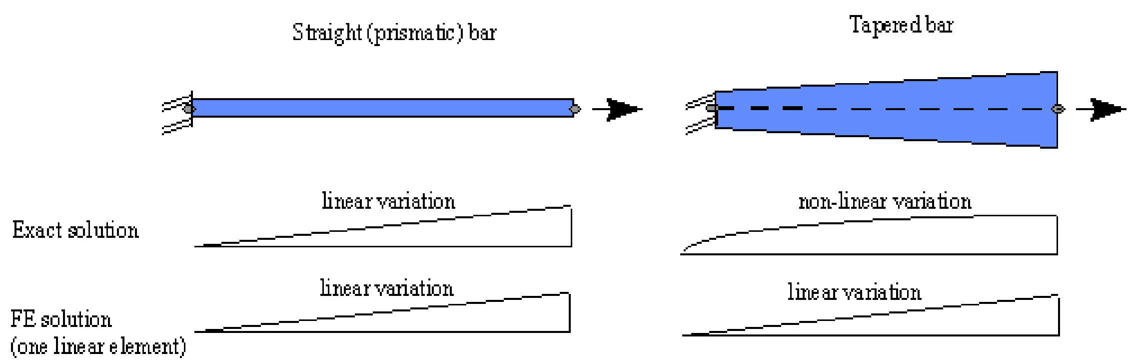

Fig: 3.4 **Approximation Error**

3. **Approximation Error**

Assumption of D.O.F makes the solution approximate. Approximation error occurs as a result of numerical calculation procedures, and includes truncation errors and round off errors. Approximation error is therefore a problem mainly concerning the FEM vendors and developers. The user can also contribute to the numerical accuracy, for example, by specifying a physical quantity, say Young's modulus, E, to an inadequate number of decimal places.

3.3.4. System Analysis / System Stiffness Matrix

The matrix equations for the individual elements are combined to form the Matrix equations for the entire system called system stiffness matrix. This tells the response of the parameters on the entire system.

3.3.5. Incorporation of Boundary and Loading Conditions

The system stiffness matrix is modified according to the over all boundary conditions. This reduces calculation work and saves time.

3.3.6. Solving of the System Equations

The system equations can be solved to give the unknown values at the nodes. If the problem is of an equilibrium nature, then the solution is obtained by solving a set of linear or non-linear equations. If the physical formulation of the problem is described as a differential equation, then the most popular solution method is the Method of Weighted Residuals. If the physical problem can be formulated as the minimization of a functional, then the Variational Formulation is usually used.

3.3.7 Post Processing / Display

The post processing stage deals with the representation of results. Typically, the deformed configuration, mode shapes, temperature, and stress distribution are displayed at this stage. C++ graphics and/or OPENGL can be used to display the graphical images .

3.4 Theoretical Overview of Elements Analysis by Virtual Work Principal

The theory of FEM for structural analysis follows the virtual work principle or the minimum total potential energy principle. The virtual work principle approach is more general as it is applicable to both linear and non-linear material behaviour.

3.4.1. Virtual Work Principle

When a rigid body that is in equilibrium is subject to virtual compatible displacements, the total virtual work of all external forces is zero; and conversely, if the total virtual work of all external forces acting on a rigid body is zero then the body is in equilibrium.

The principle of virtual work for the structural system expresses the mathematical identity of external and internal virtual work:

$$\text{External Virtual Work} = \int_v \delta\varepsilon^T \sigma \, dV \quad \text{---} \qquad (3.1)$$

The virtual internal work in the right-hand-side of the above equation may be found by summing the virtual work in the individual elements. This is the crucial step where we will need displacement functions written only for the small domain rather than over the entire system. As shown in the subsequent sections, Eq (1.1) leads to the following governing equilibrium equation for the system:

$$R = Kr + R^0 \quad \text{---} \qquad (3.2)$$

Where

R= vector of nodal forces, representing external forces applied to the system's nodes.

r= vector of system's nodal displacements, which will, by interpolation, yield displacements at any point of the finite element mesh.

R^0= vector of equivalent nodal forces, representing all external effects other than the nodal forces which are already included in the preceding nodal force vector ***R***. These external effects may include distributed or concentrated surface forces, body forces, thermal effects, initial stresses and strains.

K= system stiffness matrix, which will be established by assembling the elements' stiffness matrices : $\mathbf{k}^e$.

Once the supports' constraints are accounted for, the nodal displacements are found by solving the system of linear equations (3.2), symbolically:

$$r = K^{-1}(R - R^{0}) \qquad \text{---} \qquad (3.3)$$

Subsequently, the strains and stresses in individual elements may be found as follows:

$$\varepsilon = Bq \qquad \text{-----------} \qquad (3.4)$$

$$\sigma = E(\varepsilon - \varepsilon^{0}) + \sigma^{0} \qquad \text{----------------} \qquad (3.5)$$

Where

q= vector of element's nodal displacements--a subset of the system displacement vector **r** that pertains to the element under consideration.

B= strain-displacement matrix that transforms nodal displacements **q** to strains at any point in the element.

E= elasticity matrix that transforms effective strains to stresses at any point in the element. Also called material matrix

ε = vector of initial strains in the element.

σ^{o} = vector of initial stresses in the element.

By applying the virtual work equation (3.1) to the system, we can establish the element matrices *B*, K^{e} as well as the technique of assembling the system matrices R^{0} and *K*. Other matrices such as ϵ^{o}, σ^{o}, *R* and *E* can be directly set up from data input.

3.4.2. Interpolation or Shape Functions

Let q be the vector of nodal displacements of a typical element. The displacements at any point of the element may be found by interpolation functions as, symbolically:

$$u = Nq \qquad \text{---------} \qquad (3.6)$$

Where

u= vector of displacements at any point {x, y, z} of the element.

N= matrix of *shape functions* serving as interpolation functions.

Equation (3.6) gives rise to other quantities of great interest:

Virtual displacements consistent with virtual nodal displacements:

$$\delta u = N\delta q \qquad \text{----------} \qquad (3.6a)$$

Strains in the elements:

$$\varepsilon = Du = DNq \qquad \text{-------------} \qquad (3.7)$$

Where D= matrix of differential operators that convert displacements to strains using linear elasticity theory.

Equation (3.7) shows that matrix B in (3.4) is

$$B = DN \qquad \text{------------} \qquad (3.8)$$

Virtual strains consistent with element's virtual nodal displacements:

$$\delta\varepsilon = B\delta q \qquad \text{------------------} \qquad (3.9)$$

3.4.3. Internal Virtual Work in a Typical Element

For a typical element of volume V^e, the internal virtual work due to virtual displacements is obtained by substitution of (3.5) and (3.9) into (3.1):

$$\text{Internal virtual work} = \int_{V^e} \delta\varepsilon^T dV^e \; = \; \delta q^T \int B^T \{E(Bq - \varepsilon^0) + \sigma^0\} dV^e \qquad (3.10)$$

3.4.4. Element Matrices

Primarily for the convenience of reference, the following matrices pertaining to a typical element may now be defined:

$$\text{Element stiffness matrix} \quad k^e = \int B^T EBdV^e \qquad \text{-----} \qquad (3.11)$$

Equivalent element load vector

$$Q^{oe} = \int - B^T (E\varepsilon^0 - \sigma^0) dV^e \qquad \text{-----} \qquad (3.12)$$

These matrices are usually evaluated numerically using Gaussian quadrature for numerical integration. Their use simplifies (3.10) to the following:

$$\text{Internal virtual work} = \delta q^T (k^e + Q^{oe}) \qquad \text{---} \qquad (3.13)$$

CHAPTER 4

EXPERIMENTAL SETUP

4.1 INTRODUCTION

A **tool and cutter grinder** is used to sharpen milling cutters and tool bits along with a host of other cutting tools. It is an extremely versatile machine used to perform a variety of grinding operations: surface, cylindrical, or complex shapes. The image shows a manually operated setup, however highly automated Computer Numerical Control machines are becoming increasingly common due to the complexities involved in the process.

The operation of this machine (in particular, the manually operated variety) requires a high level of skill. The two main skills needed understand of the relationship between the grinding wheel and the metal being cut and knowledge of tool geometry. The illustrated set-up is only one of many combinations available. The huge variety in shapes and types of machining cutters requires flexibility in usage. A variety of dedicated fixtures are included that allow cylindrical grinding operations or complex angles to be ground.

Figure 4.1:- Experimental setup of tool and cutter grinder

The table moves longitudinally and laterally, the head can swivel as well as being adjustable in the horizontal plane, as visible in the first image. This flexibility in the head allows the critical clearance angles required by the various cutters to be achieved. Tool and cutter grinders can be adapted to manufacturing precision machine components.

Tool and cutter Grinder are widely used to produce parts for aerospace, medical, automotive, and other industries.

4.2 TECHNICAL SPECIFICATIONS OF TOOL AND CUTTER GRINDER

1.	Larger diameter of cutter that can be ground	254mm
2.	Maximum admit between centers	465mm
3.	Maximum length of cutting edge that can be ground	385mm
4.	Grinding spindle speed	4500 & 6000 rpm
5.	Working surface of T-slot table	645 x 150 mm
6.	Working surface of auxiliary table	655 x 118 mm
7.	Longitudinal traverse	385 mm
8.	Cross traverse	125 mm
9.	Horse power of driving motor	0.75 HP : 440 volt 3 phase : 50 cycles.
10.	Base of machine	515 x 515 mm

Figure 4.2:- Experimental setup with all components

4.3 Main Components of Experimental Setup

a) **Dynamometer**

b) **Thermometer**

c) **Dial gauge**

d) **Grinding wheel**

4.3.1 Dynamometer

A dynamometer is a device used for measuring force, moment of force (torque), or power. For example, the power produced by an engine, motor or other rotating prime mover can be calculated by simultaneously measuring torque and rotational speed(rpm). A dynamometer can also be used to determine the torque and power required to operate a driven machine such as a pump. In that case, a *motoring* or *driving* dynamometer is used. A dynamometer that is designed to be driven is called an absorption or passive dynamometer. A dynamometer that can either drive or absorb is called a universal or active dynamometer.

Figure 4.3:- Work piece mounted on dynamometer

- **Principle of Absorbing Dynamometer**

An absorbing dynamometer acts as a load that is driven by the prime mover that is under test. The dynamometer must be able to operate at any speed and load to any level of torque that the test requires. Absorbing dynamometers are not to be confused with "inertia" dynamometers, which calculate power solely by measuring power required to accelerate a known mass drive roller and provide no variable load to the prime mover. An Absorption dynamometer is usually equipped with some

means of measuring the operating torque and speed. In most dynamometers power (*P*) is not measured directly; it must be calculated from torque (τ) and angular velocity (ω) values or force (*F*) and linear velocity (v).

$$P = \tau \cdot \omega$$

or

$$P = F \cdot v$$

Table 4.1 Specifications Of Dynamometer

Calibration			Calibrated
Measuring Range	Fx, Fy, Fz	KN	±5
Sensitivity	Fx, Fy	pC/N	≈-7.5
	Fz	pC/N	≈-3.7
Natural Frequency	Fnx	KHz	≈2.3
	Fny	KHz	≈3.5
Operating temperature range		°C	0...70
Length		Mm	≈170
Width		Mm	≈100
Height		Mm	≈60

4.3.2 Thermometer

Temperature is measured with thermometers that may be calibrated to a variety of temperature scales. Celsius scale is used for most temperature measuring purposes. The entire scientific world measures temperature using the Celsius scale and thermodynamic temperature using the Kelvin scale, which is just the Celsius scale shifted downwards so that 0 K[1]= −273.15 °C, or absolute zero.

- **Types of Thermometers Mechanism**:-

Digital Thermometers

Digital thermometers use thermocouples or thermistors to sense the change in temperature and display the temperature on a digital display. They are widely used as clinical, outdoor and food thermometers. Infrared thermometers use the infrared sensor to determine the temperature and have a digital display.

Figure 4. 4 Digital Thermometer

Mercury Thermometers:-

Mercury thermometers have mercury filled in a glass tube and have a glass bulb at the bottom. As the temperature increases, the mercury rises in the glass tube. The glass tube is calibrated in Celsius, Fahrenheit or both. The rise in mercury determines the temperature according to the calibration. Alcohol thermometers have ethanol or toluene instead of mercury in the glass tube. All the other mechanism of the thermometer are same as that of the mercury thermometer. They are used as clinical thermometers and outdoor thermometers.

- **Thermometer Specifications**

The following are definitions and options that are important to know in order to select the best thermometer for the particular task: -

1. Temperature range: The maximum temperature range of the application needs to be known to select the appropriate thermometer. In general, it is better to overstate the range slightly to allow some room for potential abuse. Another option is to identify a smaller range that is used 90% of the time and buy the majority of the units in that range to save cost, while getting a few more expensive units at the full range for the occasions that they are needed.

2. Scale: Some units come in Fahrenheit or Celsius exclusive forms, while others are user switchable. While it is nice to have both in a unit, if only one scale is commonly used, an non-switchable unit may be preferable to avoid confusion during usage.

3. Accuracy: Higher accuracy usually means higher price. The level of accuracy depends on the application. Generally ±0.5 to 1C accuracy is sufficient in the food industry whereas the pharmaceutical industry may require ±0.2 to 0.5C accuracy or better. It is important to note the scale used in comparisons though ±0.2C accuracy is not the same as ±0.2F accuracy.

4. Resolution: Often confused with accuracy, it is often 0.1 degree regardless of the accuracy. Many suppliers purposefully omit accuracy and list resolution on cheaper inaccurate product to make them look better.

5. Water-Resistance: Waterproof models are 2-3X the price of water resistant or not rated thermometers. However, if the application does involve exposure to water, the higher initial cost for a waterproof model may be worthwhile rather than having to constantly replace non-waterproof thermometers that fail from water exposure.

2.3 Thermocouple

When two wires composed of dissimilar metals are joined at both ends and one of the ends is heated, there is a continuous current which flows in the thermoelectric circuit. If this circuit is broken at the center, the net open circuit voltage is a function of the junction temperature and the composition of the two metals. All dissimilar metals exhibit this effect.

4.3.3 DIAL GAUGE/DIAL INDICATOR

Dial indicators, also known as dial gauges and probe indicators, are instruments used to accurately measure small linear distances, and are frequently used in industrial and mechanical processes. They are named so because the measurement results are displayed in a magnified way by means of a dial.

Figure 4.5 Dial Indicator

A special variety of the dial indicator is the dial test indicator (DTI) which is primarily used in machine setups. The DTI measures displacement at an angle of a lever or plunger perpendicular to the axis of the indicator. A regular dial indicator measures linear displacement along that axis. Dial indicators may be used to check the variation in tolerance during the inspection process of a machined part, measure the deflection of a beam or ring under laboratory conditions, as well as many other situations where a small measurement needs to be registered or indicated. Dial indicators typically measure ranges from 0.25 mm to 300 mm (0.015 in to 12.0 in).

4.3.4 GRINDING WHEEL

Grinding wheel is cutting tool used for machining operations such as surface finishing, metal cutting etc. Grinding wheel is made up of different types of abrasives such as aluminum oxide, silicon carbide, and diamond etc.

Figure 4.6 Grinding wheel

In this abrasives are acts as cutting edges which will cut the material in the form of small chip.

Specifications of Grinding Wheel

Straight cup grinding wheel, 60grit grinding wheel is used having dimensions are 4"Diameter x 2"Wide x 20mm Hole (100 x 50 x 20mm)

4.4 EXPERIMENTAL PROCEDURE

An experimental set-up is developed for the measurement of forces and temperature during the grinding process. In this setup Tool and cutter grinder is used for experiments which are drived through an electric motor and with the help of flat belt. In this setup there is a possibility to vary the rpm of motor i.e 6000 and 4500 rpm. The grinding wheel is mounted on the arbor and is placed in the proper position so that grinding is possible. Before commencement of experiment, proper height of table is set with the help of hand lever which is mechanized with the help of tail and pinion mechanism. The dynamometer is mounted on the table with the help of fasteners which are further tightened on T- slots. The work piece is mounted on a dynamometer (Kistler 9257A) linked to an acquisition data system in order to measure also the loads during grinding. The force is displaced on the display meter which is connected with the dynamometer. Cross slide is used for giving a motion to the table in y-axis which is operated with the help of gear mechanism. Dial gauge indicator is used to calculate the depth of cut which is given to the work piece. The dial gauge is having a plunger which is moving in to and fro motion. As it moves in up and down motion, indication is given on the dial gauge. The least count of dial gauge indicator is 0.01 mm. As we start the motor, grinding wheel is rotated at particular rpm according to the positioning of flat belt and work piece is mounted on the dynamometer. As grinding wheel start machining forces are displayed on the display meter of the dynamometer and we get final readings of force. Temperature is measured with the help of thermometer using thermocouple.

CHAPTER 5

MODELING AND ANALYSIS

5.1. FINITE ELEMENT MODELING

It is very difficult to exactly model a process like grinding in which there are still researches are going on to find out the real mechanism of material removal. There is always a need of some assumptions to model any complex process. These assumptions are made, keeping in mind the difficulties involved in the theoretical calculation and the importance of the parameters that are taken and those which are ignored. In modeling we always ignore the things that are of less importance and have little impact on the process. The assumptions are always made depending upon the details and accuracy required in modeling.

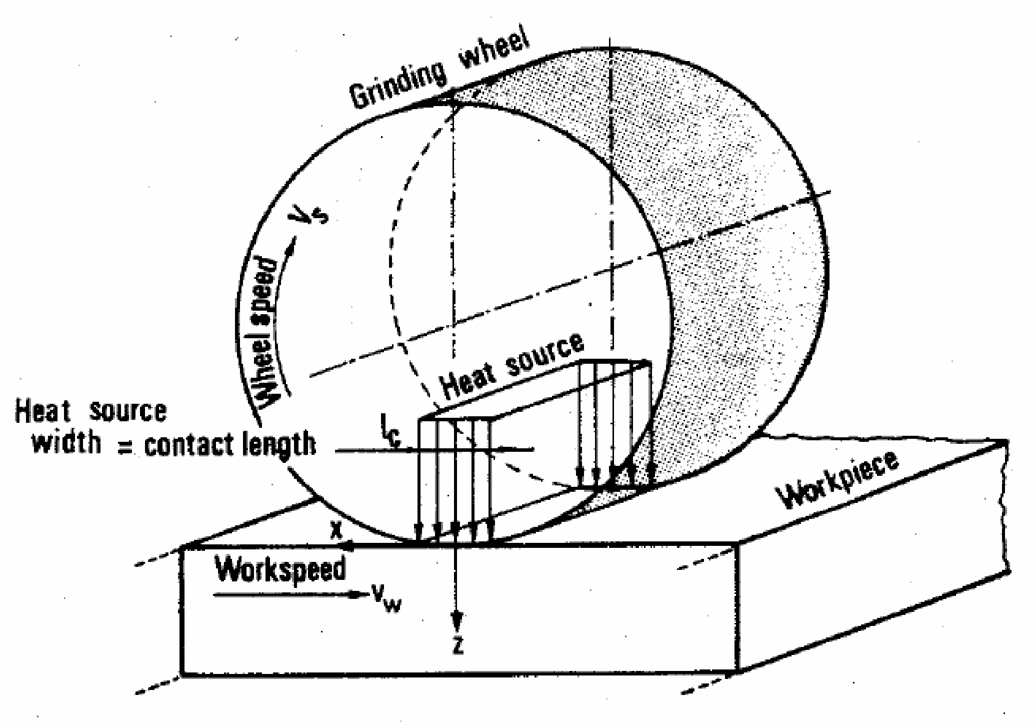

Figure 5.1 Basic grinding parameters with application of heat source on work piece [ref 6]

5.2. THERMAL MODELING

Steps involved in Thermal Modeling using finite element modeling

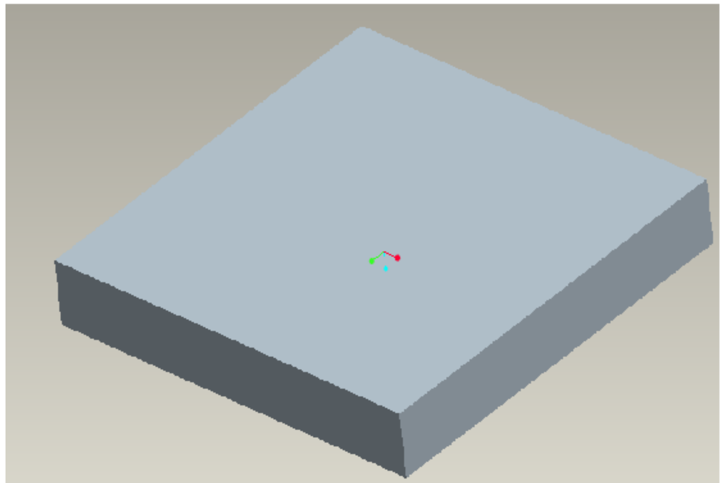

Figure 5.2: 3-D model of the work piece

- **Planning the Analysis**

In this step a compromise between the computer time and accuracy of the analysis is made. The various parameters set in this step of our analysis are given below:

Temperature modeling

1. Analysis type – thermal H-method.
2. Steady state or Transient?
3. Thermal or Structural?
4. Properties of the material?
5. Objective of analysis- to find out the temperature distribution in the work piece when the process of grinding is done.
6. Units- SI

- **Determine the Problem Domain**

In this step the geometry of the problem is defined. A 3-D isometric figure of the problem is made

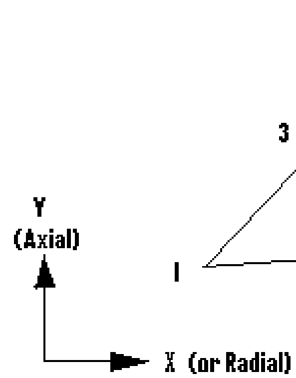

Figure: 5.3 Triangular elements with 3 Nodes

The element that is used in this analysis with its degree of freedom is shown in the figure 5.2. Since in the finite element analysis the results are available only on the nodes, the geometry of the problem is meshed such that the nodes can be found on the locations where the values of the degree of freedom (temperature in thermal analysis and x-y-z translation in stress analysis) are needed. To meet all the requirements meshing is used.

- **Applying the Boundary Conditions**

The tool with specific dimensions has been considered as the domain. On the domain Heat flux is applied on the surface up to 16 mm, 20 mm and 24 mm and Gauss distribution convection is used for the other region on surface which is caused due to cooling by atmospheric temp.

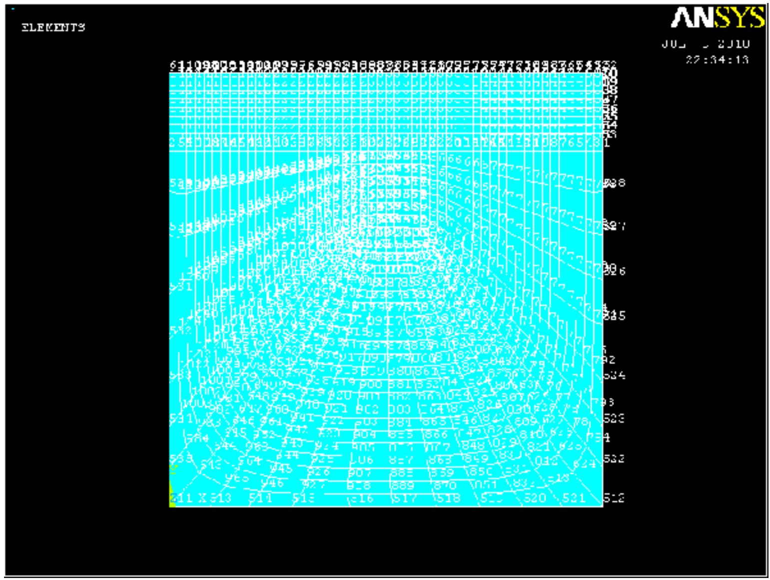

Figure 5.4 Meshing of Work piece

- **Solve the Problem**

In the solution procedure, frontal solver is used. It involves

1) Defining the load and apply the convection and the heat flux region on the work piece depending upon the requirements.
2) After defining the load initial conditions are defined like temperature.
3) Final analysis is done using general post processor and we get the final result of temperature distribution on the work piece.
4) After getting the temperature distribution graphs are plotted between temperature and distance.

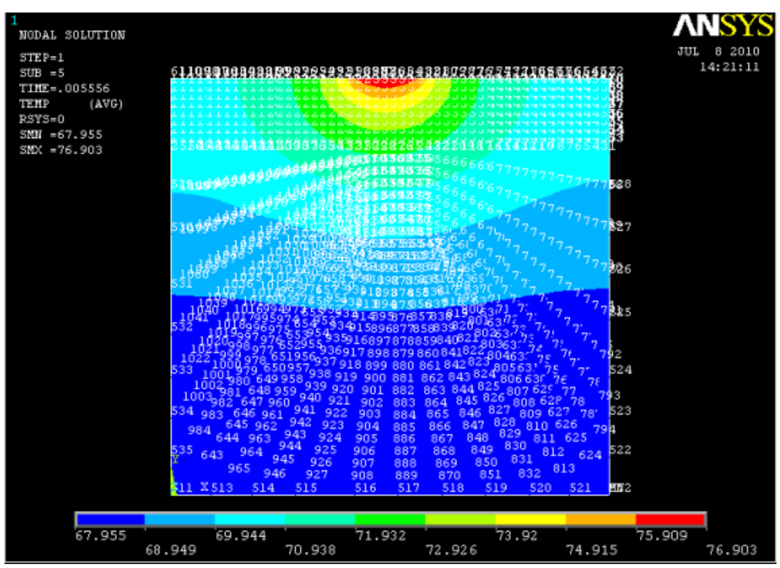

Figure 5.5 Temperature distributions on work piece

5.3. STRUCTURAL MODELING

Steps Involved in Structural Modeling Using Finite Element Modeling

- **Determine the Problem Domain**

In this step the geometry of the problem is defined. A 3-D isometric figure of the problem is made by giving dimensions of the 3-D model. These are further model by using direct selection of volume or by using joining vertices approach and then from vertices, lines are made and further faces and volumes are created.

- **Creating a Finite Element Mesh**

In finite element mesh, the work piece is distributed into the small elements or nodes

- **Applying the Boundary Conditions**

After meshing the work piece, boundary conditions were applied to it. The following are the boundary conditions according to the material properties like as, Density, Poisson ratio etc. All DOF is applied to the work piece so that there is zero displacement in it.

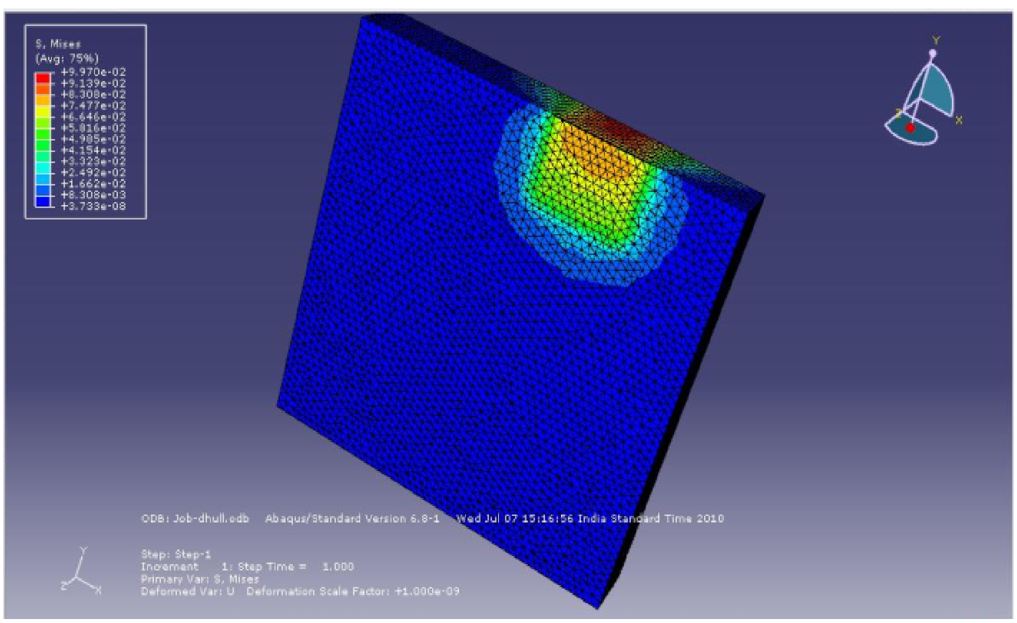

Figure 5.6 Stress Distribution on the work piece using ABAQUS software

- **Convergence Monitor**

The convergence monitor for displacement is selected as 1.0e-08 for accuracy in the results. The solution is achieved whenever the convergence monitor reaches at 1.0e-08.

- **Solve the Problem**

In the solution procedure, frontal solver is used. It involves

a) After the individual element matrices are calculated, the solver reads in the degree of freedom (DOF) for the first element.

b) The program eliminates any degrees of freedom that can be expressed in terms of the other DOF.

Chapter 6

RESULTS AND DISCUSSION

6.1 GRAPHS FOR TEMPERATURE VS DEPTH OF CUT FOR DIFFERENT MATERIALS:

- **Material Mild Steel**
- **Speed 6000 rpm**

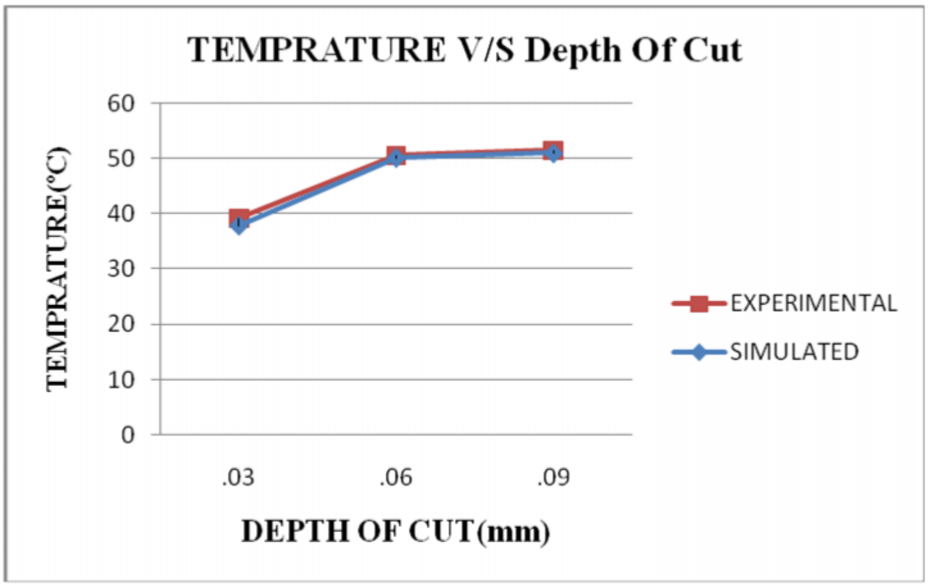

Figure 6.1 Variation between depth of cut and temperature at 0.0667 feed

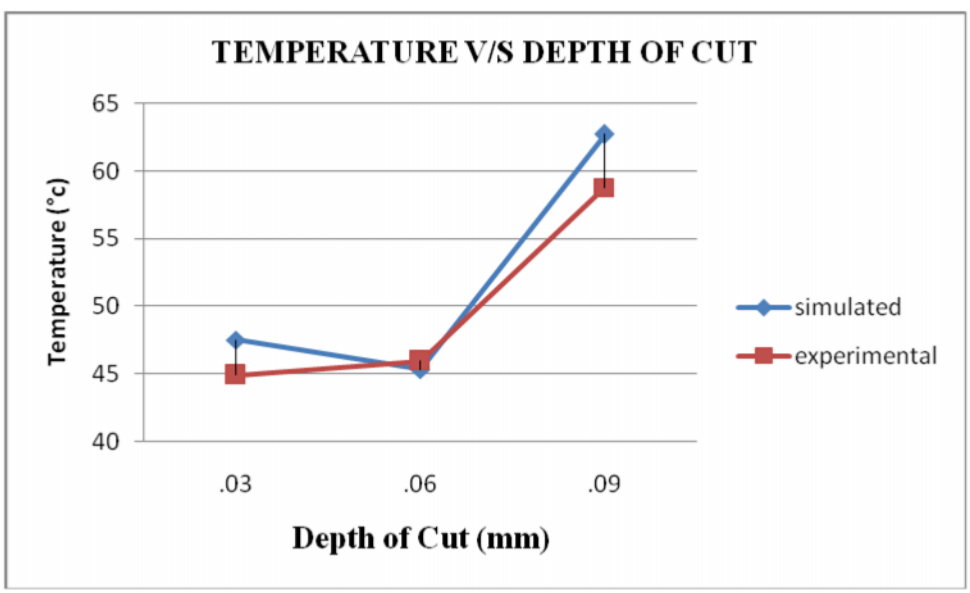

Figure 6.2 Variation between depth of cut and temperature at 0.1 feed

- **Material High Chromium Steel**
- **Speed 6000 rpm**

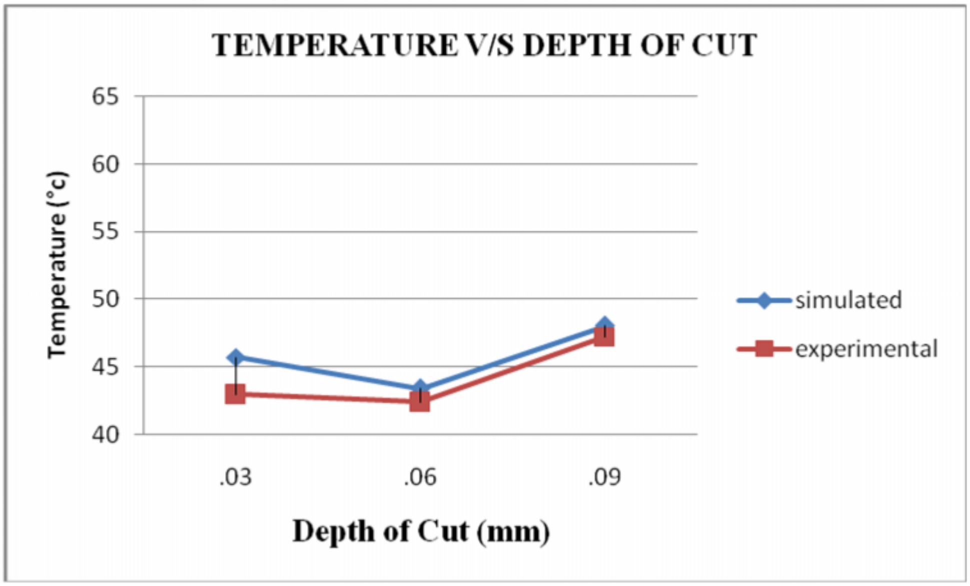

Figure 6.3 Variation between depth of cut and temperature at 0.0667 feed

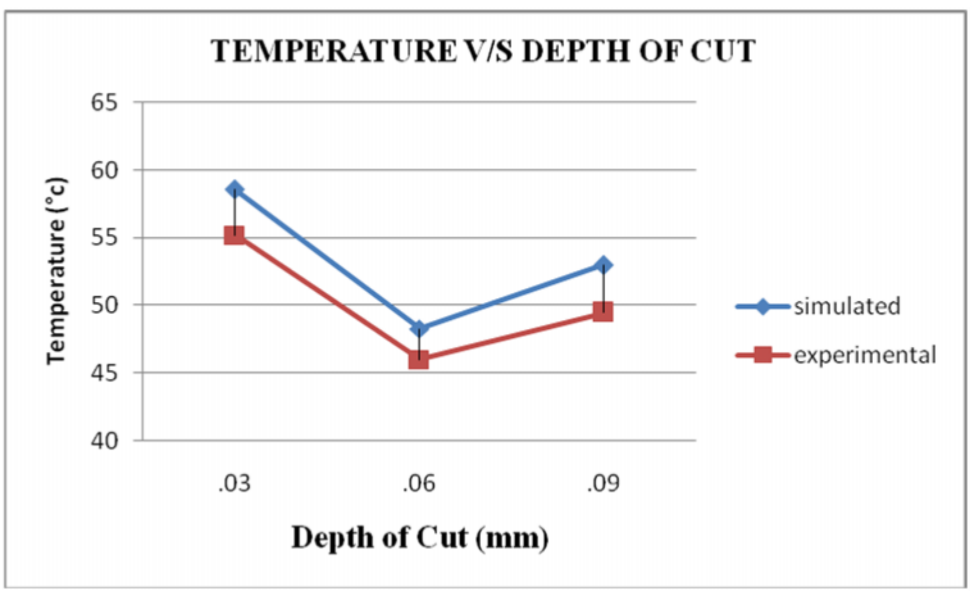

Figure 6.4 Variation between depth of cut and temperature at 0.1 feed

- **Material Stainless Steel**
- **Speed 6000 rpm**

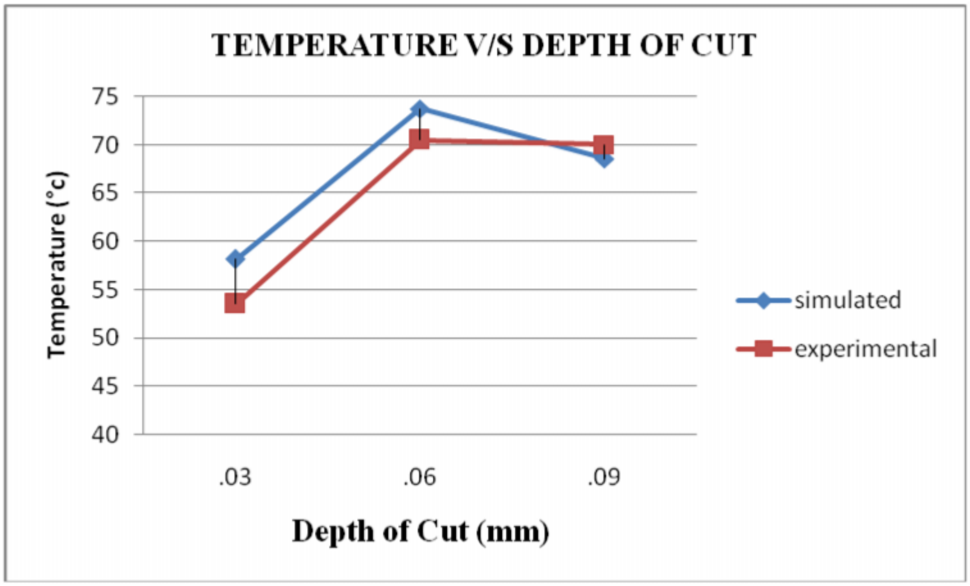

Figure 6.5 Variation between depth of cut and temperature at 0.0667 feed

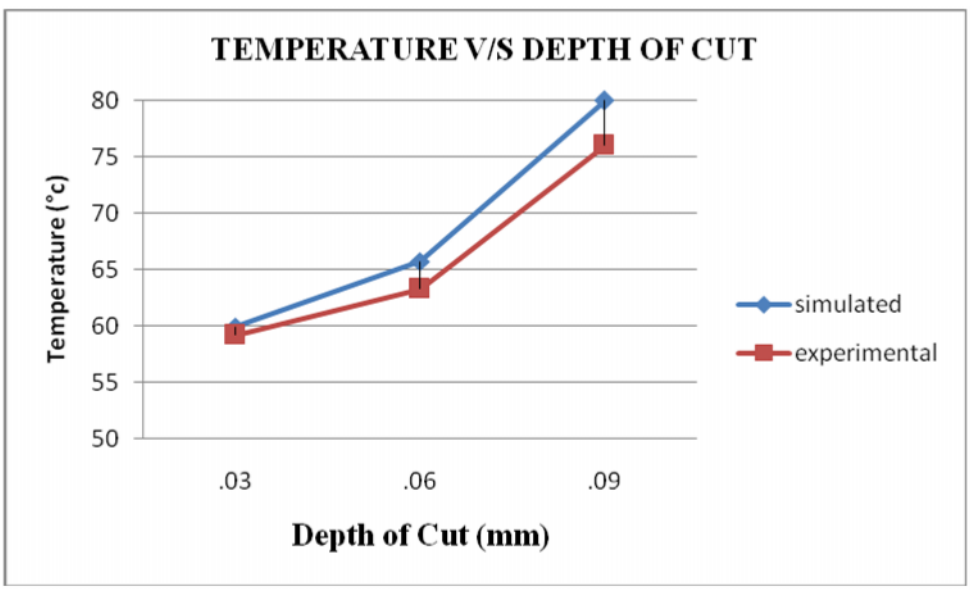

Figure 6.6 Variation between depth of cut and temperature at 0.1 feed

- **Material Mild Steel**
- **Speed 4500 rpm**

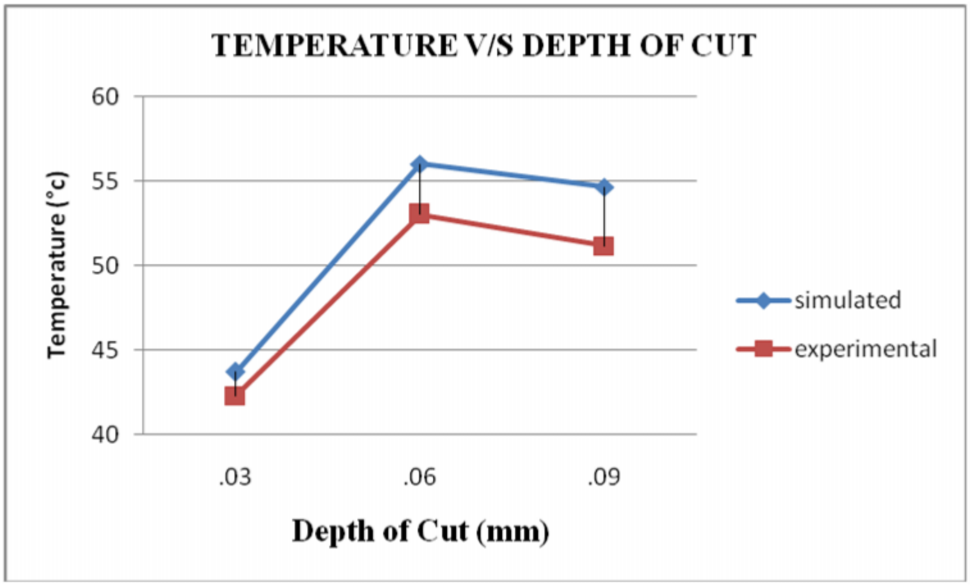

Figure 6.7 Variation between depth of cut and temperature at 0.0667 feed

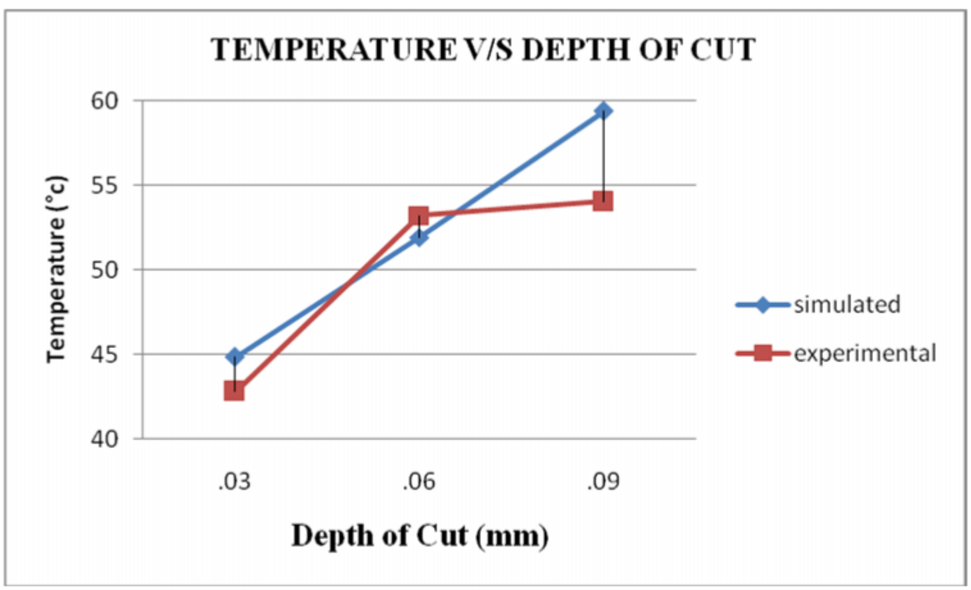

Figure 6.8 Variation between depth of cut and temperature at 0.1 feed

- **Material High Chromium Steel**
- **Speed 4500 rpm**

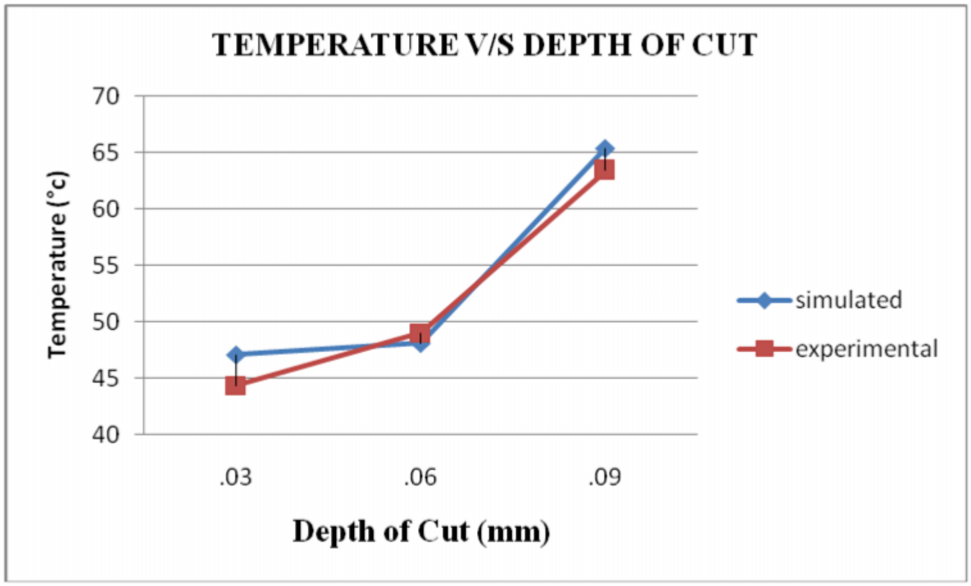

Figure 6.9 Variation between depth of cut and temperature at 0.0667 feed

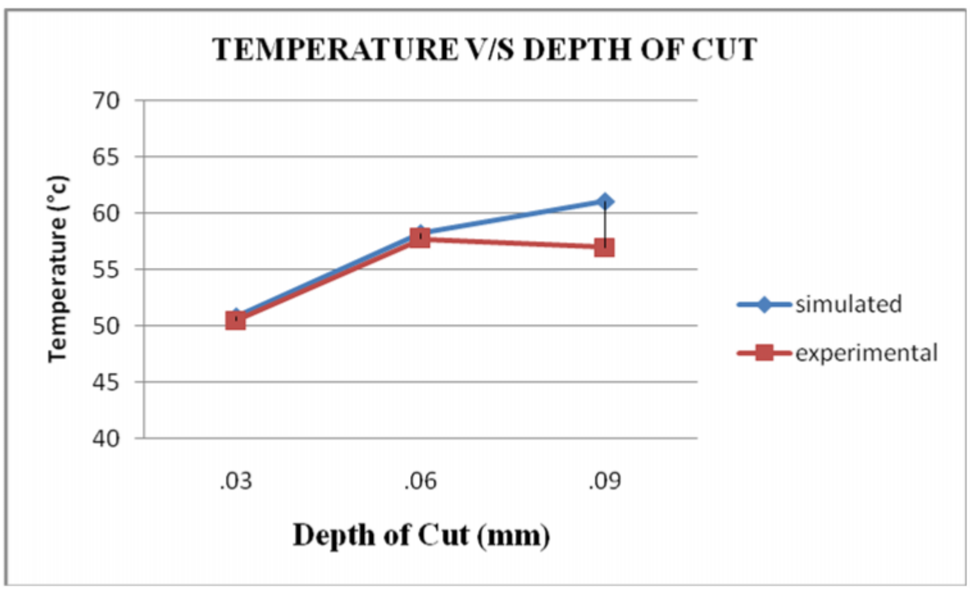

Figure 6.10 Variation between depth of cut and temperature at 0.1 feed

- **Material Stainless Steel**
- **Speed 4500 rpm**

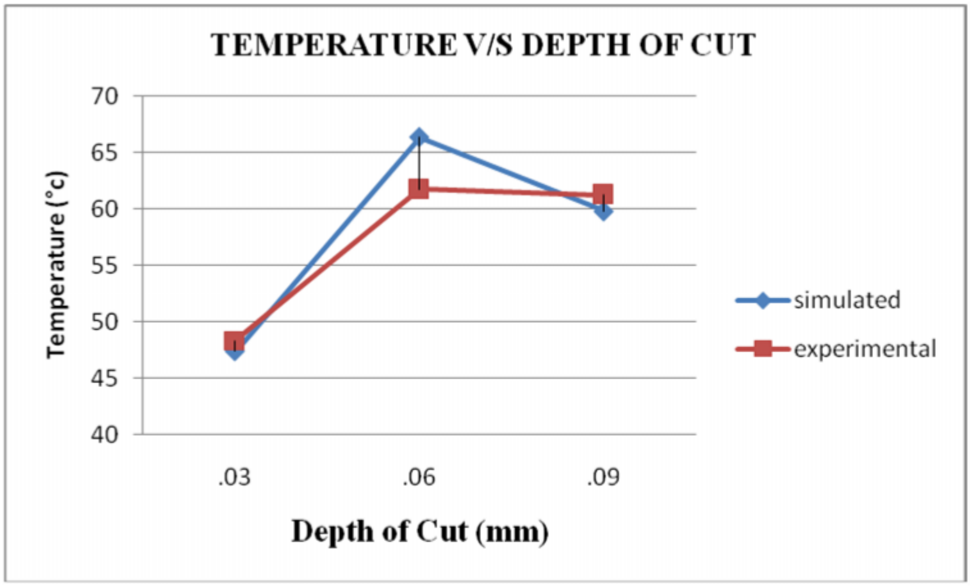

Figure 6.11 Variation between depth of cut and temperature at 0.0667 feed

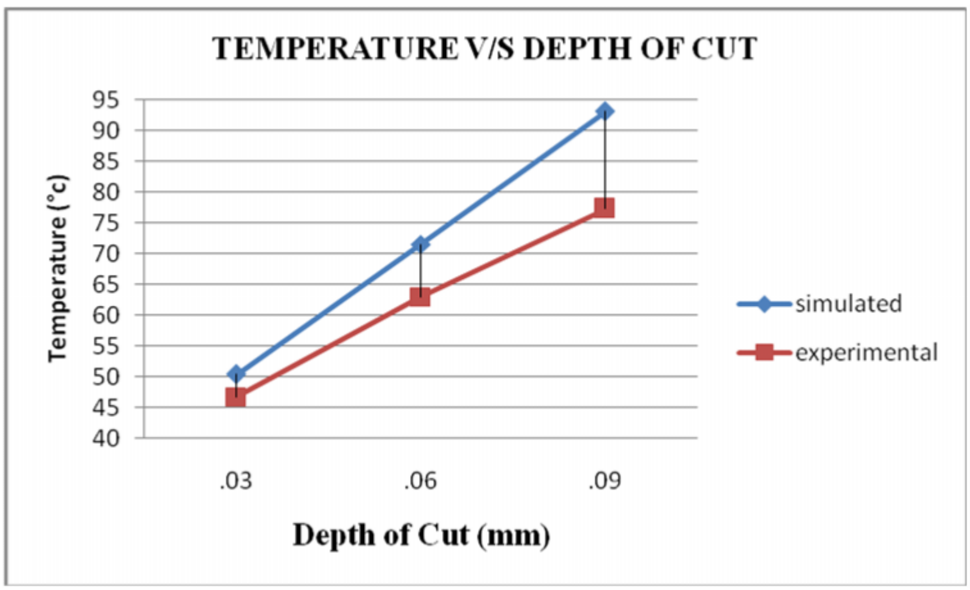

Figure 6.12 Variation between depth of cut and temperature at 0.1 feed

6.2 RESULTS AND DISCUSSIONS FOR TEMPERATURE VS DEPTH OF CUT FOR DIFFERENT MATERIALS:

1. In figure 6.1 for mild steel one can observe that temperature for simulated graphs is almost similar as temperatures obtained from experimental observation. Maximum temperature occurs at 51°C at 0.09 mm depth of cut.

2. In figure 6.2 for mild steel one can observe that temperature for simulated graphs is almost similar as temperatures obtained from experimental observation. Maximum temperature occurs at 63°C at 0.09 mm depth of cut.

3. In figure 6.3 for high chromium steel it is observed that with increase in depth of cut temperature rises.

4. In figure 6.4 for high chromium steel and for 0.1 mm/rev feed temperature at lesser depth of cut is more than temperature for higher depth of cut.

5. In figure 6.5 for stainless steel one can observe that temperature for simulated graphs is more than temperatures obtained from experimental observation. But at 0.09 mm depth of cut the temperature for experimental observations overshoots the temp of simulated observations.

6. In figure 6.6 for stainless steel it is observed that with increase in depth of cut temperature rises.

7. In figure 6.7 for mild steel it is observed that with increase in depth of cut temperature rises.

8. In figure 6.8 for mild steel for 0.06 depth of cut one can experience difference in variation. The simulated curve follows the linear pattern.

9. In figure 6.9 for high chromium steel (4500 rpm) it is observed that with increase in depth of cut temperature rises.

10. In figure 6.10 for high chromium steel and for 0.1 mm/rev feed till 0.06 depth of cut the experimental as well as simulated data show same results except for 0.09 mm depth of cut.

11. In figure 6.11 for stainless steel one can observe that temperature for simulated graphs is more than temperatures obtained from experimental observation at 0.06. But at 0.09 mm depth of cut the temperature for experimental observations overshoots the temp of simulated observations.

12. In figure 6.12 for stainless steel it is observed that with rise in depth of cut temperature rises and temperature for simulated graphs is more than temperature for experimental graphs.

6.3 GRAPHS FOR STRESS VS DEPTH OF CUT FOR DIFFERENT MATERIALS:

- **Mild Steel**
- **Speed 6000 rpm**

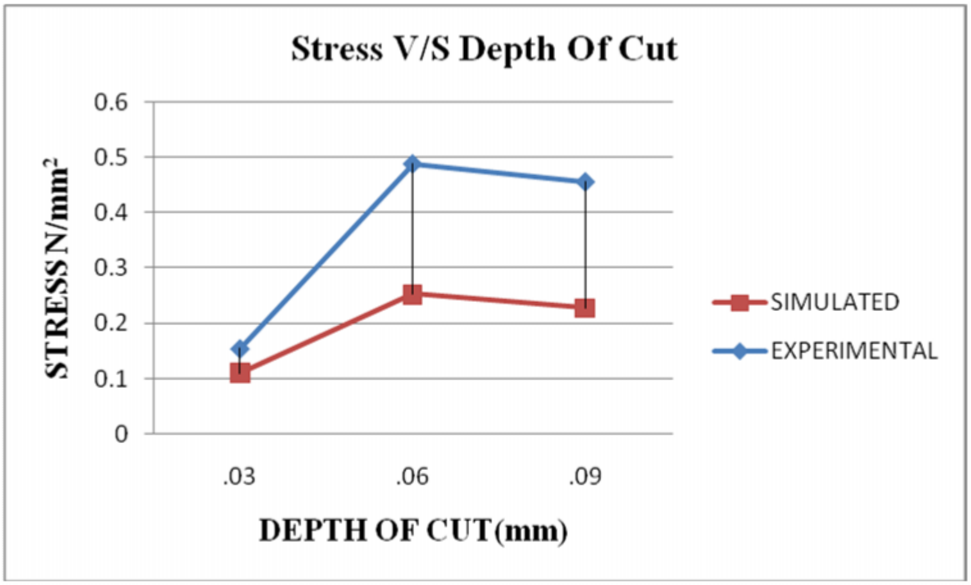

Figure 6.13 Variation of stresses with depth of cut at 0.0667mm/rev

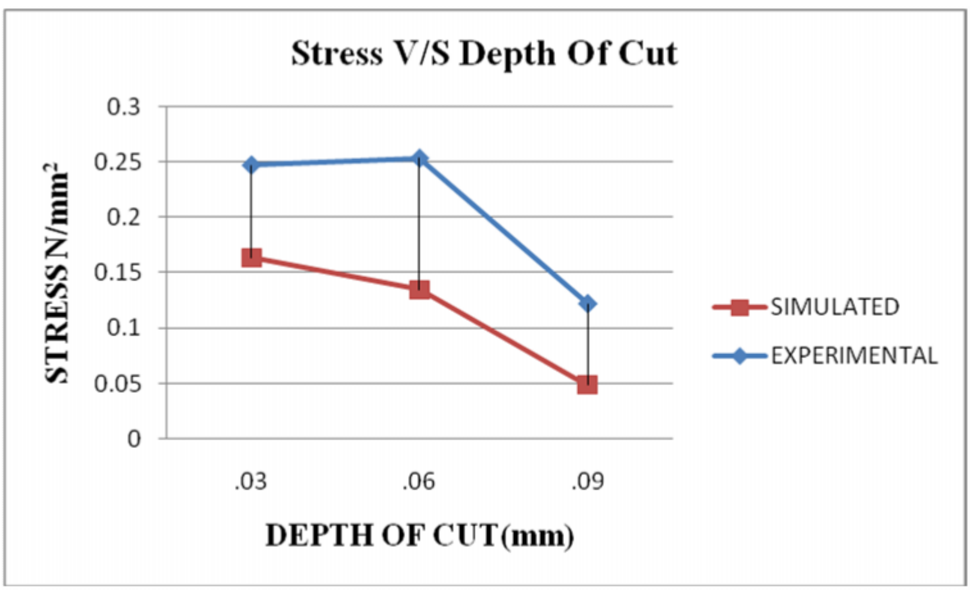

Figure 6.14 Variation of stresses with depth of cut at 0.1mm/rev

- **High chromium Steel**
- **Speed 6000 rpm**

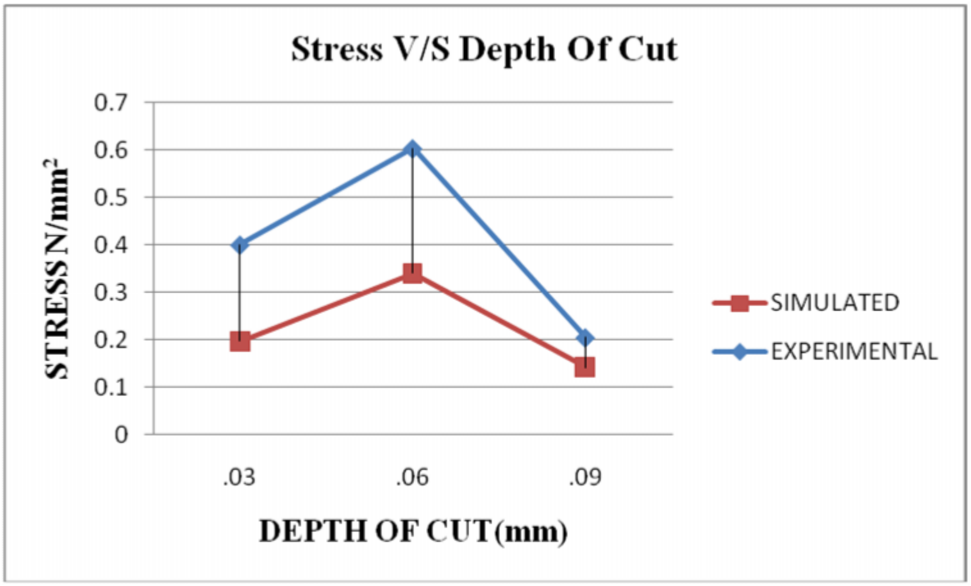

Figure 6.15 Variation of stresses with depth of cut at 0.0667mm/rev

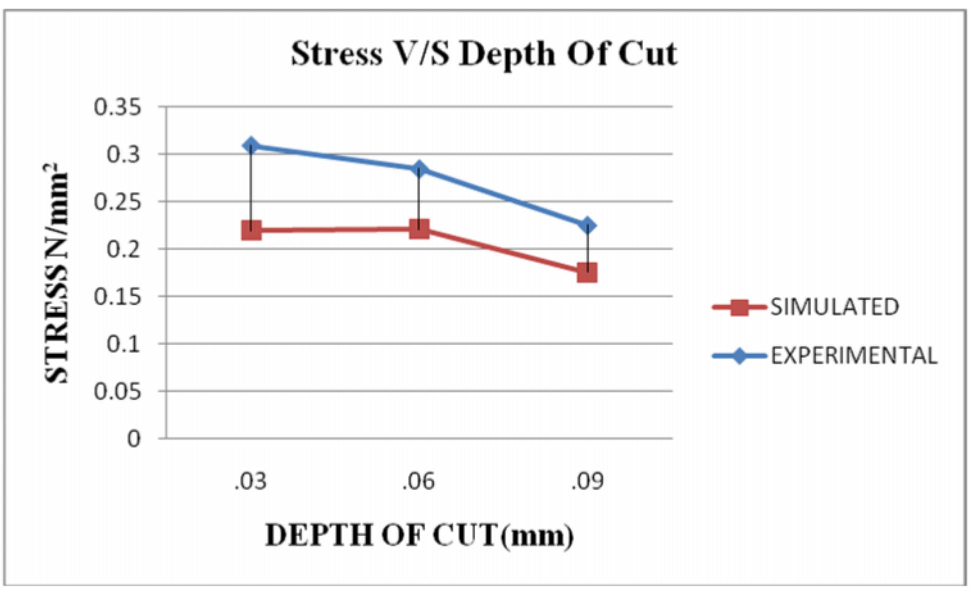

Figure 6.16 Variation of stresses with depth of cut at 0.1mm/rev

- **Stainless Steel**
- **Speed 6000 rpm**

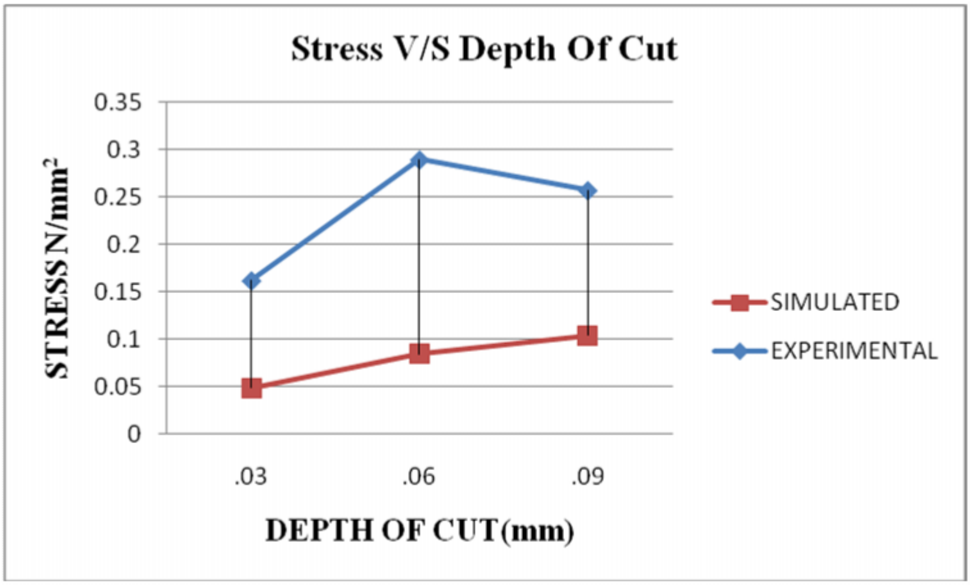

Figure 6.17 Variation of stresses with depth of cut at 0.0667mm/rev

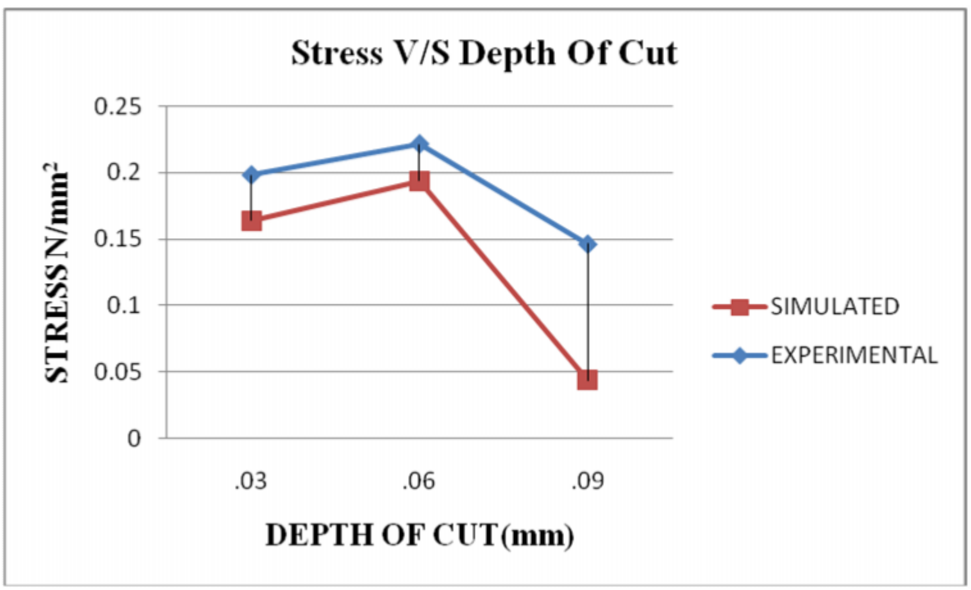

Figure 6.18 Variation of stresses with depth of cut at 0.1mm/rev

- **Mild Steel**
- **Speed 4500 rpm**

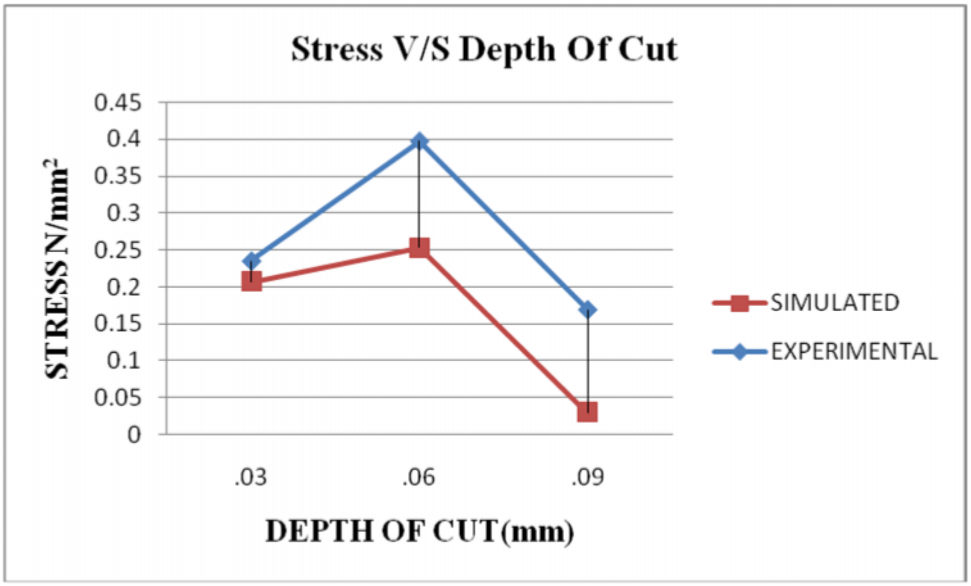

Figure 6.19 Variation of stresses with depth of cut at 0.0667mm/rev

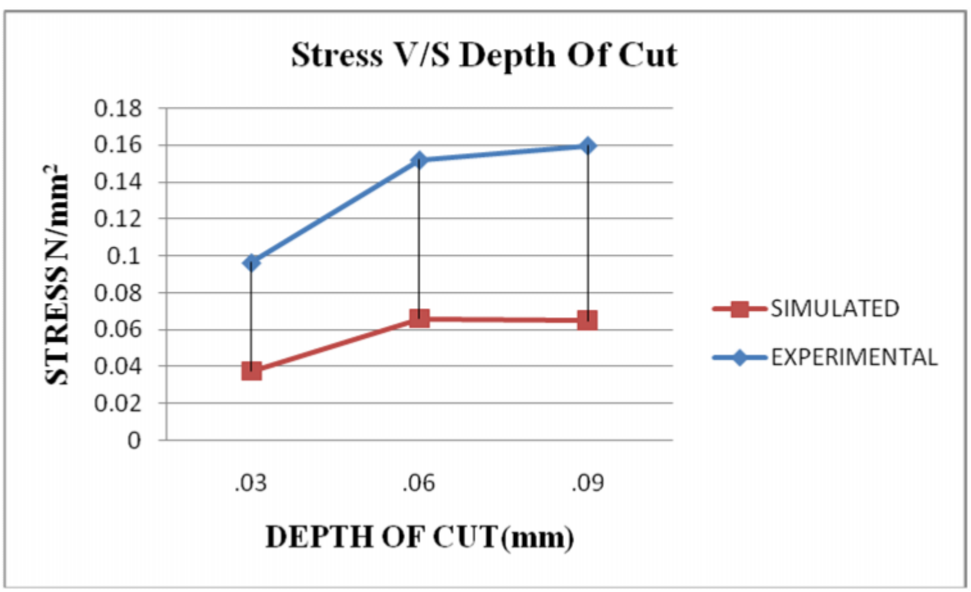

Figure 6.20 Variation of stresses with depth of cut at 0.1mm/rev

- **High Chromium Steel**
- **Speed 4500 rpm**

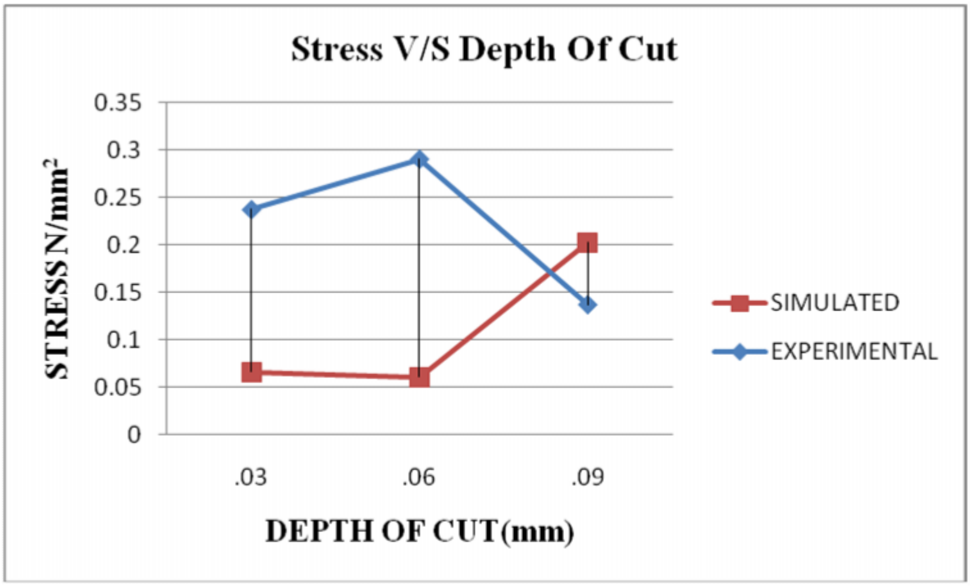

Figure 6.21 Variation of stresses with depth of cut at 0.0667mm/rev

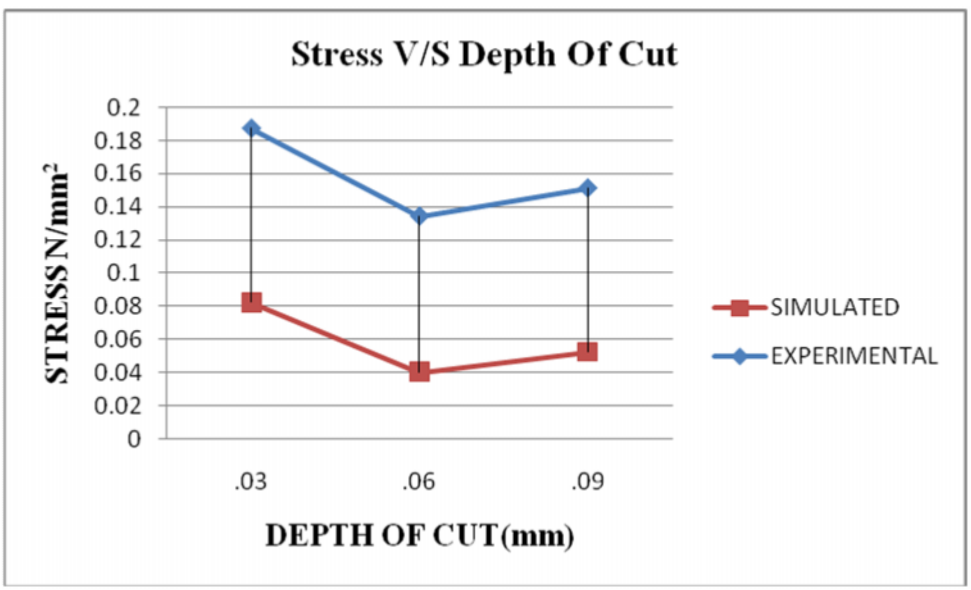

Figure 6.22 Variation of stresses with depth of cut at 0.1mm/rev

- **Stainless Steel**
- **Speed 4500 rpm**

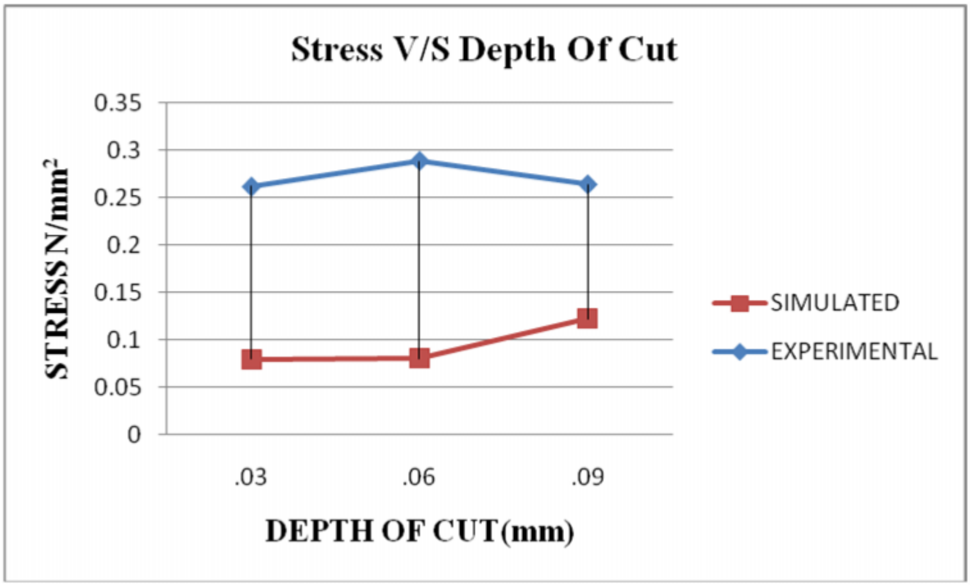

Figure 6.23 Variation of stresses with depth of cut at 0.0667mm/rev

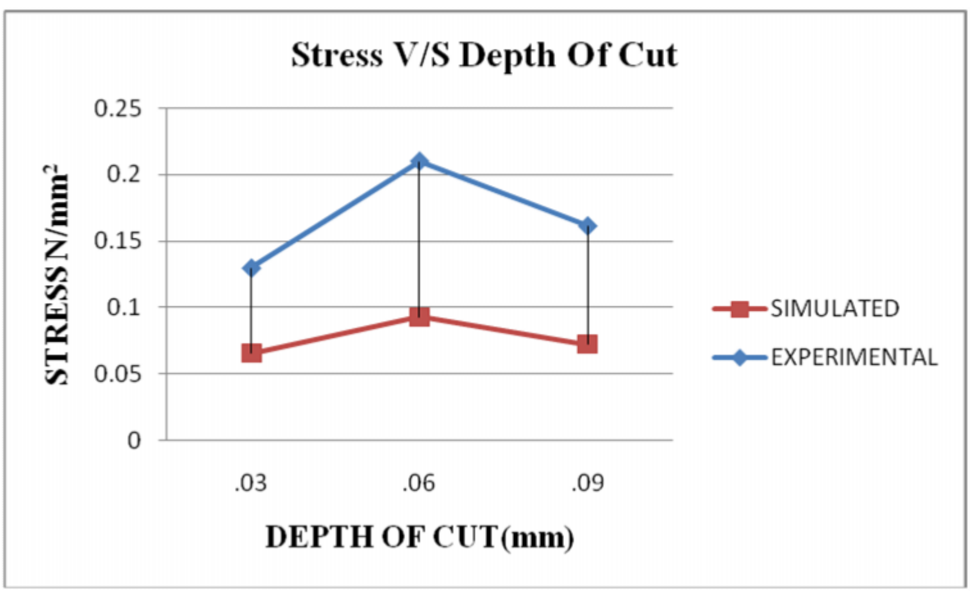

Figure 6.24 Variation of stresses with depth of cut at 0.1mm/rev

6.4 RESULTS AND DISCUSSIONS FOR STRESS VS DEPTH OF CUT FOR DIFFERENT MATERIALS:

1. In figure 6.13 for mild steel one can observe that stresses for simulated graphs are quite less as stresses obtained from experimental observation. Maximum stresses occur at 0.5 N/mm^2 for 0.06 depth of cut.

2. In figure 6.14 for mild steel it is observed that with increase in depth of cut amount of stresses reduces.

3. In figure 6.15 for high chromium steel it is observed that with increase in depth of cut amount of stresses increases till 0.06 depth of cut and then it suddenly it gets a sharp decline afterwards.

4. In figure 6.16 for high chromium steel and for 0.1 mm/rev feed at 6000 rpm with increase in depth of cut amount of stresses reduces.

5. In figure 6.17 for stainless steel one can observe that stresses for simulated graph is considerably less than stresses for experimental graphs.

6. In figure 6.18 for stainless steel it is observed that with increase in depth of cut amount of stresses increases till 0.06 depth of cut and then it suddenly it gets a sharp decline afterwards.

7. In figure 6.19 for mild steel it is observed that with increase in depth of cut amount of stresses increases till 0.06 depth of cut and then it suddenly it gets a sharp decline afterwards.

8. In figure 6.20 for mild steel one can observe that stresses for simulated graphs are quite less as stresses obtained from experimental observation. Maximum stresses occur at 0.4 N/mm^2 for 0.06 depth of cut.

9. In figure 6.21 for high chromium steel (4500 rpm) it is observed that till 0.06 mm feed the behavior of both the curves is similar as in previous figures but after 0.06 till 0.09 mm the stresses for experimental declines and for simulation it inclines.

10. In figure 6.22 for high chromium steel and for 0.1 mm/rev feed till 0.06 depth of cut the experimental as well as simulated data show same declining behavior and after it both of rises.

11. In figure 6.23 for stainless steel one can observe that stresses for simulated graphs is less than stresses obtained from experimental observation at 0.06mm depth of cut.

12. In figure 6.24 for stainless steel it is observed that with rise in depth of cut stresses rises till 0.06 then it reduces for both simulated as well as experimental results.

6.5 GRAPHS FOR FORCE VS TIME AND TEMPERATURE V/S TIME OF DIFFERENT MATERIALS

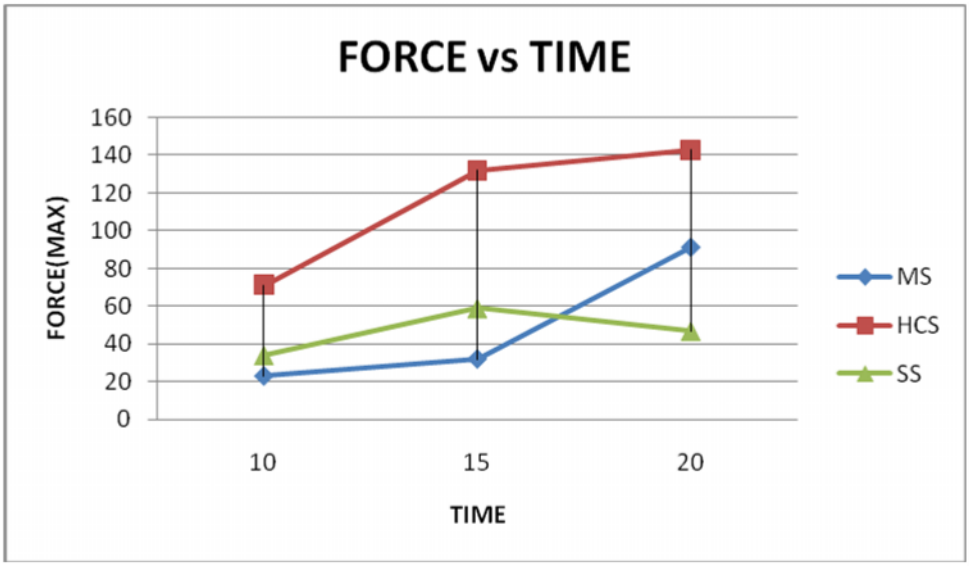

Fig 6.25 Graphical Represantaion of Force (Newton) Vs Time (Seconds), at constant speed 6000 rpm, feed 0.0667mm/rev and depth of cut 0.03mm

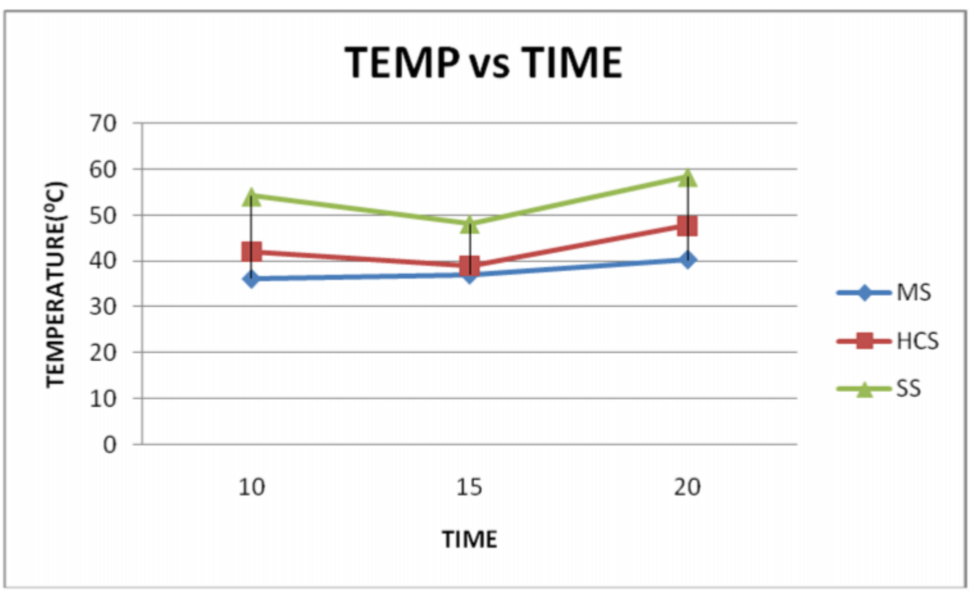

Fig 6.26 Graphical Represantaion of Temprature (ºC) Vs Time (Seconds), at constant speed 6000 rpm, feed 0.0667mm/rev and depth of cut 0.03mm

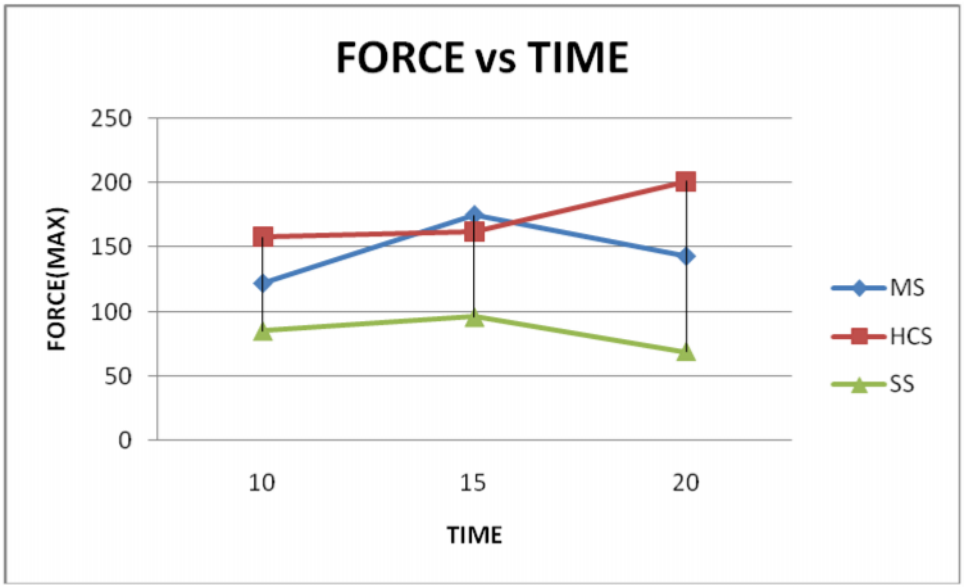

Fig 6.27 Graphical Represantaion of Force (Newton) Vs Time (Seconds), at constant speed 6000 rpm, feed 0.0667mm/rev and depth of cut 0.06mm

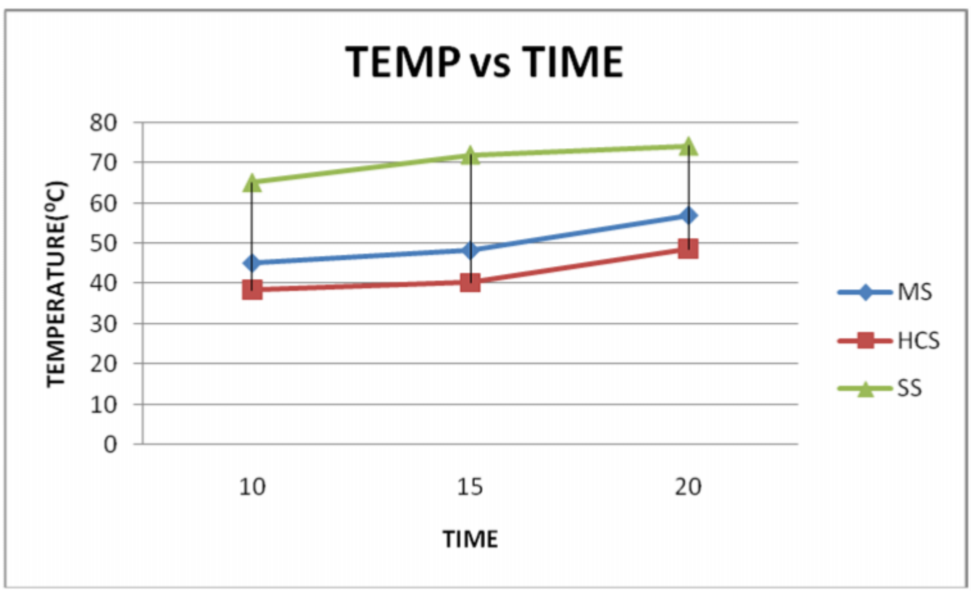

Fig 6.28 Graphical Represantaion of Temprature (ºC) Vs Time (Seconds), at constant speed 6000 rpm, feed 0.0667mm/rev and depth of cut 0.06mm

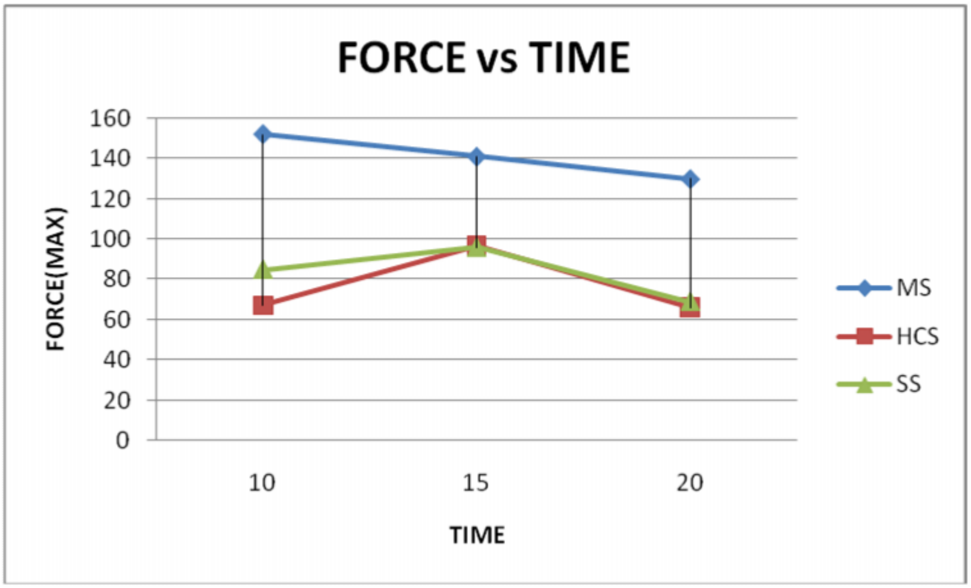

Fig 6.29 Graphical Represantaion of Force (Newton) Vs Time (Seconds), at constant speed 6000 rpm, feed 0.0667mm/rev and depth of cut 0.09mm

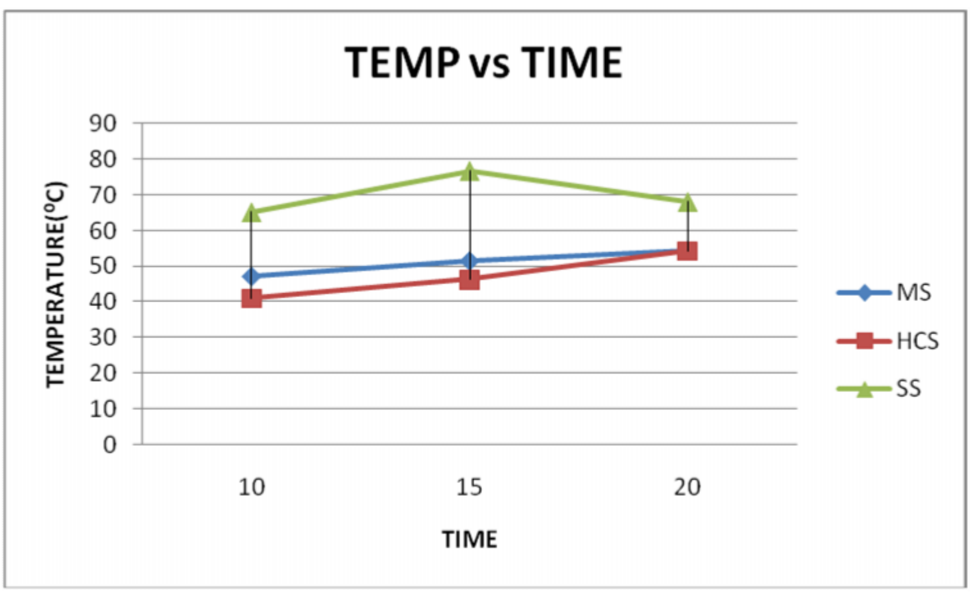

Fig 6.30 Graphical Represantaion of Temprature (ºC) Vs Time (Seconds), at constant speed 6000 rpm, feed 0.0667mm/rev and depth of cut 0.09mm

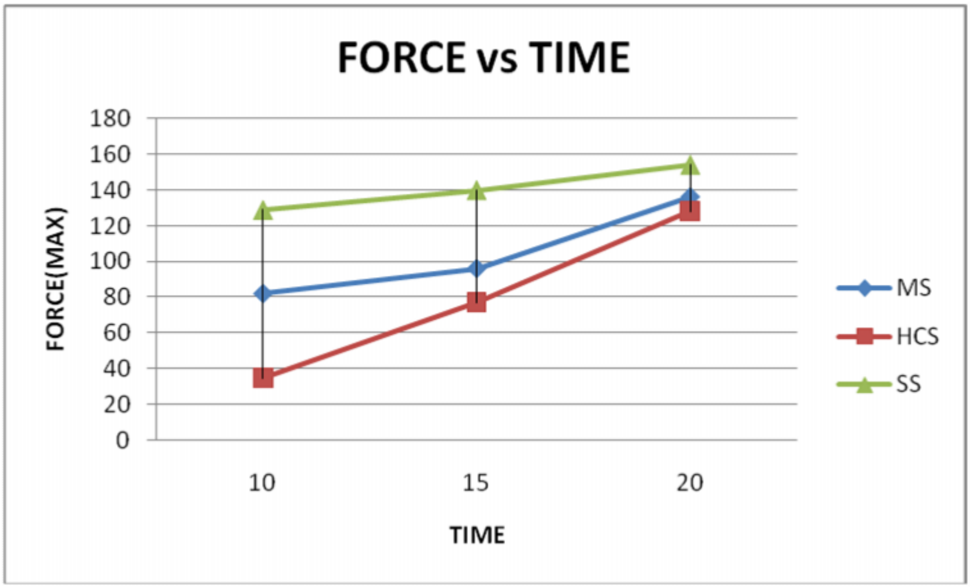

Fig 6.31 Graphical Represantaion of Force (Newton) Vs Time (Seconds), at constant speed 6000 rpm, feed 0.0833mm/rev and depth of cut 0.03mm

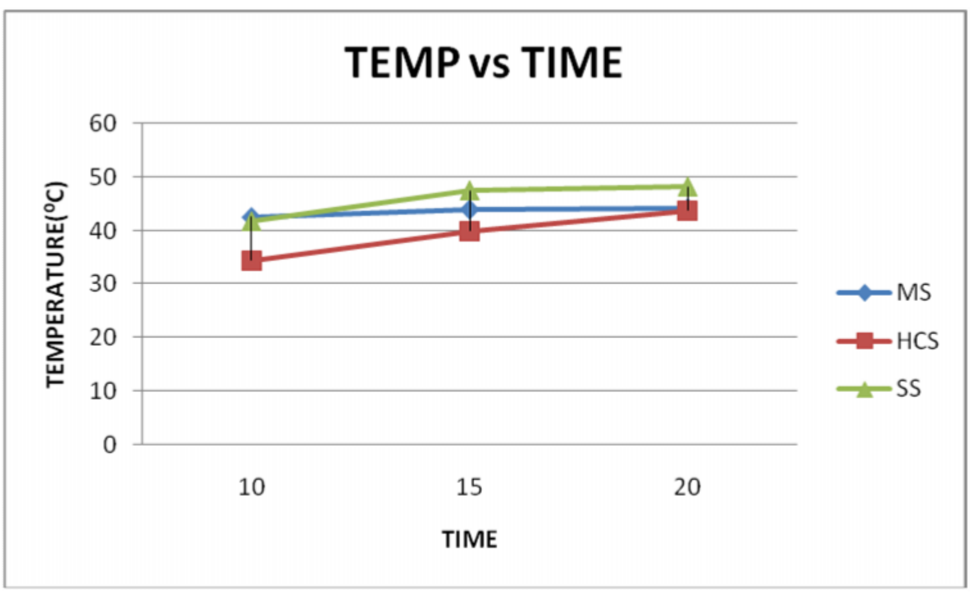

Fig 6.32 Graphical Represantaion of Temprature (ºC) Vs Time (Seconds), at constant speed 6000 rpm, feed 0.0833mm/rev and depth of cut 0.03mm

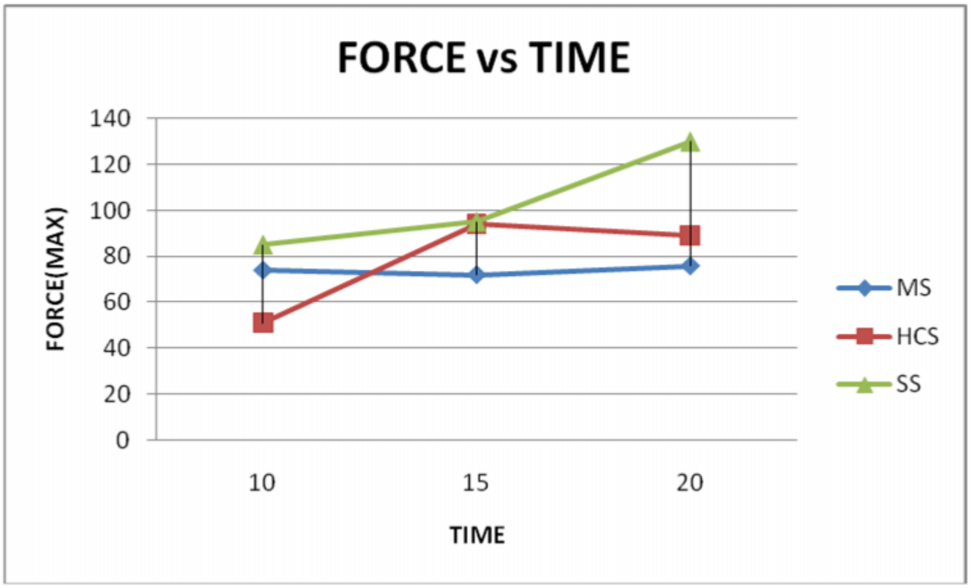

Fig 6.33 Graphical Represantaion of Force (Newton) Vs Time (Seconds), at constant speed 6000 rpm, feed 0.833mm/rev and depth of cut 0.06mm

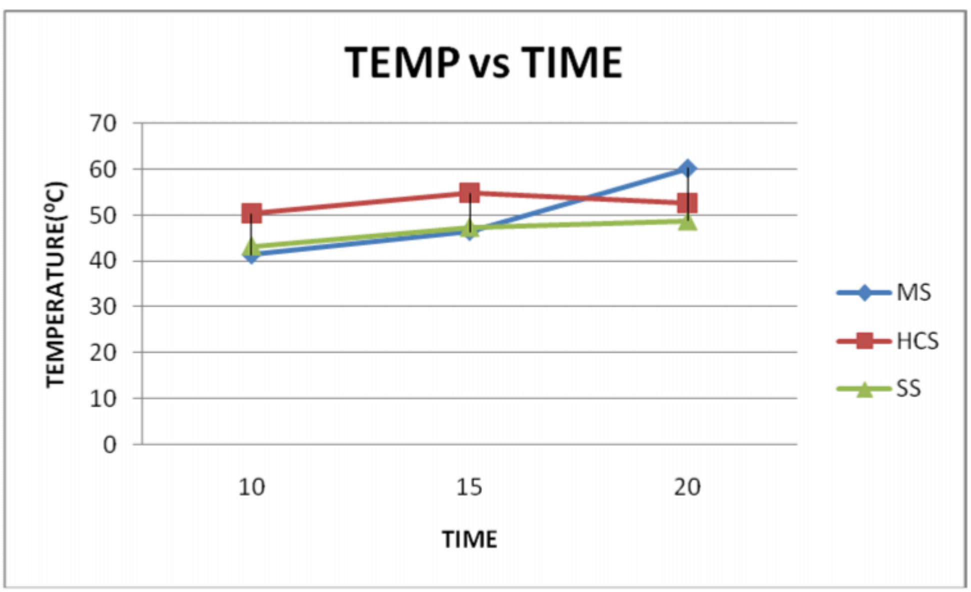

Fig 6.34 Graphical Represantaion of Temprature (ºC) Vs Time (Seconds), at constant speed 6000 rpm, feed 0.0833mm/rev and depth of cut 0.06mm

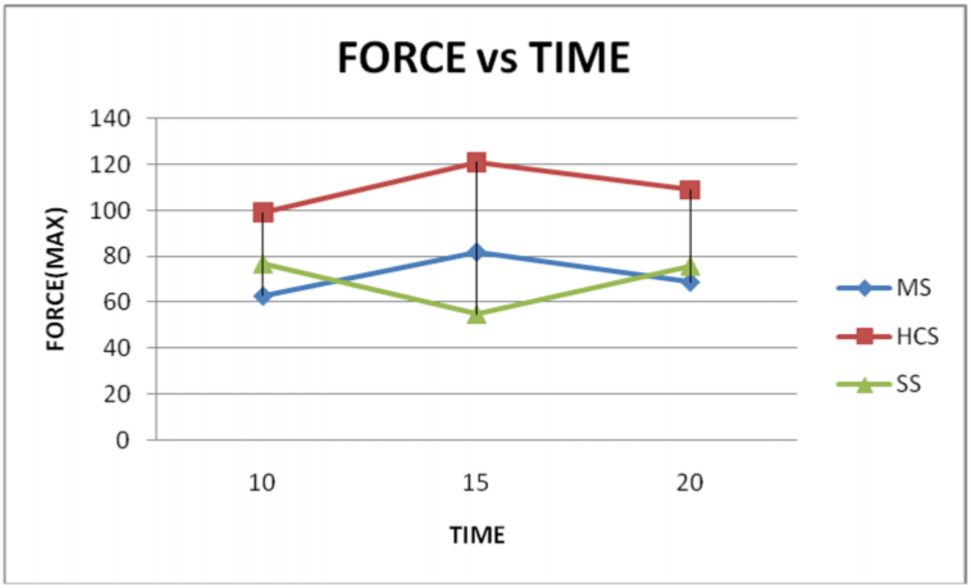

Fig 6.35 Graphical Represantaion of Force (Newton) Vs Time (Seconds), at constant speed 6000 rpm, feed 0.0833mm/rev and depth of cut 0.09mm

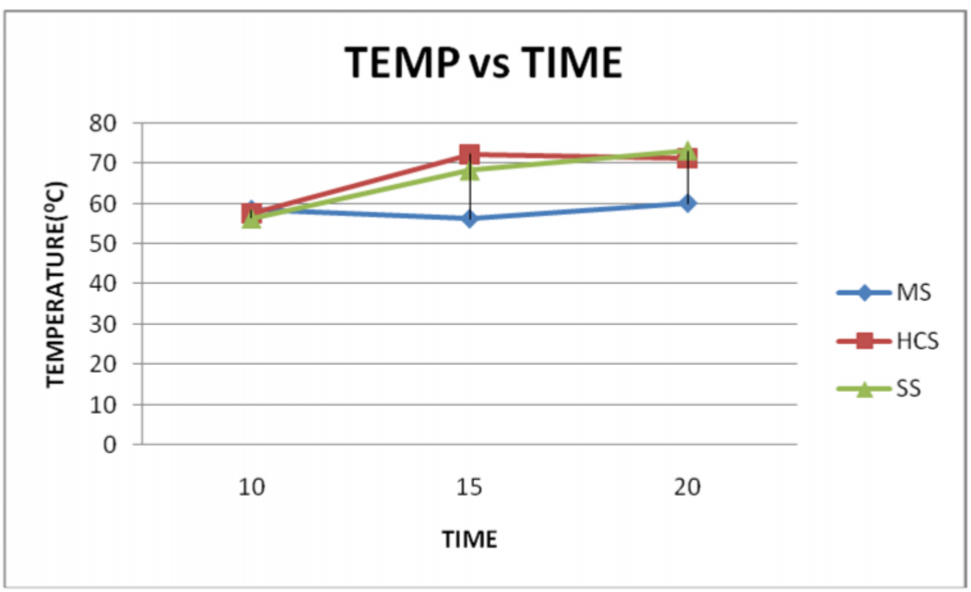

Fig 6.36 Graphical Represantaion of Temprature (ºC) Vs Time (Seconds), at constant speed 6000 rpm, feed 0.0833mm/rev and depth of cut 0.09mm

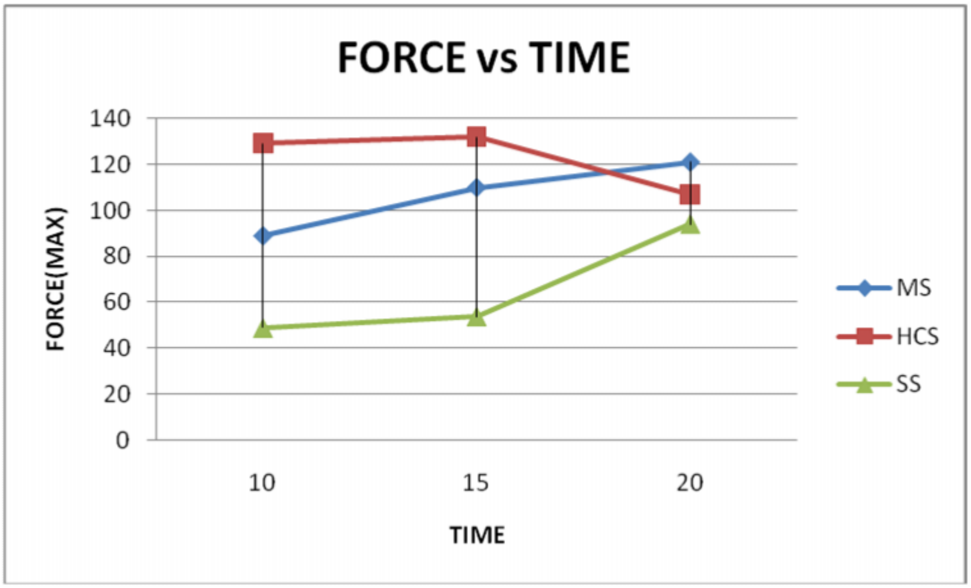

Fig 6.37 Graphical Represantaion of Force (Newton) Vs Time (Seconds), at constant speed 6000 rpm, feed 0.1mm/rev and depth of cut 0.03mm

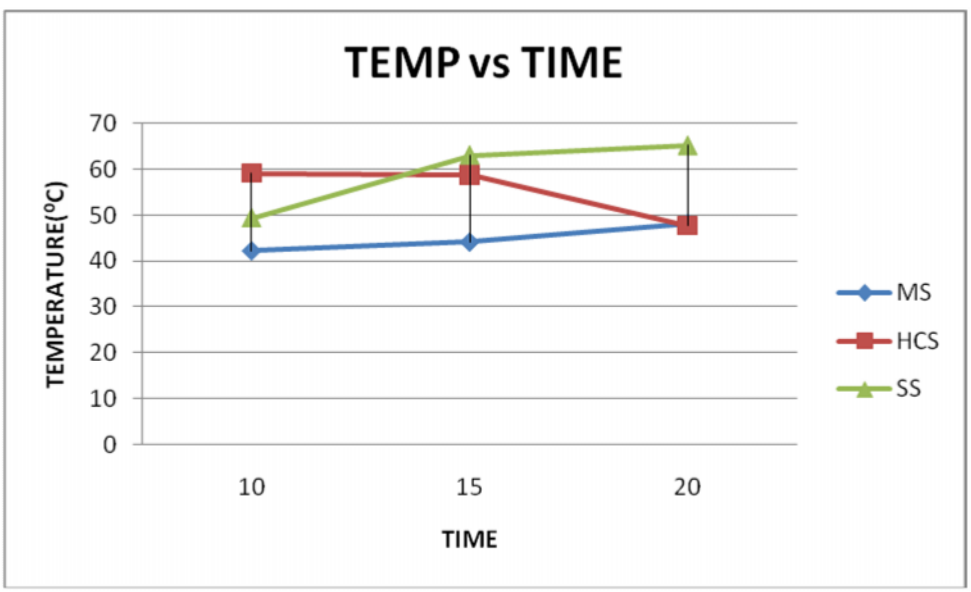

Fig 6.38 Graphical Represantaion of Temprature (ºC) Vs Time (Seconds), at constant speed 6000 rpm, feed 0.1mm/rev and depth of cut 0.03mm

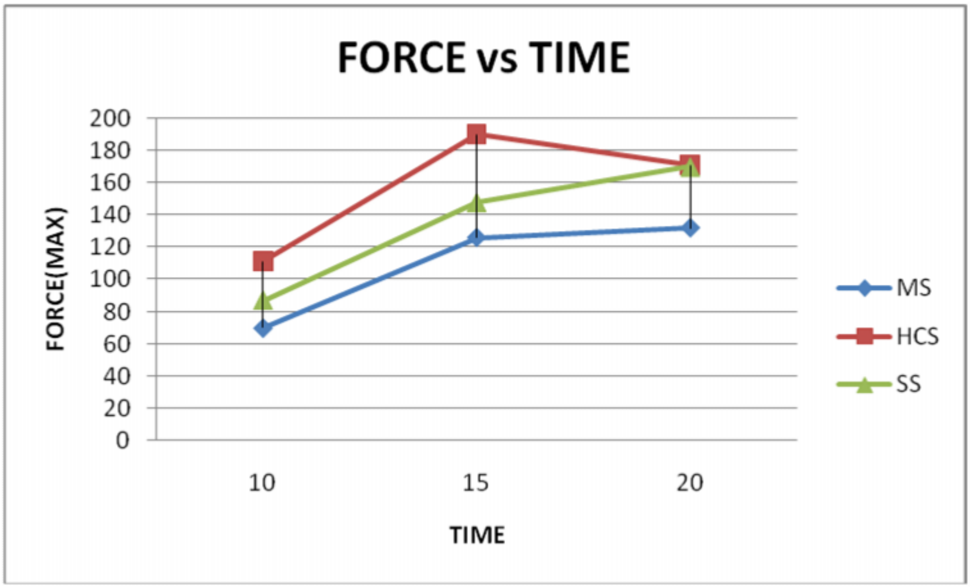

Fig 6.39 Graphical Represantaion of Force (Newton) Vs Time (Seconds), at constant speed 6000 rpm, feed 0.1mm/rev and depth of cut 0.06mm

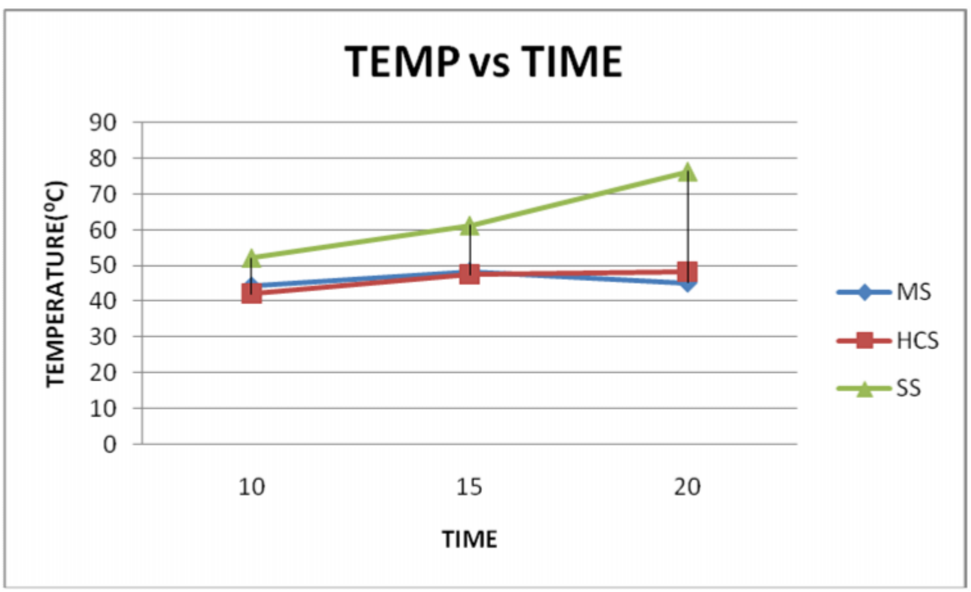

Fig 6.40 Graphical Represantaion of Temprature (ºC) Vs Time (Seconds), at constant speed 6000 rpm, feed 0.1mm/rev and depth of cut 0.06mm

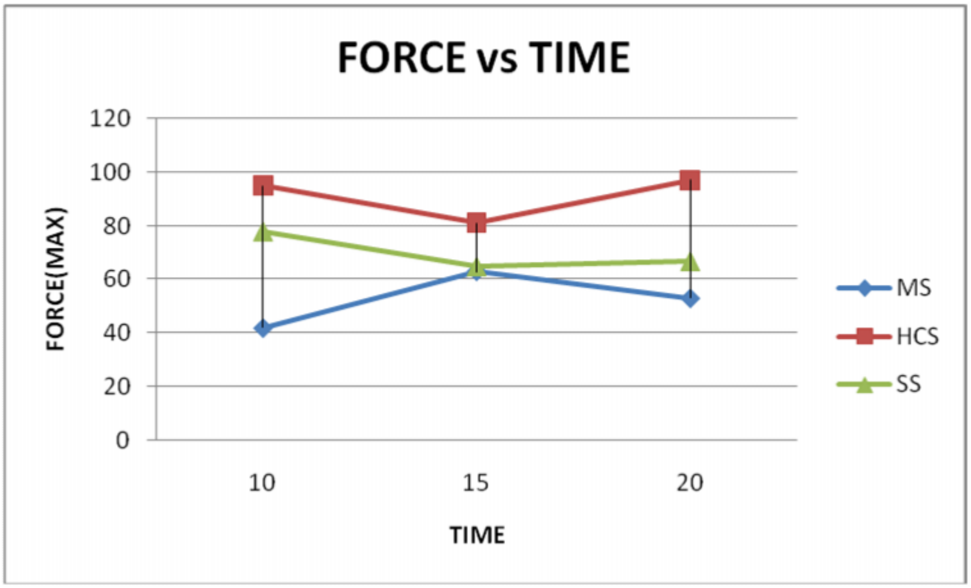

Fig 6.41 Graphical Represantaion of Force (Newton) Vs Time (Seconds), at constant speed 6000 rpm, feed 0.1mm/rev and depth of cut 0.09mm

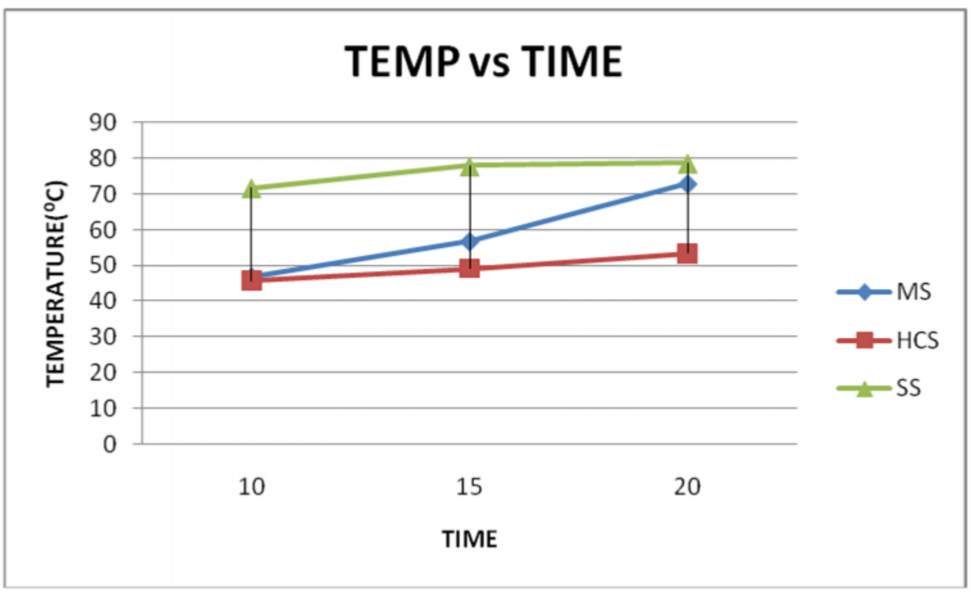

Fig 6.42 Graphical Represantaion of Temprature (ºC) Vs Time (Seconds), at constant speed 6000 rpm, feed 0.1mm/rev and depth of cut 0.09mm

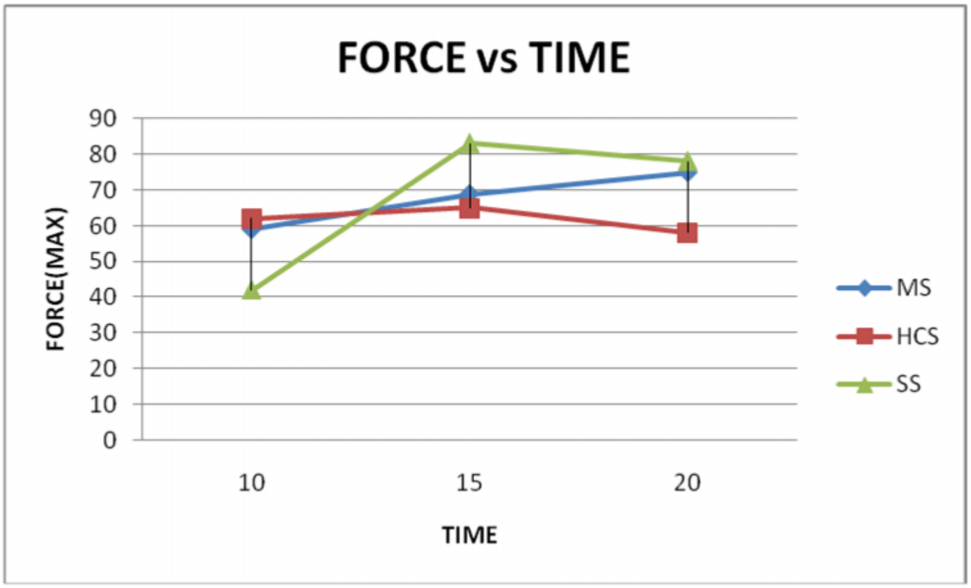

Fig 6.43 Graphical Represantaion of Force (Newton) Vs Time (Seconds), at constant speed 4500 rpm, feed 0.0667mm/rev and depth of cut 0.03mm

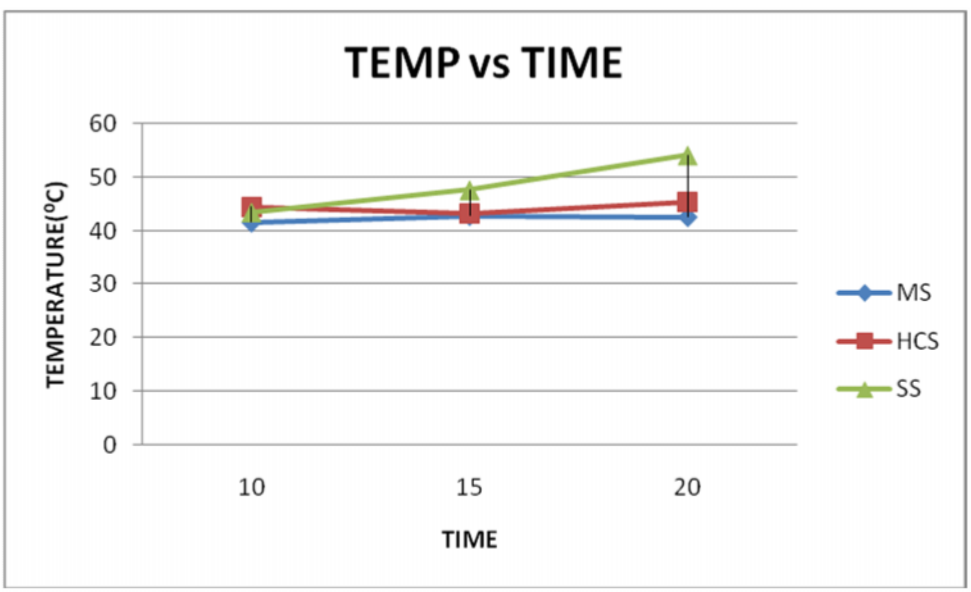

Fig 6.44 Graphical Represantaion of Temprature (°C) Vs Time (Seconds), at constant speed 4500 rpm, feed 0.0667mm/rev and depth of cut 0.03mm

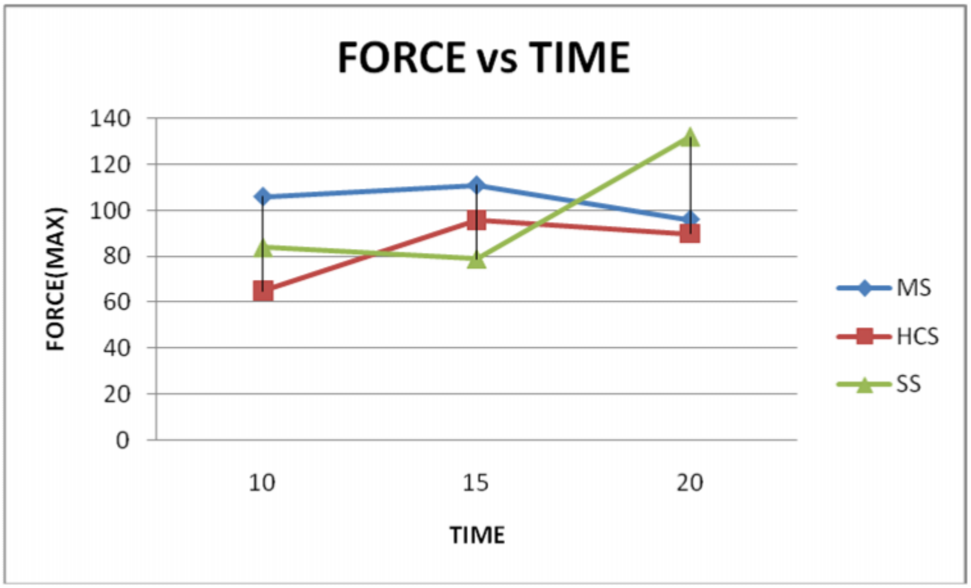

Fig 6.45 Graphical Represantaion of Force (Newton) Vs Time (Seconds), at constant speed 4500 rpm, feed 0.0667mm/rev and depth of cut 0.06mm

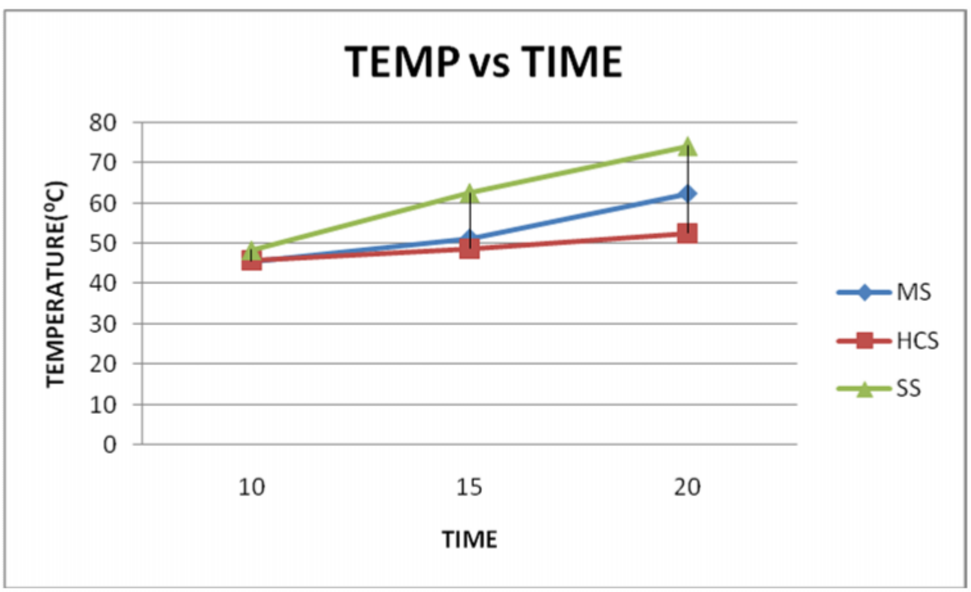

Fig 6.46 Graphical Represantaion of Temprature (ºC) Vs Time (Seconds), at constant speed 4500 rpm, feed 0.0667mm/rev and depth of cut 0.06mm

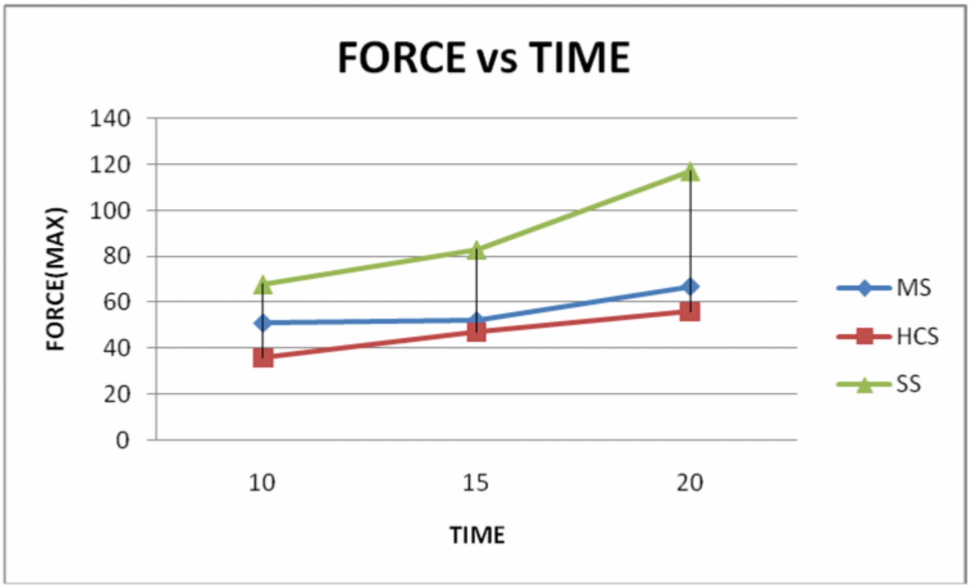

Fig 6.47 Graphical Represantaion of Force (Newton) Vs Time (Seconds), at constant speed 4500 rpm, feed 0.0667mm/rev and depth of cut 0.09mm

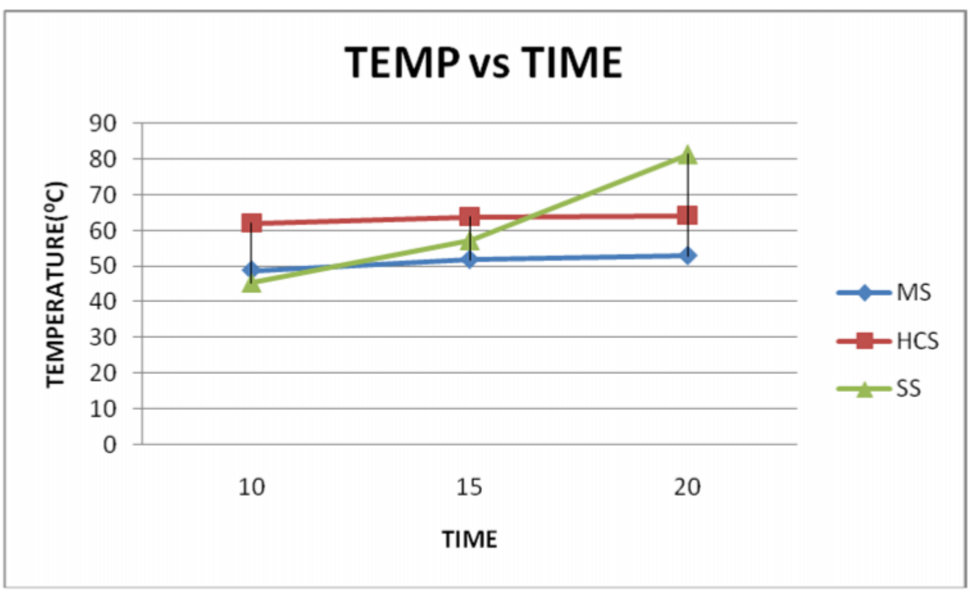

Fig 6.48 Graphical Represantaion of Temprature (ºC) Vs Time (Seconds), at constant speed 4500 rpm, feed 0.0667mm/rev and depth of cut 0.09mm

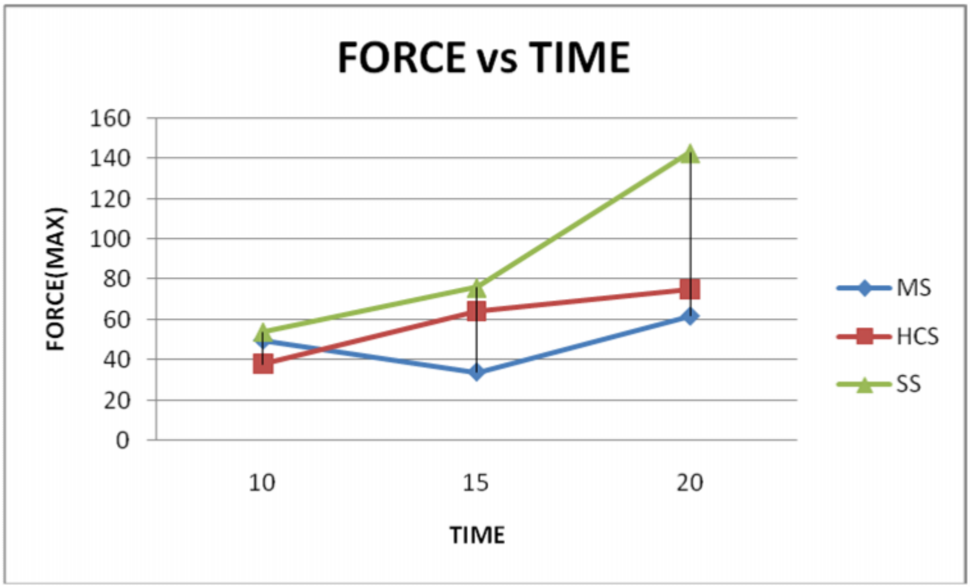

Fig 6.49 Graphical Represantaion of Force (Newton) Vs Time (Seconds), at constant speed 4500 rpm, feed 0.0833mm/rev and depth of cut 0.03mm

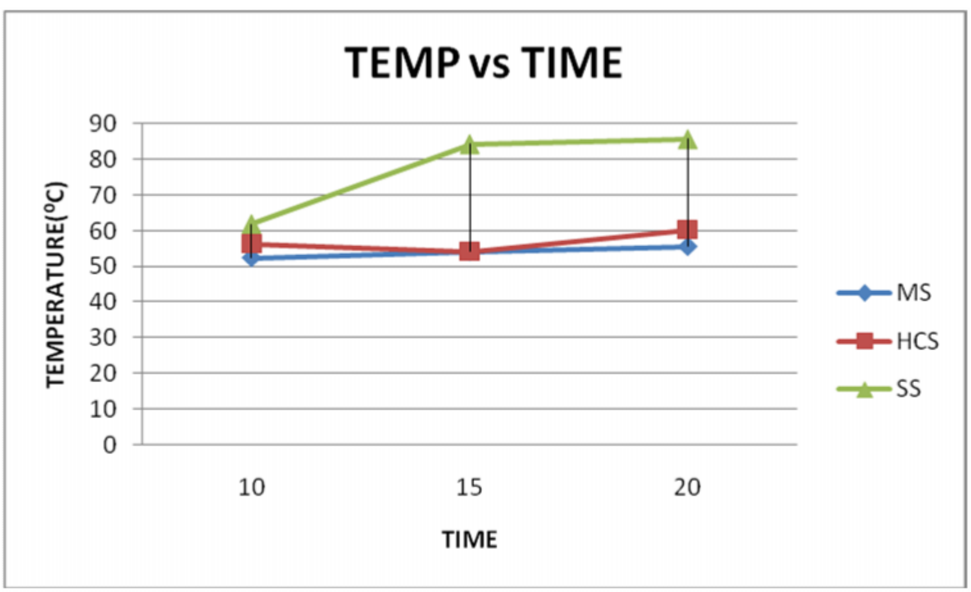

Fig 6.50 Graphical Represantaion of Temprature (ºC) Vs Time (Seconds), at constant speed 4500 rpm, feed 0.0833mm/rev and depth of cut 0.03mm

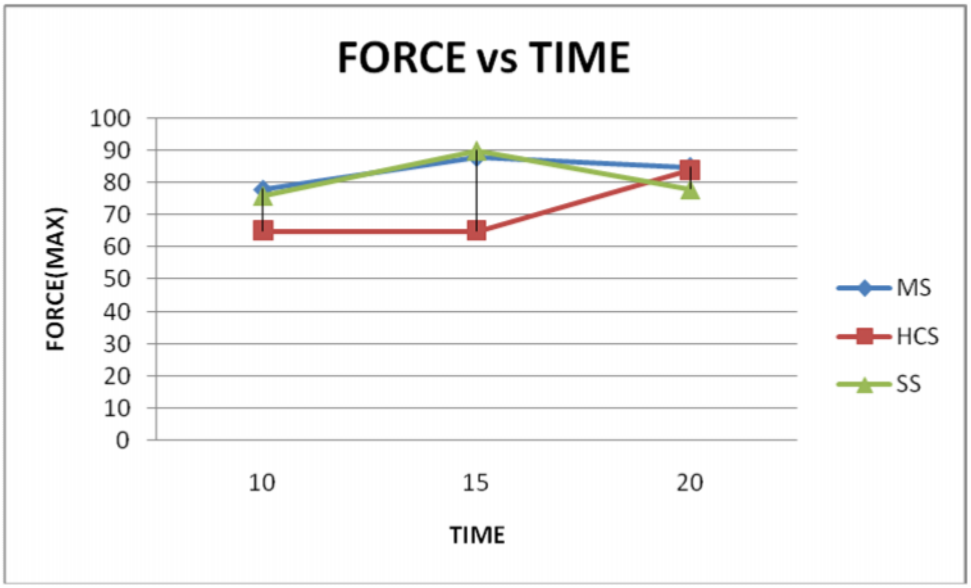

Fig 6.51 Graphical Represantaion of Force (Newton) Vs Time (Seconds), at constant speed 4500 rpm, feed 0.0833mm/rev and depth of cut 0.06mm

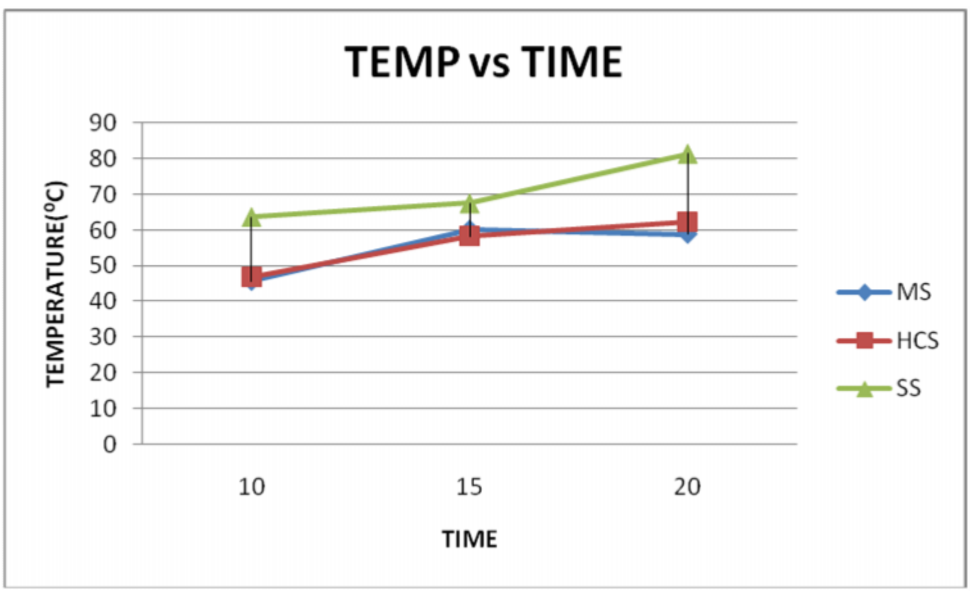

Fig 6.52 Graphical Represantaion of Temprature (ºC) Vs Time (Seconds), at constant speed 4500 rpm, feed 0.0833mm/rev and depth of cut 0.06mm

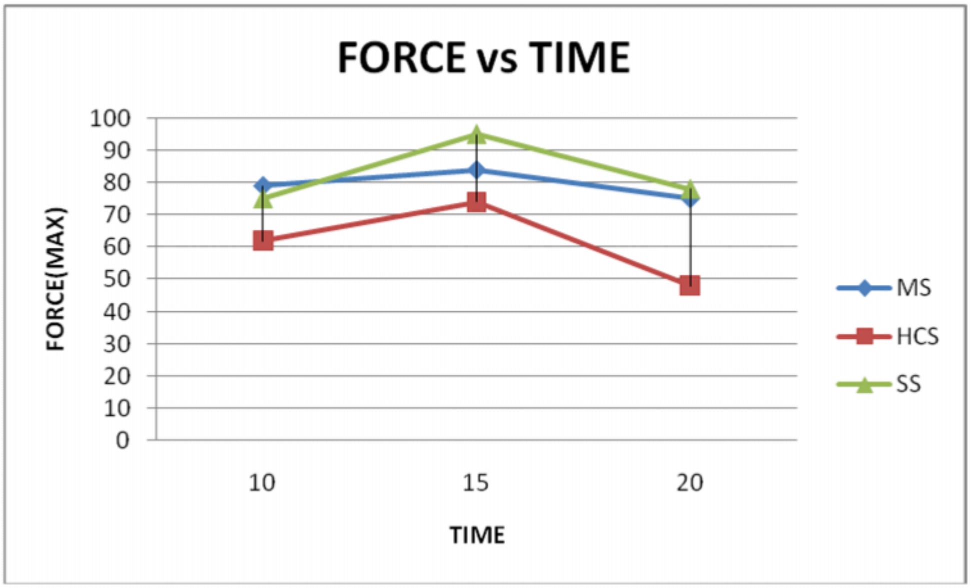

Fig 6.53 Graphical Represantaion of Force (Newton) Vs Time (Seconds), at constant speed 4500 rpm, feed 0.0833mm/rev and depth of cut 0.09mm

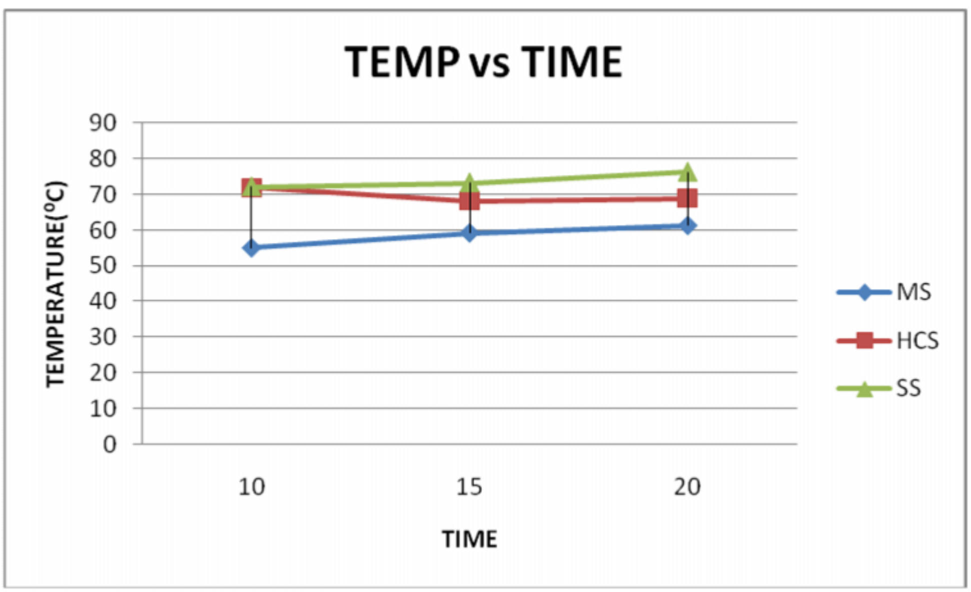

Fig 6.54 Graphical Represantaion of Temprature (ºC) Vs Time (Seconds), at constant speed 4500 rpm, feed 0.0833mm/rev and depth of cut 0.09mm

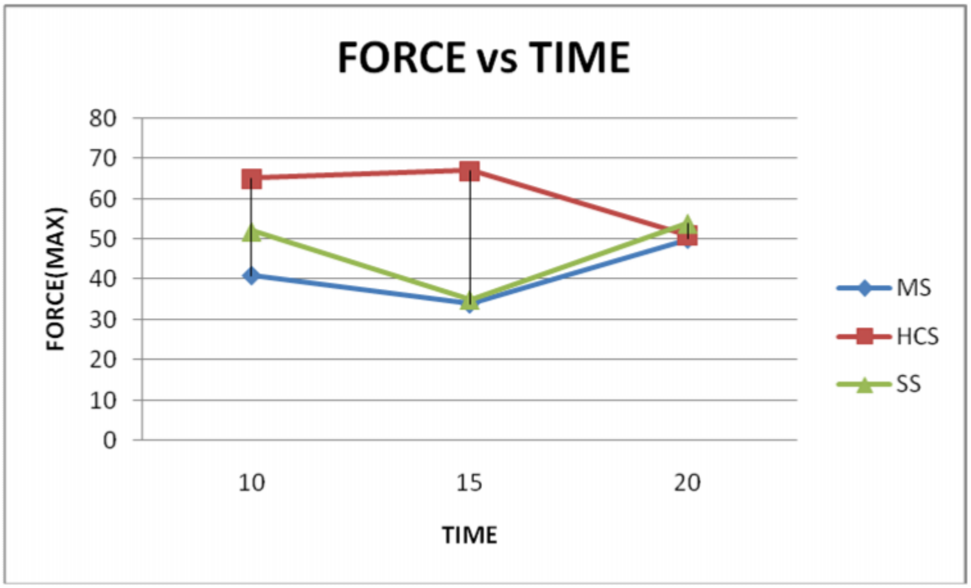

Fig 6.55 Graphical Represantaion of Force (Newton) Vs Time (Seconds), at constant speed 4500 rpm, feed 0.1mm/rev and depth of cut 0.03mm

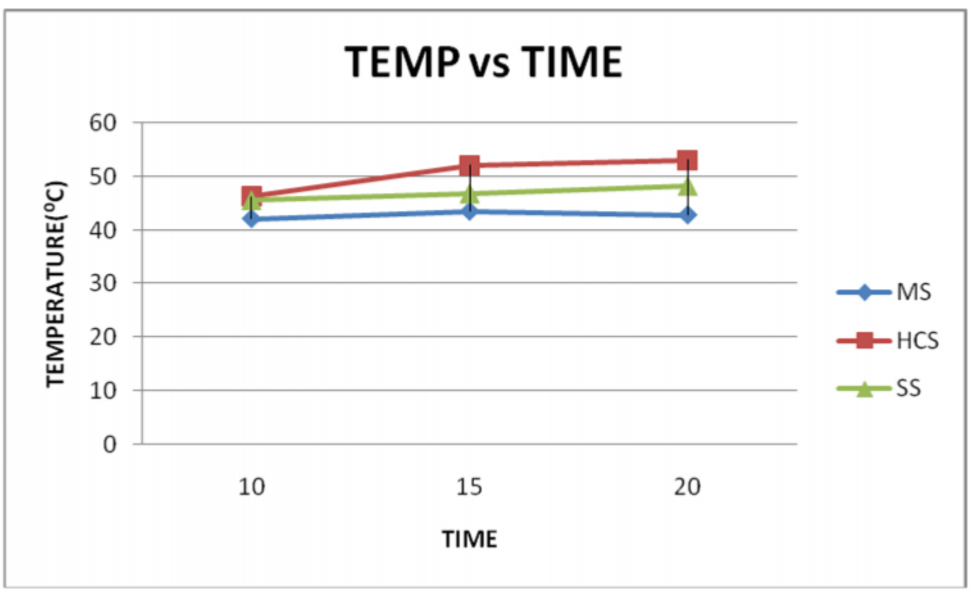

Fig 6.56 Graphical Represantaion of Temprature (ºC) Vs Time (Seconds), at constant speed 4500 rpm, feed 0.1mm/rev and depth of cut 0.03mm

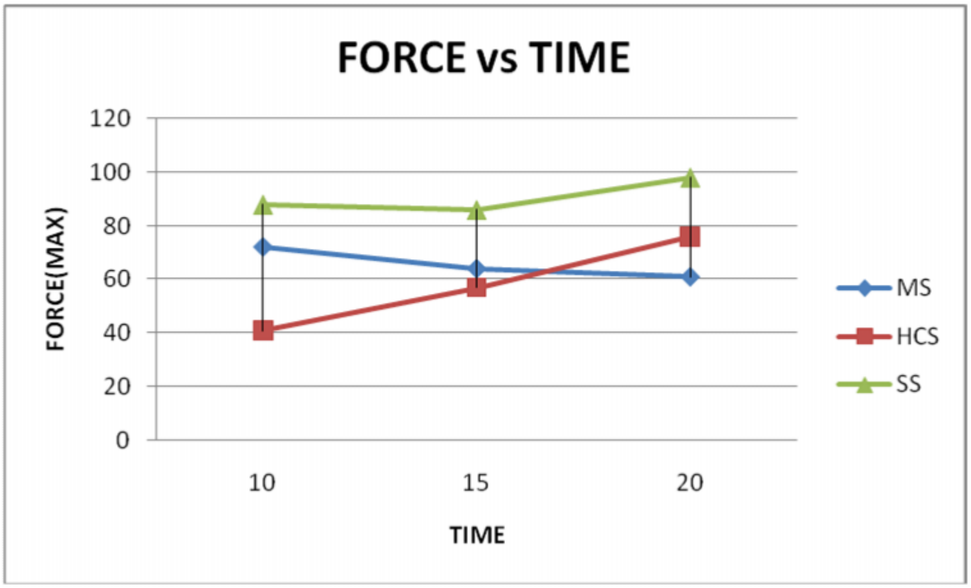

Fig 6.57 Graphical Represantaion of Force (Newton) Vs Time (Seconds), at constant speed 4500 rpm, feed 0.1mm/rev and depth of cut 0.06mm

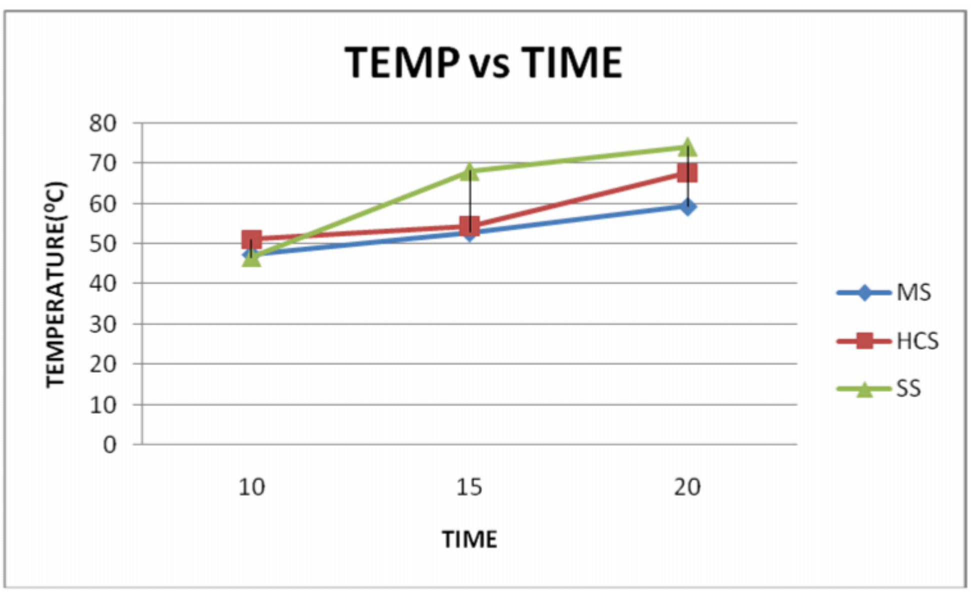

Fig 6.58 Graphical Represantaion of Temprature (ºC) Vs Time (Seconds), at constant speed 4500 rpm, feed 0.1mm/rev and depth of cut 0.06mm

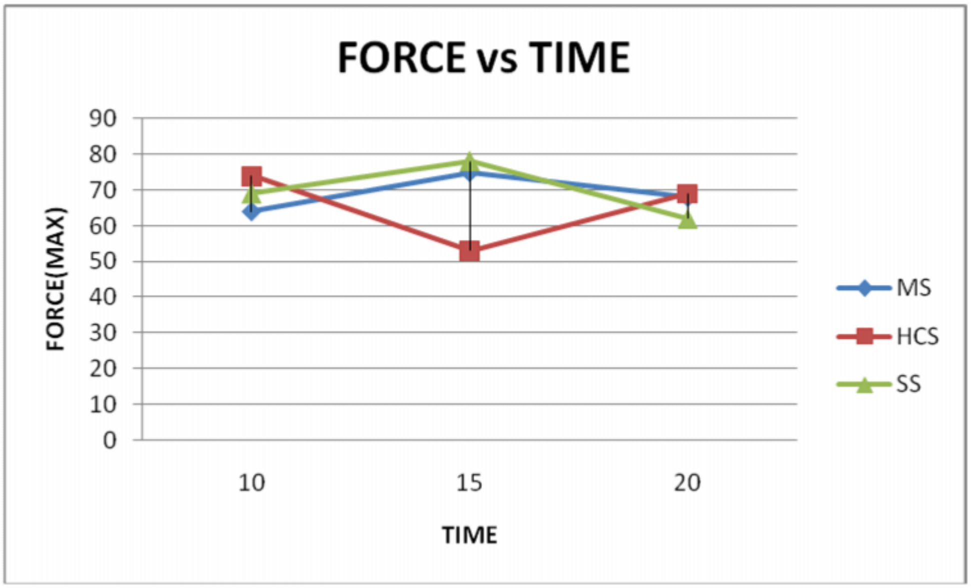

Fig 6.59 Graphical Represantaion of Force (Newton) Vs Time (Seconds), at constant speed 4500 rpm, feed 0.1mm/rev and depth of cut 0.09mm

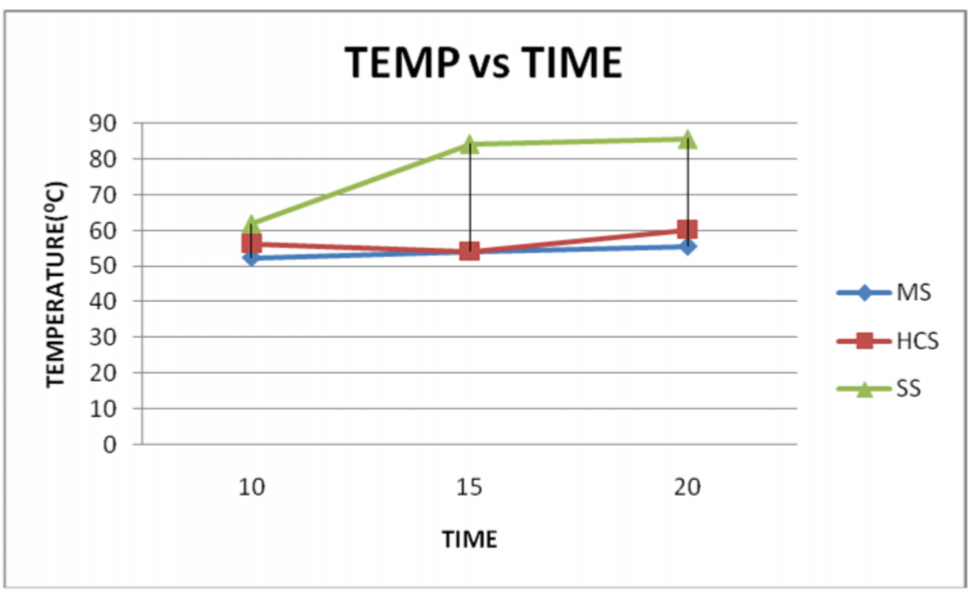

Fig 6.60 Graphical Represantaion of Temprature (ºC) Vs Time (Seconds), at constant speed 4500 rpm, feed 0.1mm/rev and depth of cut 0.09mm

6.6 Results of Temperature distribution on work piece using ANSYS Software

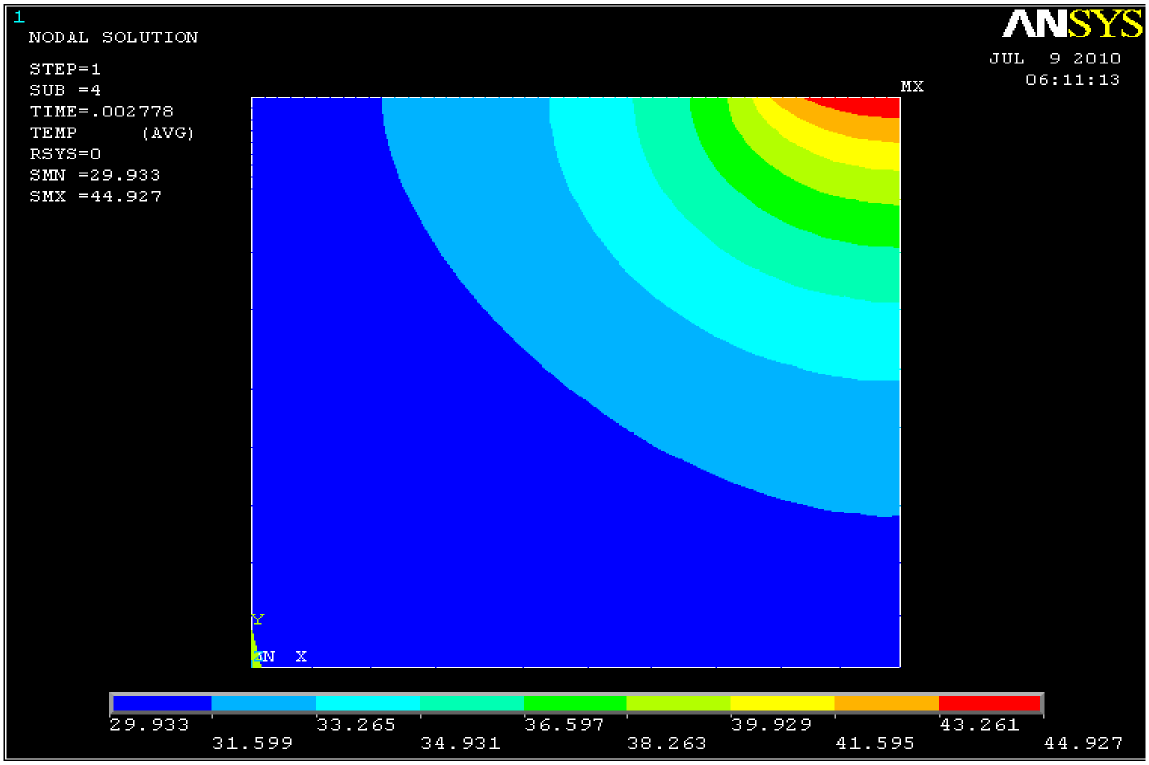

Fig 6.61 For constant speed 4500 rpm, constant feed of 0.0667 mm/rev, Depth of cut 0.03 mm, and for time 10 seconds the temperature using software is 44.9 ºC and with experimentation is 44.5 ºC.

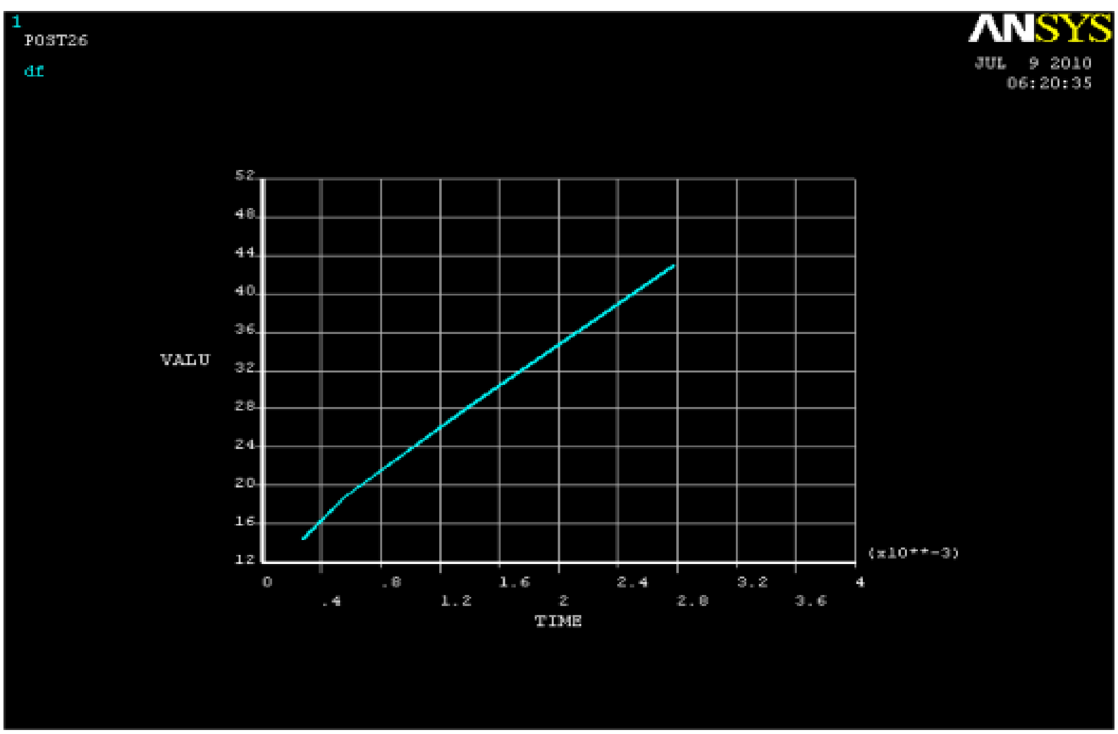

Variation between time and temperature

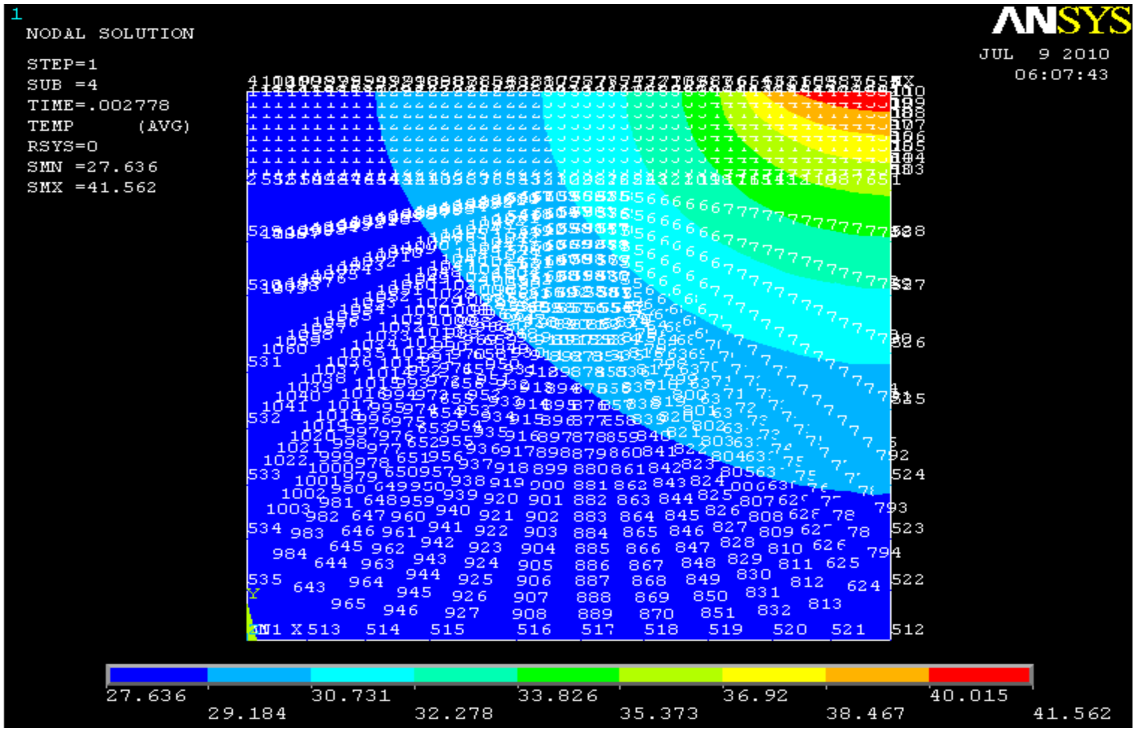

Fig 6.62 For constant speed 4500 rpm, constant feed of 0.0667 mm/rev, Depth of cut 0.03 mm, and for time 10 seconds the temperature using software is 41.5 ºC and with experimentation is 43.4 ºC.

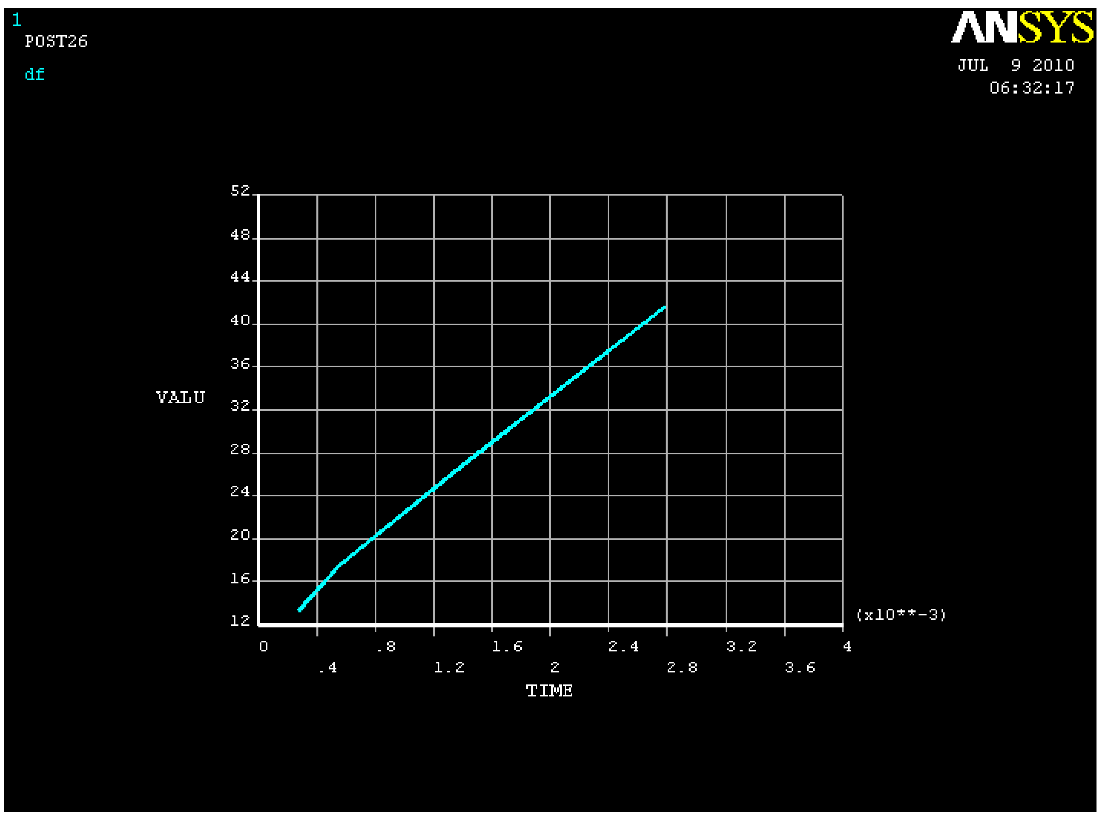

Variation between time and temperature

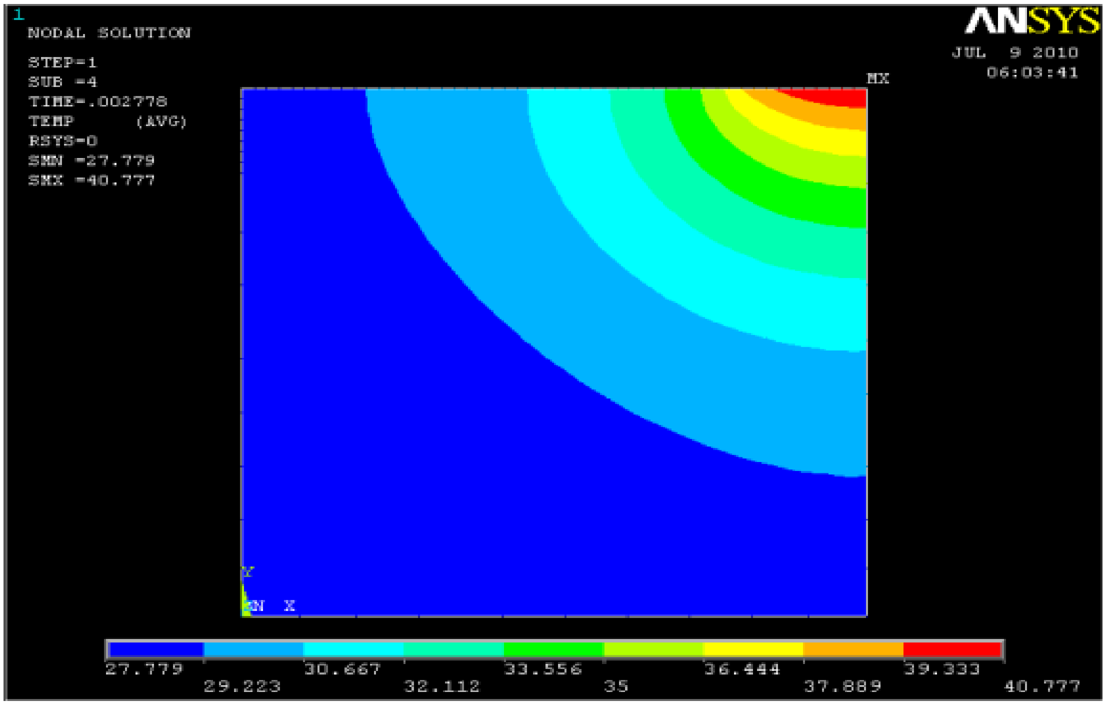

Fig 6.63 For constant speed 4500 rpm, constant feed of 0.0667 mm/rev, Depth of cut 0.03 mm, and for time 10 seconds the temperature using software is 40.7 ºC and with experimentation is 41.6 ºC.

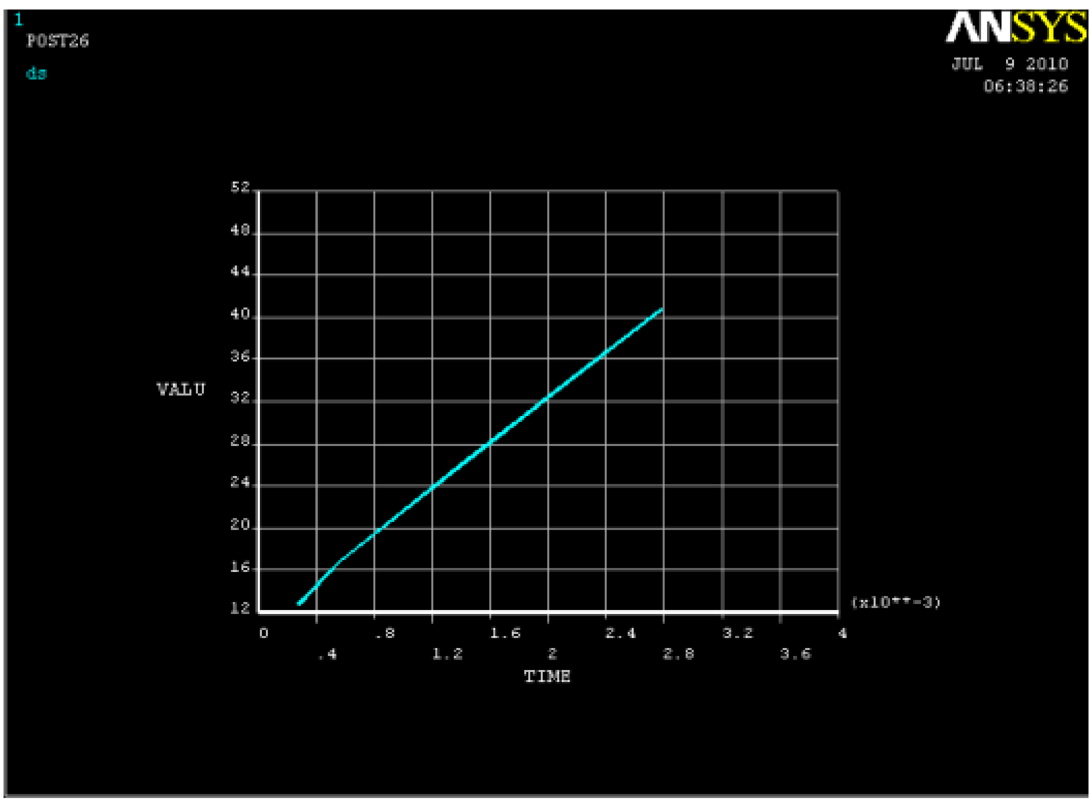

Variation between time and temperature

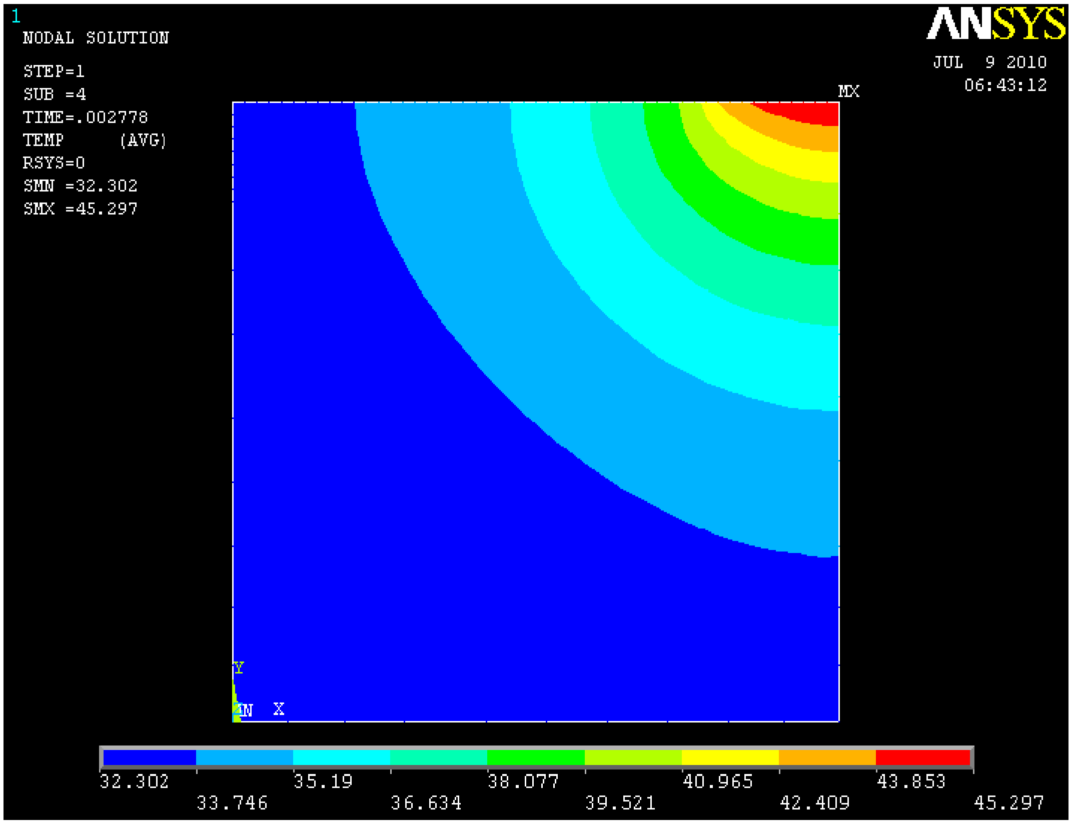

Fig 6.64 For constant speed 4500 rpm, constant feed of 0.0833 mm/rev, Depth of cut 0.03 mm, and for time 10 seconds the temperature using software is 45.2 ºC and with experimentation is 45.4 ºC.

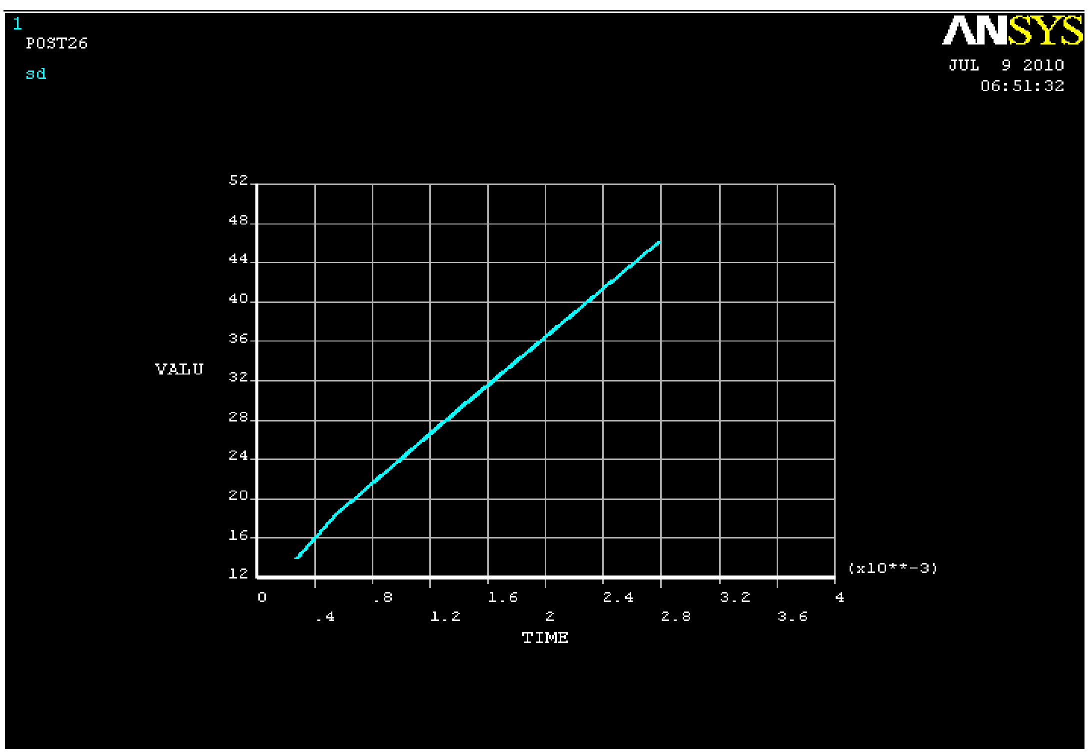

Variation between time and temperature

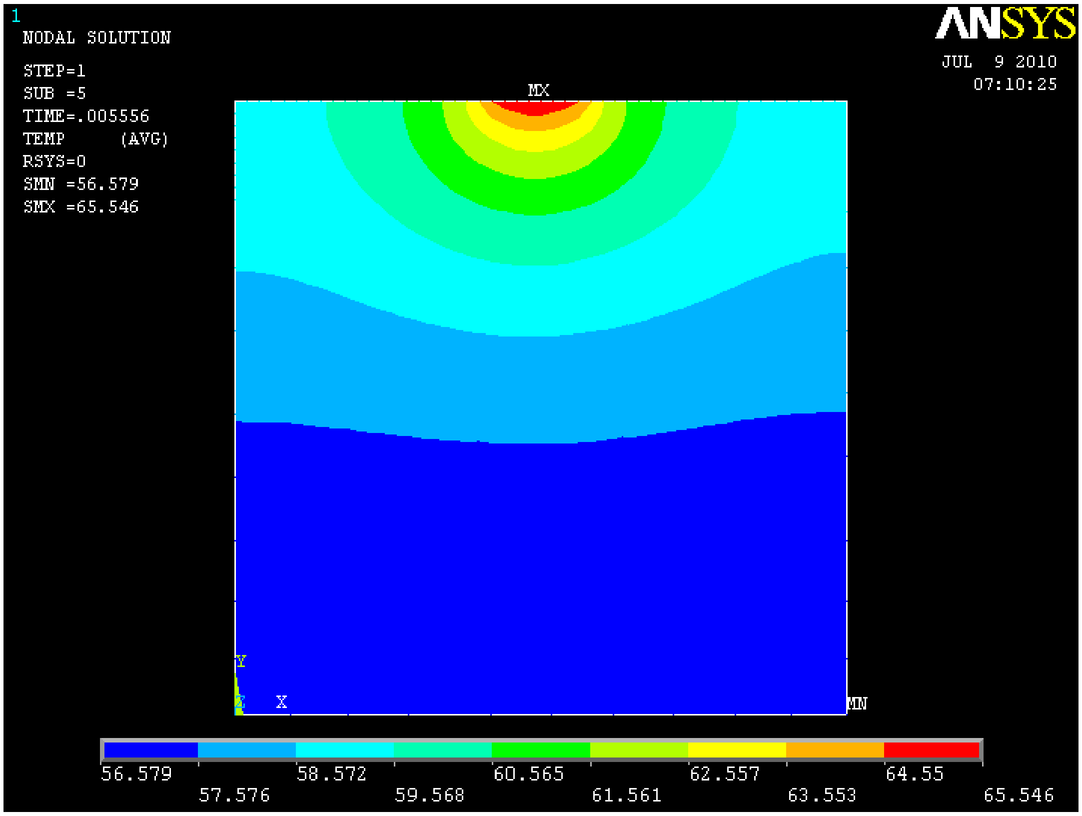

Fig 6.65 For constant speed 6000 rpm, constant feed of 0.0833 mm/rev, Depth of cut 0.09 mm, and for time 20 seconds the temperature using software is 65.5 ºC and with experimentation is 60.1 ºC.

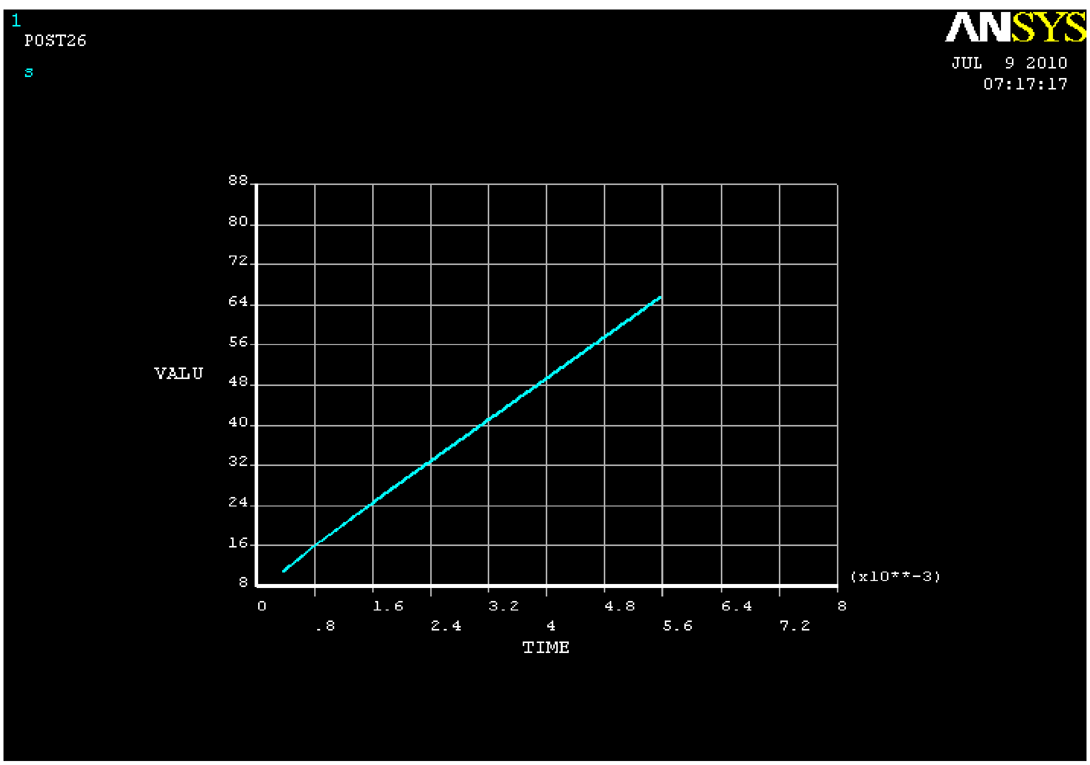

Variation between time and temperature

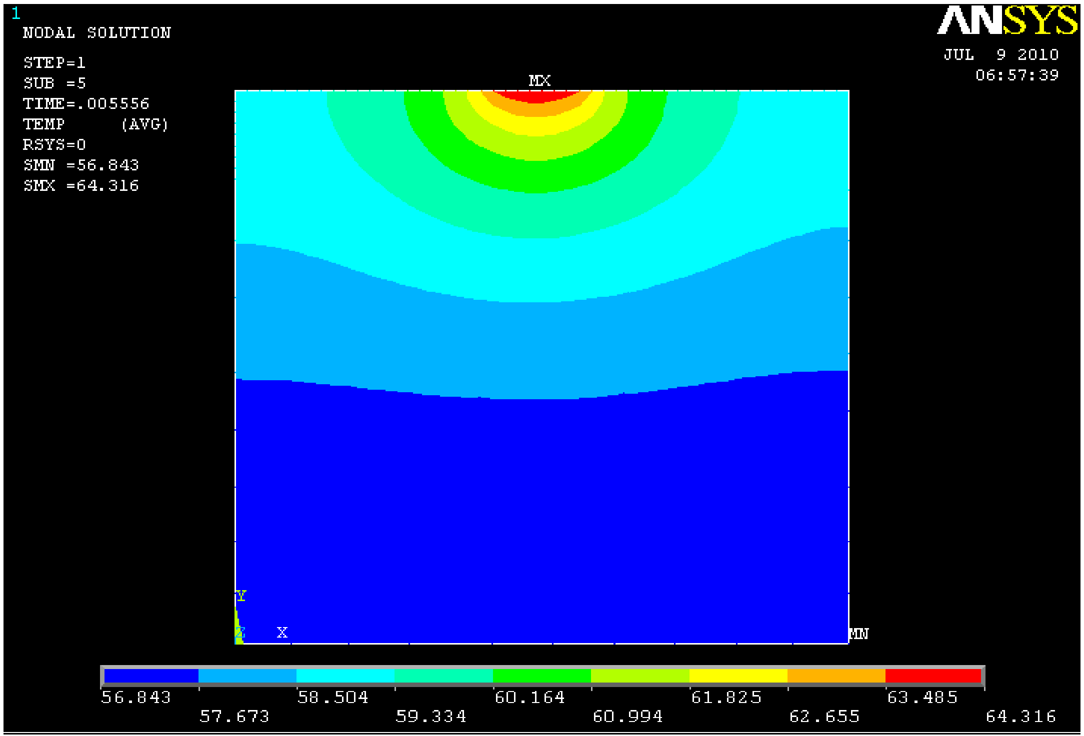

Fig 6.66 For constant speed 6000 rpm, constant feed of 0.0833 mm/rev, Depth of cut 0.09 mm, and for time 15 seconds the temperature using software is 64.3 ºC and with experimentation is 57.5 ºC.

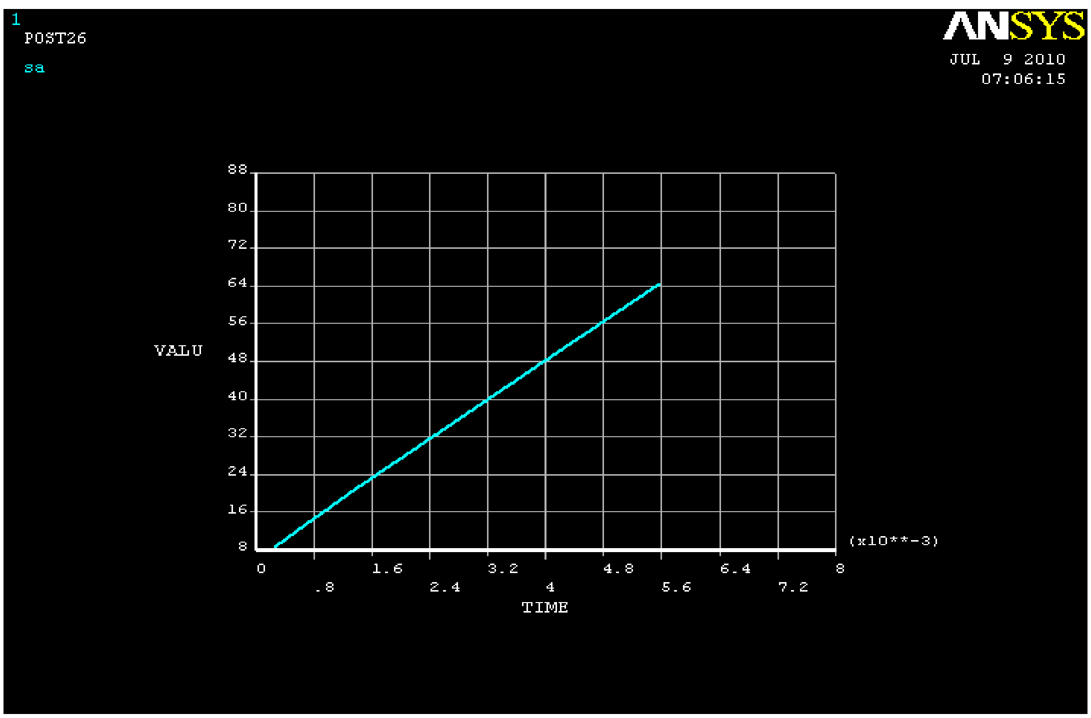

Variation between time and temperature

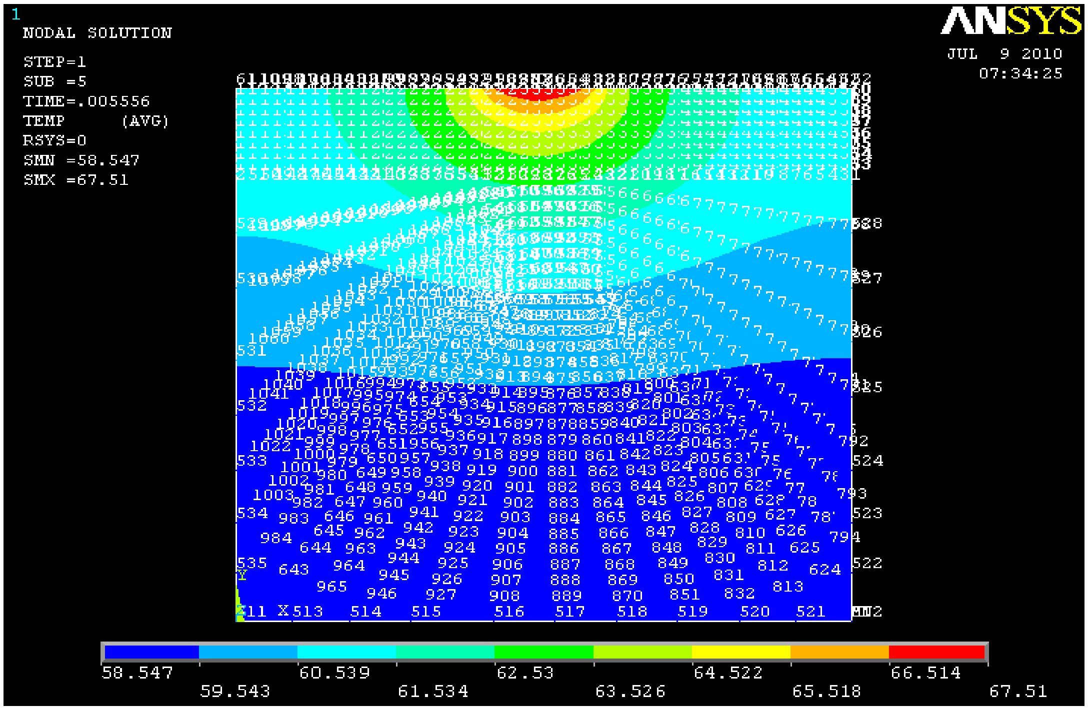

Fig 6.67 For constant speed 4500 rpm, constant feed of 0.0677 mm/rev, Depth of cut 0.09 mm, and for time 20 seconds the temperature using software is 67.5 ºC and with experimentation is 64.2 ºC.

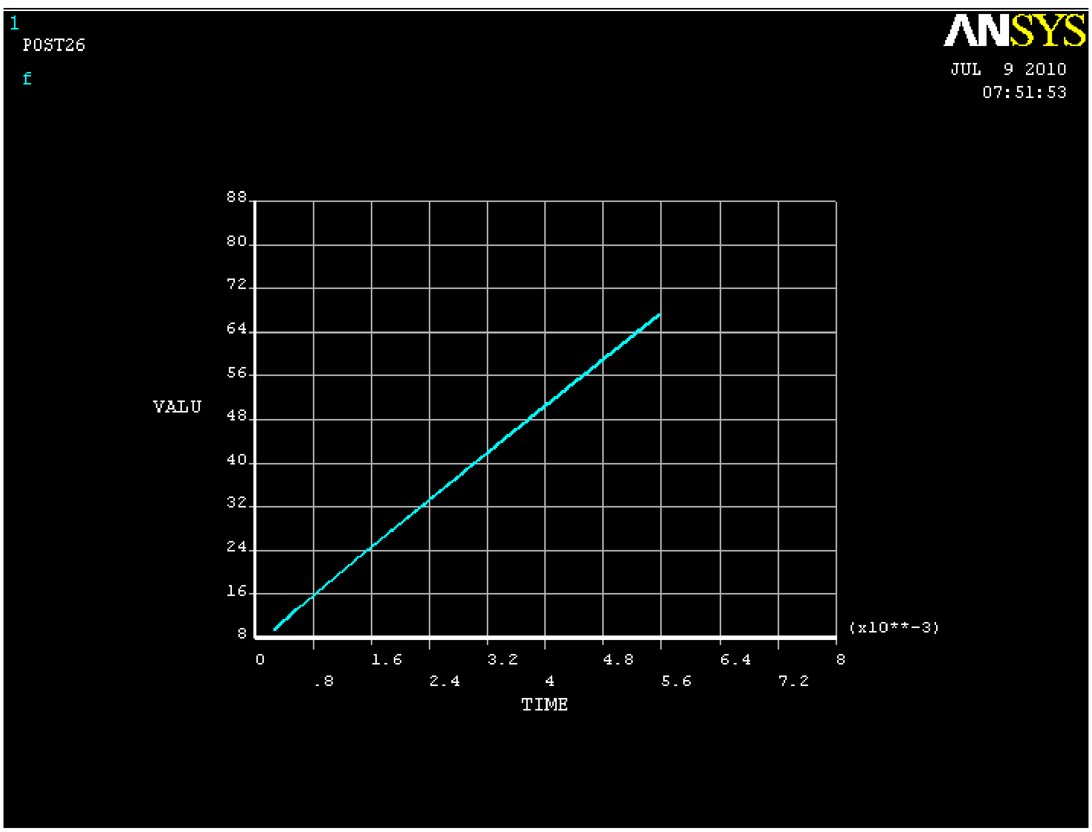

Variation between time and temperature

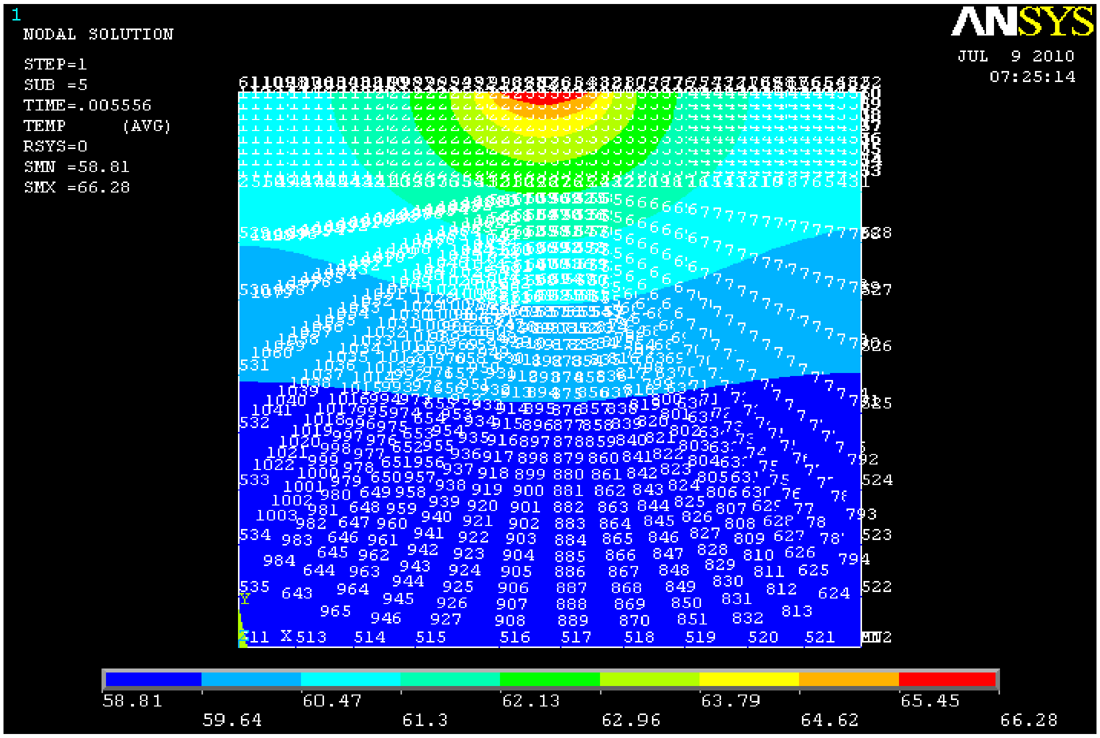

Fig 6.68 For constant speed 4500 rpm, constant feed of 0.0667 mm/rev, Depth of cut 0.06 mm, and for time 20 seconds the temperature using software is 66.2 ºC and with experimentation is 62.3 ºC.

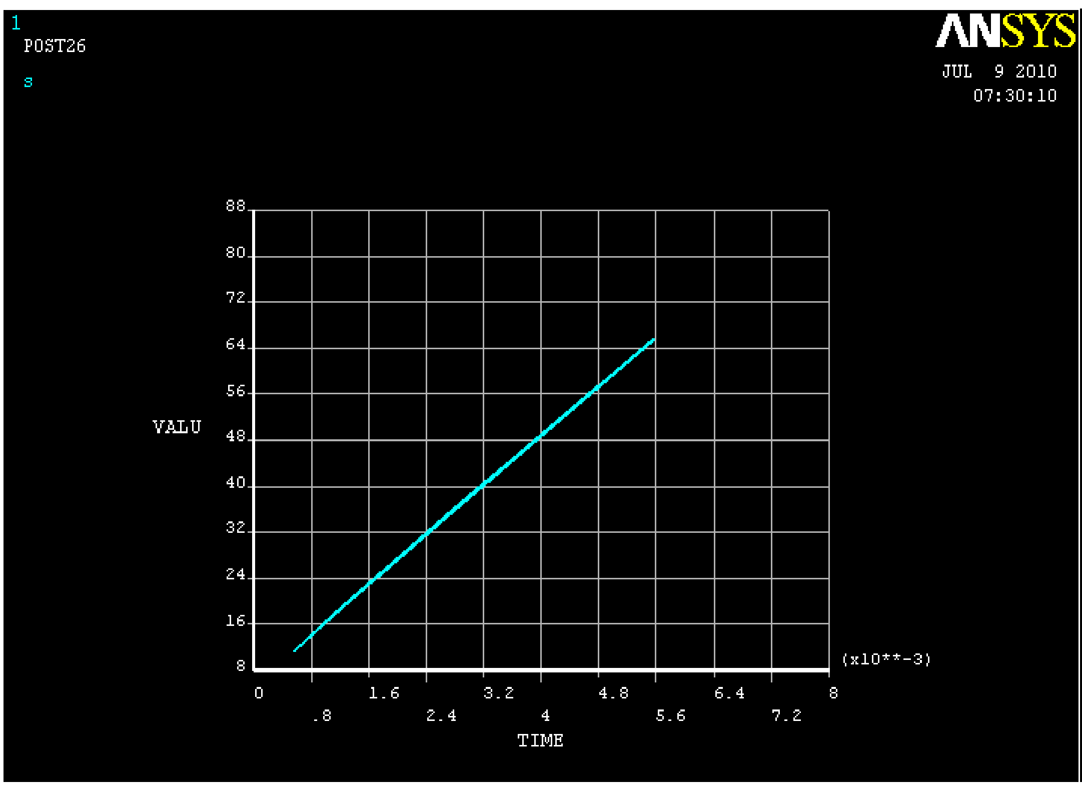

Variation between time and temperature

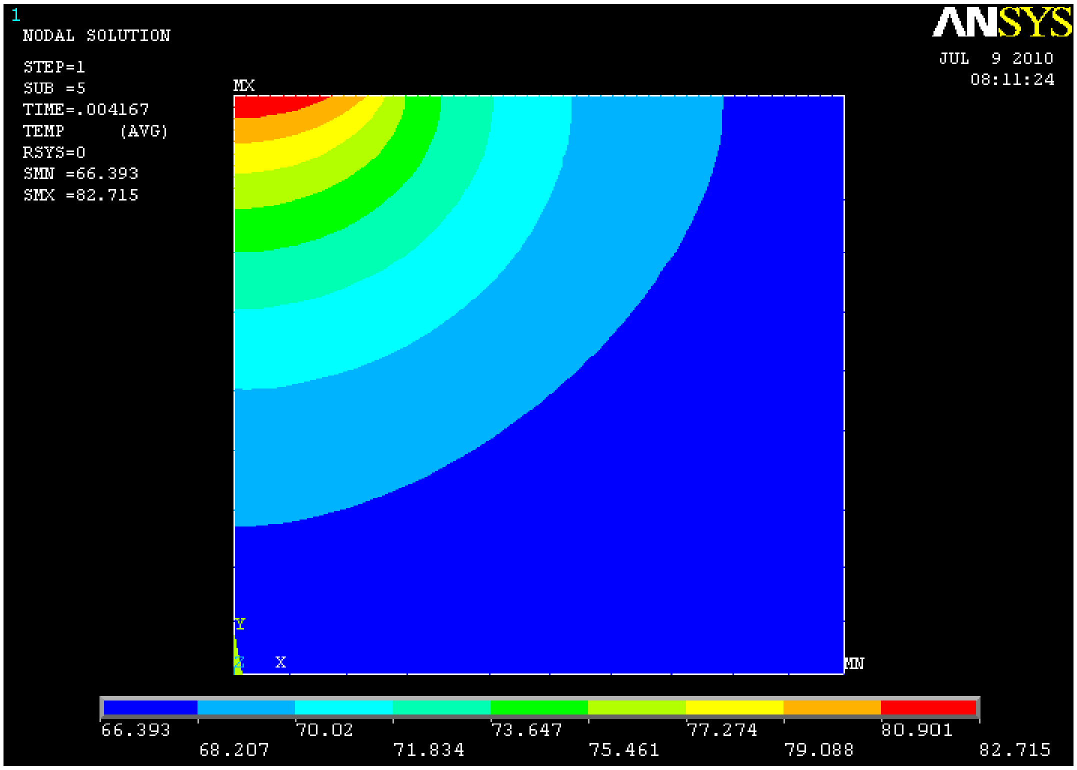

Fig 6.69 For constant speed 4500 rpm, constant feed of 0.0833 mm/rev, Depth of cut 0.09 mm, and for time 20 seconds the temperature using software is 82.7 ºC and with experimentation is 76.2ºC.

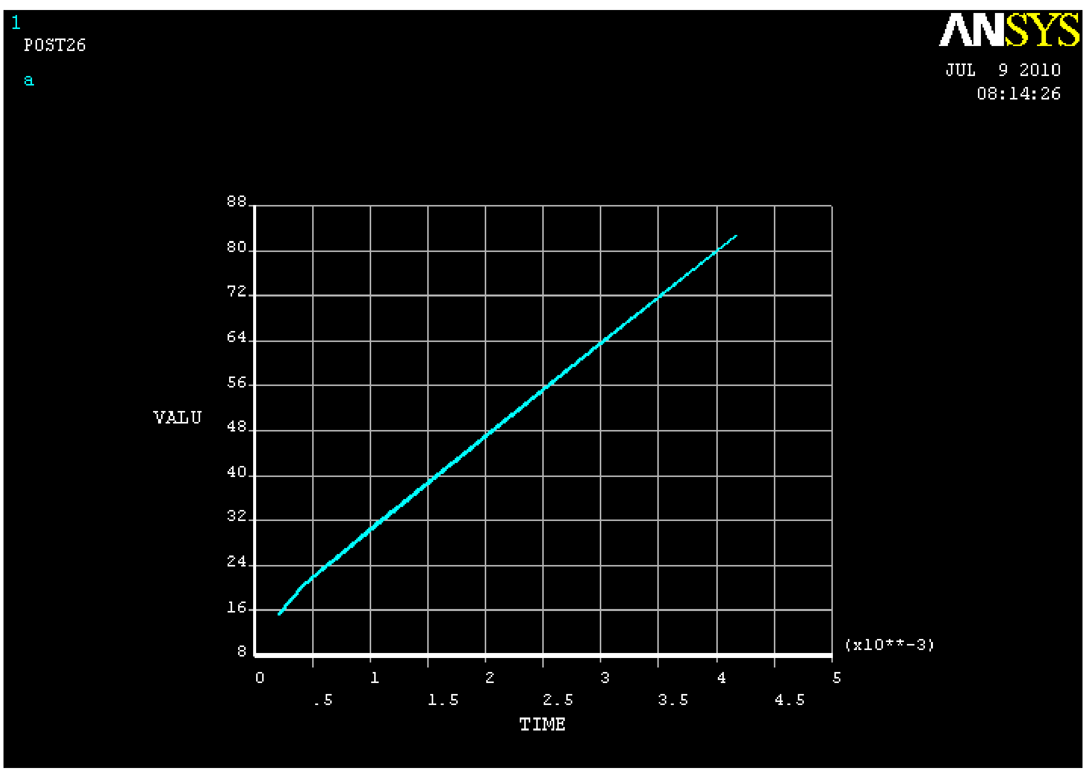

Variation between time and temperature

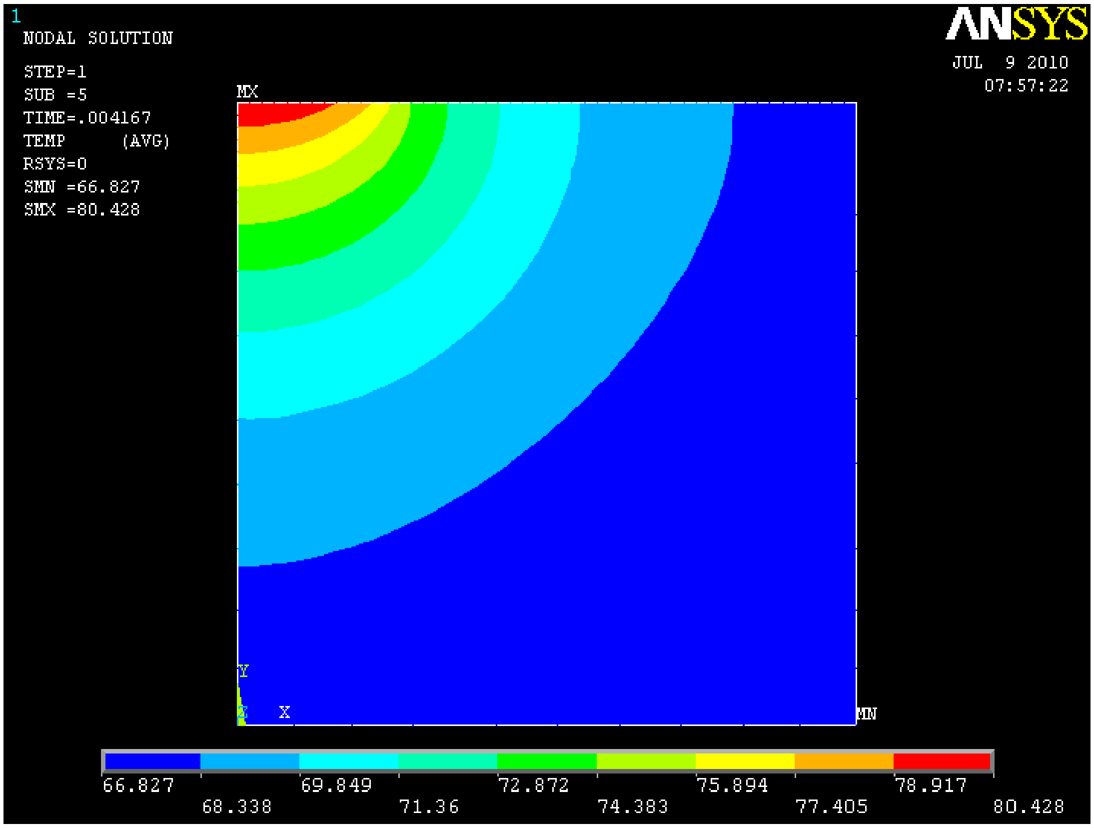

Fig 6.70 For constant speed 6000 rpm, constant feed of 0.1 mm/rev, Depth of cut 0.09 mm, and for time 20 seconds the temperature using software is 80.4 ºC and with experimentation is 77.8 ºC.

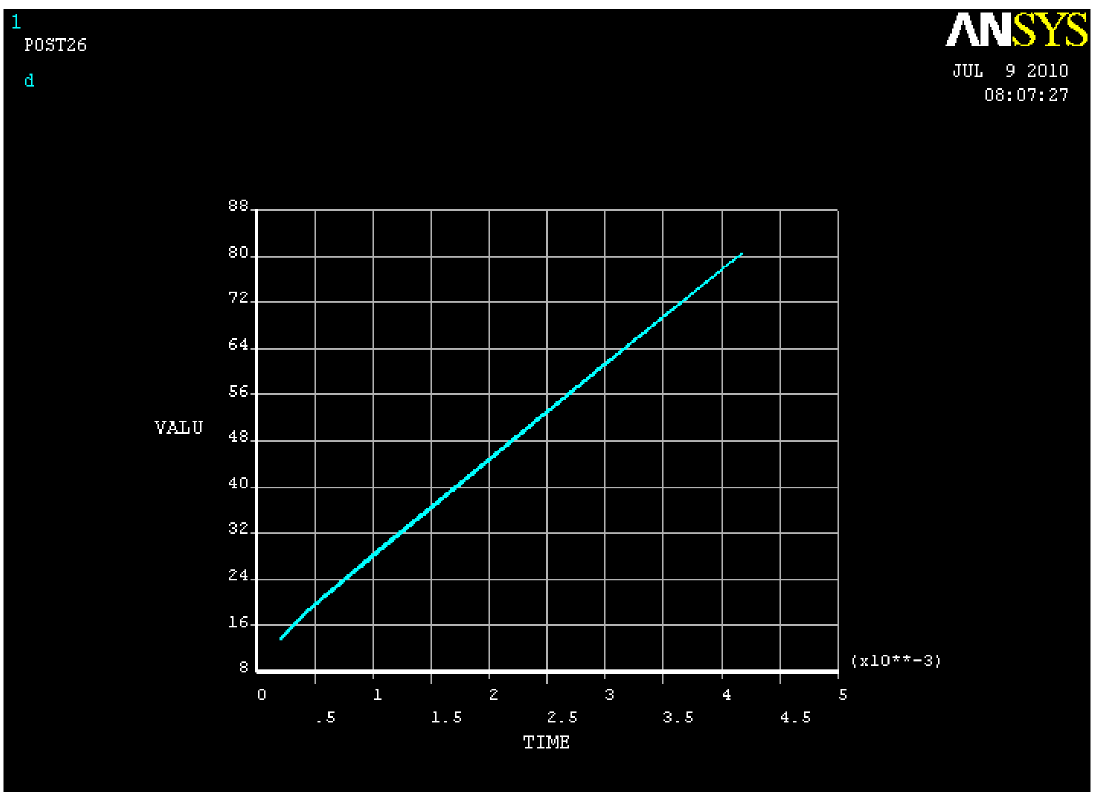

Variation between time and temperature

6.8 Results of Stress distribution on work piece using ABAQUS Software

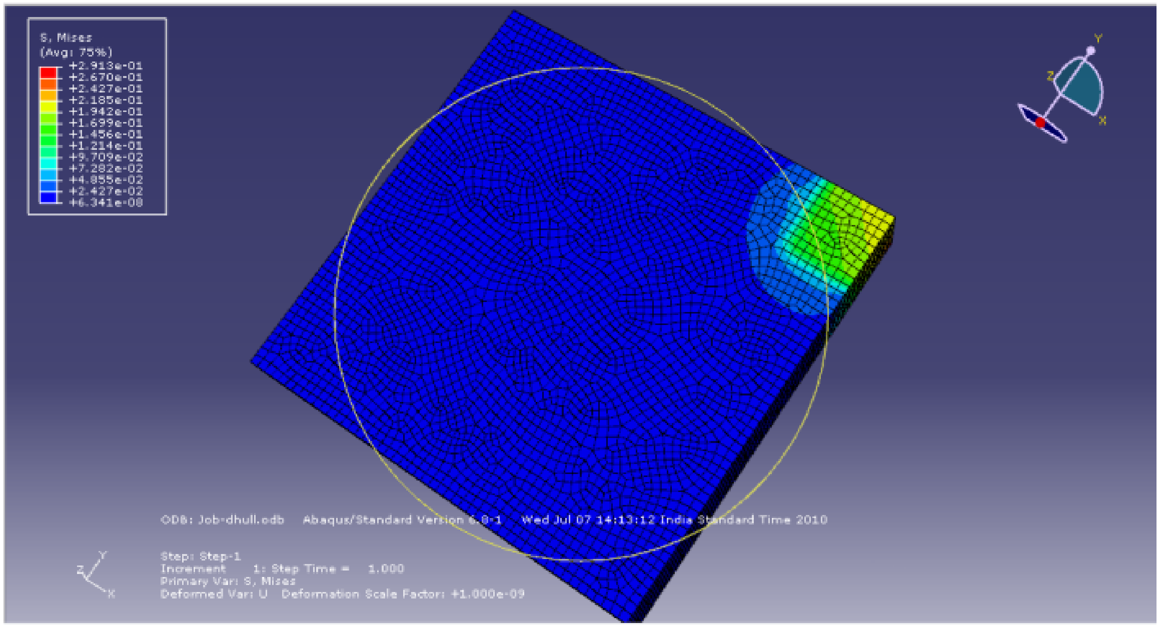

Fig 6.71 For same force of 157 N the stresses obtained using software is 0.2913 N/ mm^2 and with experimentation is 0.545139 N/ mm^2 for area 288 mm^2 of workpiec

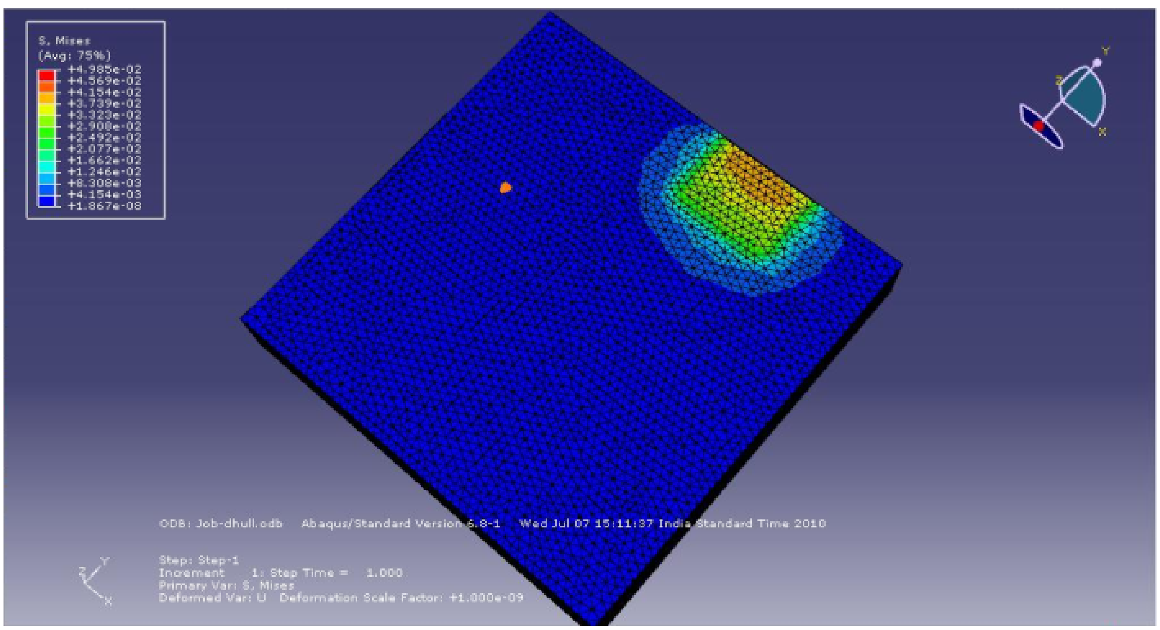

Fig 6.72 For same force of 200 N the stresses obtained using software is 0.4905 N/mm2 and with experimentation is 0.6979 N/ mm^2 for area 432 mm^2 of workpiece

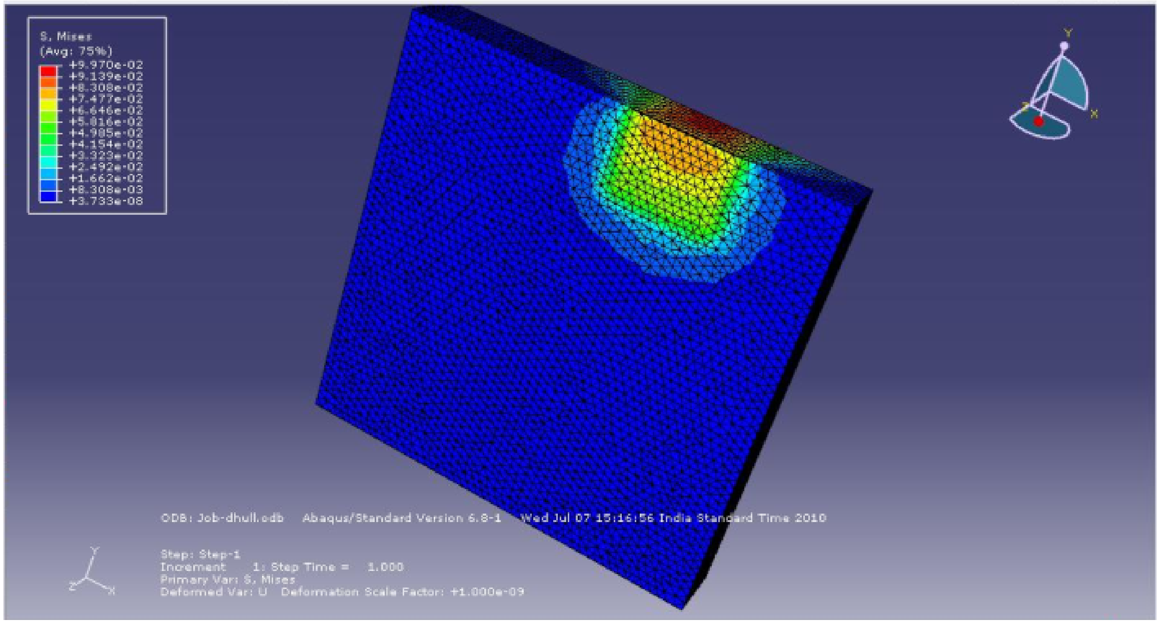

Fig 6.73 For same force of 51 N the stresses obtained using software is 0.0997 N/mm2 and with experimentation is 0.14166 N/mm^2 for area 360mm^2 of workpiece

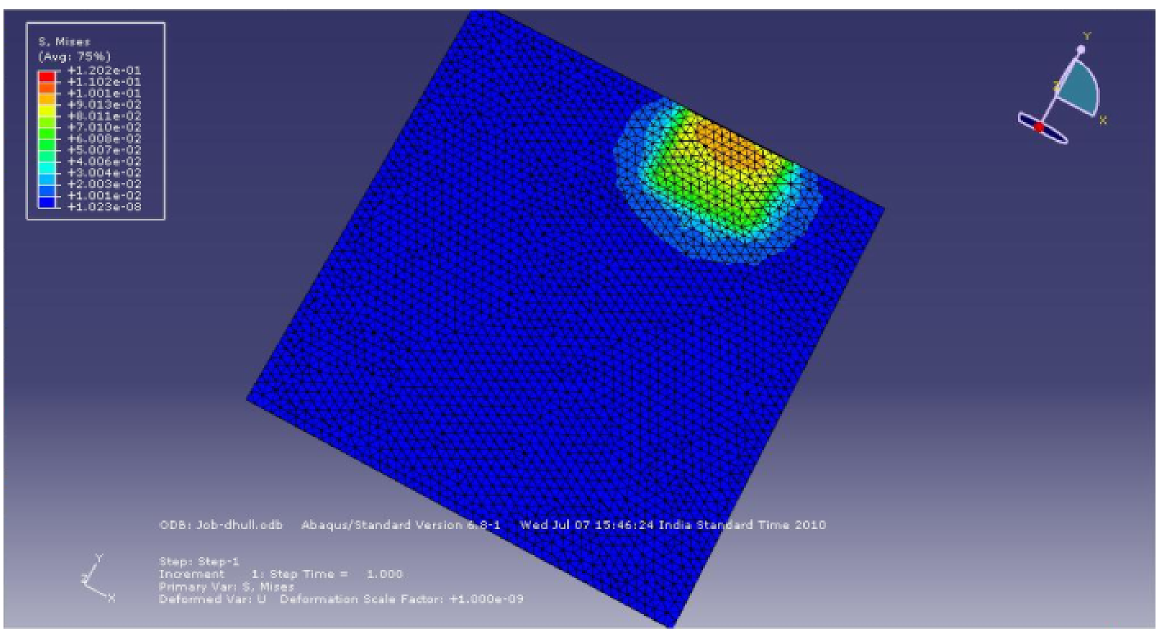

Fig 6.74 For same force of 110 N the stresses obtained using software is 0.1202 N/mm2 and with experimentation is 0.254 N/mm^2 for area 432mm^2 of workpiece

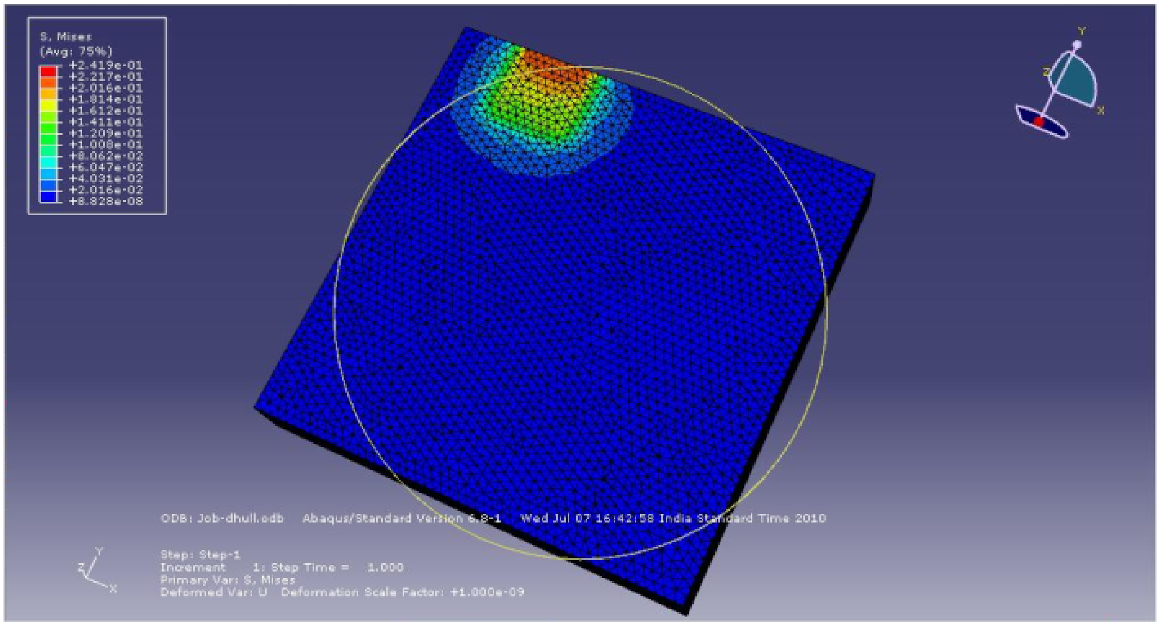

Fig 6.75 For same force of 132 N the stresses obtained using software is 0.243 N/mm2 and with experimentation is 0.3055 N/mm^2 for area 432 mm^2 of workpiece

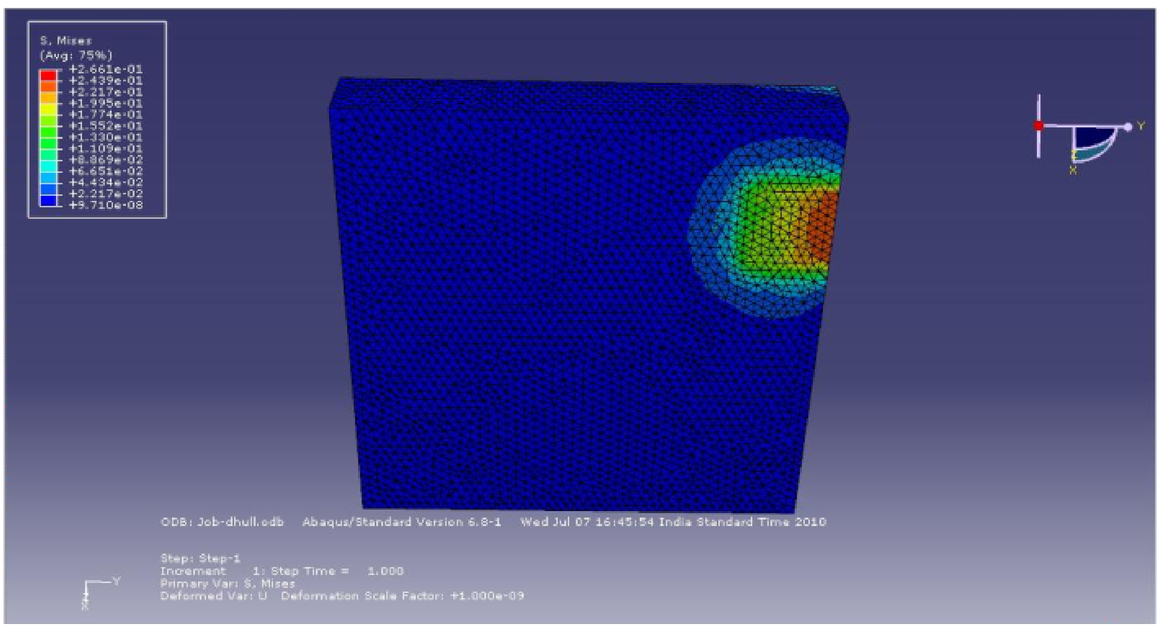

Fig 6.76 For same force of 135 N the stresses obtained using software is 0.266 N/mm2 and with experimentation is 0.3125 N/mm^2 for area 432 mm^2 of workpiece

CHAPTER 7

CONCLUSION AND SCOPE FOR FUTURE WORK

7.1 CONCLUSION

The objective of the present work is to collect the data based on four parameters i.e. speed, feed, time, and depth of cut.

On the basis of present study following conclusions can be drawn:

a) For the same force applied stresses generated in software are considerably less than stresses generated in case of experiment.

b) For constant feed and speed temperature generated in case of software is more than temperature in case of experiment.

c) The maximum temperature is for stainless steel out of the three materials on which present work was performed.

d) The maximum force is for high chromium steel out of the three materials on which present work was performed.

e) The minimum temperature is for mild steel out of the three materials on which present work was performed.

f) With increase in depth of cut temperature rises.

g) With increase in depth of cut stresses increases.

h) With rise in time temperature rises.

7.2. SCOPE FOR FUTURE WORK

The present work may be extended in one of the following ways. Directions in which the work can be further carried out in future are:

a) There are different types of grinders like cylindrical grinder, surface grinder, etc which are under application, calculate the data for temperature and verify the results and choose the most appropriate grinder for experimental and simulated comparison.

b) In the present work the different materials used are Mild Steel, High Chromium Steel and Stainless Steel. Choose materials like alloys which are in use on the same Tool and Cutter Grinder and verify the results

c) All the measurements can be repeated at least 2-3 times to cover more variations for varying parameters and to get more accurate results.

d) In modern day world there are highly accurate and precise temperature measuring instruments like laser application based thermometer evaluate the result and find out variation in results.

e) Since the number of parameters are more than 4 one can apply design of experiments and validate the results.

REFERENCES

1. W.B. Rowe, M.N. Morgan, S.C.E. Black and B. Mills., A Simplified Approach to Control of Thermal Damage in Grinding, *CRIP Annals Manufacturing Technology*, vol 45, 1996, pp 299-302
2. P. N. Moulik, H.T.Y. Yang and S. Chandrasekar, Simulation of Thermal Stresses Due to Grinding, *International Journal of Mechanical Science*, Vol 43, 2001, pp 831-851
3. W.B. Rowe and T. Jin., Temperatures in High Efficiency Deep Grinding (HEDG), *CIRP Annals Manufacturing Technology*, Vol 50, 2001, pp 205-208.
4. Fritz Klocke, Thorsten Beck, Stefan Hoppe, Tilo Krieg, Norbert Müller, Tobias Nothe, Hans-Willi Raedt and Kevin Sweeney., FEM Application in Manufacturing Technology, *Journal of Material Processing Technology*. Vol 120, 2002, pp 450-457.
5. H. H. Tsai and H. Hocheng., Prediction of a Thermally Induced Concave Ground Surface of the Workpiece in Surface Grinding, *Journal of Material Processing Technology*, vol 122, 2002, pp 148-159.
6. Athanasios G. Mamalis. The Temperature Fields and the Heat Affected Zones in Grinding, *Production Systems and Information Engineering,* Vol.1. (2003), pp 3-16.
7. Hédi Hamdi, Hassan Zahouani and Jean-Michel Bergheau., Residual Stresses Computation in a Grinding Process, *Journal of Material Processing Technology*, vol 147, 2004, pp 277-285.
8. Y.B. Guo, David W. Yen., FEM Study on Mechanisms of Discontinuous Chip Formation, *Journal of Material Processing Technology*, vol 155-156,(2004), pp 1350-1356.
9. TECHNICAL SOURCES: Thermal Damage, Residual Stress and Grinding the Abrasive Engineering Society, REVISED 10/22/04.
10. Y. Altintas and M. Weck., Chatter Stability of Metal Cutting and Grinding, *CRIP Annals Manufacturing Ttechnology, vol 53,2004, pp 619-642.*

11. T. Jin and D.J. Stephenson., Three Dimensional Finite Element Simulation of Transient Heat Transfer in High Efficiency Deep, *CIRP Annals Manufacturing Technology*, Vol 53, 2004, pp 259-262.
12. J.C. Aurich, H. Sudermann, H. Bil., Characterisation of Burr Formation in Grinding and Prospects for Modelling CIRP Annals, *Journal of Manufacturing Technology*, Vol 54, Issue 1, 2005, pp 313-316.
13. Martin. Baker, Finite Element Investigation of the Flow Stress Dependence of Chip Formation, *Journal of Material Processing, vol 167, 2005.*
14. D.A. Doman, A. Warkentin, R. Bauer, Finite Element Modeling Approaches in Grinding a Survey of Recent Grinding Wheel Topography Models, *International Journal of Machine Tools an Manufacture, vol* 46, 2006, pp 343–352.
15. J. Kopac and P. Krajnik., High-performance Grinding Faculty of Mechanical Engineering, *Journal of Material Processing Tehchnology*, vol 125, 2006, pp 278-284..
16. Martin Baker, Finite Element Simulation of High-Speed Cutting Forces, *Journal of Material Processing Technology*, vol 176, 2006, pp 117-126.
17. D. Zhang, D.G. Chetwynd, X. Liu and Y. Tian., Investigation of a 3-DOF Micro-positioning Table for Surface Grinding, *Internal Journal of Mechanical Science,* vol 48, 2006, pp 1401-1408.
18. A. Lefebvre, P. Vieville, P. Lipinski and C. Lescalier., Numerical Analysis of Grinding Temperature Measurement by the Foil/Work piece Thermocouple Method, *International of Journal of Machine Tools and Manufacturing*, vol 46, 2006, pp 1716-1726.
19. E. Brinksmeier, J.C. Aurich, E. Govekar, C. Heinzel, H.-W. Hoffmeister, F. Klocke, J. Peters, R. Rentsch, D.J. Stephenson, E. Uhlmann, K. Weinert and M. Wittmann., Advances in Modeling and Simulation of Grinding Processes , *CIRP Annals Manufacturing Technology,* vol 55, 2006, pp 667-696.
20. M.A. Davies, T. Ueda, R. M'Saoubi, B. Mullany and A.L. Cooke., The Measurement of Temperature in Material Removal Processes, *CIRP Annals Manufacturing Technology*, Vol 56, 2007, pp 581-604.
21. S. Malkin, C. Guo., Thermal Analysis of Grinding CIRP Annals, *Journal of Manufacturing Technology*, Vol 56, Issue 2, 2007, pp 760-782.

22. K. Salonitis, T. Chondros and G. Chryssolouris, Grinding Wheel Effect in the Grind-Hardening Process, *International Journal of Advanced Manufacturing Technology*, vol 38, 2008, pp 48-58.

23. A. Brosse, P. Naisson, H. Hamdi and J.M. Bergheau., Temperature Measurement and Heat Flux Characterization in Grinding Using Thermography, *Journal of Materials Processing Technology*, Vol 201, 2008, pp 590-595

24. Park, Hyung Wook., Development of Micro-grinding Mechanics and Machine Tools, Georgia Institute of Technology, 2008

25. P. Chen, W. Qu, M. H. Miller and A. Chandra., Thermal Effects in Vibration Assisted Grinding Michigan Technological University, Houghton, MI.

26. Huang-Cheng Chang and J.J. Junz Wang., A Stochastic Grinding Force Model Considering Random Grit Distribution, *International Journal of Machine Tools and Manufacture*, vol 48, 2008, pp 1335-1344.

27. J. C. Aurich, D. Biermann, H. Blum, C. Brecher, C. Carstensen, B. Denkena, F. Klocke, M. Kröger, P. Steinmann and K. Weinert Modelling and Simulation of Process: Machine Interaction in Grinding ,*Journal of Production Engineering*, Vol 3, 2009, pp 111-120.

APPENDIX

TABLE NO.1

Readings for Mild Steel for 6000 rpm										
Sr.no	Speed	Feed	Depth of Cut	Time	Forces(N)		Temp	simulated temp	stress	simulated stress
	(rpm)	(mm/rev)	(mm)	(sec)	Max	Min(-)	(°c)	(°c)	N/mm^2	N/mm^2
1	6000	0.0667	0.03	10	31	23	36.2	37.5	0.107639	0.07975
2	6000	0.0667	0.03	15	32	20	37.1	38.2	0.111111	0.08087
3	6000	0.0667	0.03	20	71	75	40.3	41.8	0.246528	0.17086
4	6000	0.0667	0.06	10	122	147	45.2	44.7	0.423611	0.21365
5	6000	0.0667	0.06	15	157	123	48.3	49.8	0.545139	0.2913
6	6000	0.0667	0.06	20	143	121	56.9	57.3	0.496528	0.25383
7	6000	0.0667	0.09	10	123	53	47.1	48.2	0.427083	0.21041
8	6000	0.0667	0.09	15	141	62	51.4	50.3	0.489583	0.24357
9	6000	0.0667	0.09	20	130	99	54.4	55.8	0.451389	0.23088
10	6000	0.0833	0.03	10	82	55	42.5	43.5	0.227778	0.18765
11	6000	0.0833	0.03	15	96	91	43.9	44.7	0.266667	0.19987
12	6000	0.0833	0.03	20	136	35	44.1	44.9	0.377778	0.22869
13	6000	0.0833	0.06	10	74	81	41.4	42.4	0.205556	0.17836
14	6000	0.0833	0.06	15	72	77	46.5	45.9	0.2	0.17471
15	6000	0.0833	0.06	20	76	105	60.2	63.8	0.211111	0.18063
16	6000	0.0833	0.09	10	63	60	58.5	55.3	0.175	0.16456
17	6000	0.0833	0.09	15	82	60	56.3	57.2	0.227778	0.1957
18	6000	0.0833	0.09	20	69	70	60.1	65.54	0.191667	0.1657
19	6000	0.1	0.03	10	89	68	42.3	43.9	0.206019	0.2362
20	6000	0.1	0.03	15	110	65	44.2	45.8	0.25463	0.1202
21	6000	0.1	0.03	20	121	58	48.3	52.9	0.280093	0.1346
22	6000	0.1	0.06	10	70	71	44.3	44.1	0.162037	0.098
23	6000	0.1	0.06	15	126	105	48.4	45.9	0.291667	0.1423
24	6000	0.1	0.06	20	132	108	45.2	46.1	0.305556	0.1635
25	6000	0.1	0.09	10	42	45	46.8	49.7	0.097222	0.0235
26	6000	0.1	0.09	15	63	37	56.7	60.8	0.145833	0.0645
27	6000	0.1	0.09	20	53	65	72.9	77.7	0.122685	0.0587

TABLE NO.2

Readings for High Chromium Steel for 6000 rpm										
Sr.no	Speed	Feed	Depth of Cut	Time	Forces(N)		Temp	simulated temp	stress	Simulated stress
	(rpm)	(mm/rev)	(mm)	(sec)	Max	Min(-)	(°c)	(°c)	N/mm^2	N/mm^2
1	6000	0.0667	0.03	10	71	51	42.1	43.7	0.246528	0.13778
2	6000	0.0667	0.03	15	132	99	39	45.3	0.458333	0.2172
3	6000	0.0667	0.03	20	143	127	47.8	48.2	0.496528	0.2364
4	6000	0.0667	0.06	10	158	143	38.4	37.9	0.548611	0.2623
5	6000	0.0667	0.06	15	162	133	40.2	41.8	0.5625	0.266
6	6000	0.0667	0.06	20	201	179	48.6	50.6	0.697917	0.4905
7	6000	0.0667	0.09	10	67	132	41.1	39.9	0.232639	0.261
8	6000	0.0667	0.09	15	72	42	46.3	45.9	0.2	0.0745
9	6000	0.0667	0.09	20	66	79	54.3	58.3	0.183333	0.0912
10	6000	0.0833	0.03	10	35	33	34.4	33.9	0.097222	0.0397
11	6000	0.0833	0.03	15	77	65	39.9	40.8	0.213889	0.0734
12	6000	0.0833	0.03	20	95	74	43.7	44.1	0.263889	0.1034
13	6000	0.0833	0.06	10	51	130	50.4	53.9	0.141667	0.0997
14	6000	0.0833	0.06	15	69	144	54.8	58.2	0.191667	0.105
15	6000	0.0833	0.06	20	89	74	52.7	60.8	0.247222	0.1278
16	6000	0.0833	0.09	10	99	92	57.5	58.2	0.275	0.1495
17	6000	0.0833	0.09	15	121	71	72.3	74.9	0.280093	0.1873
18	6000	0.0833	0.09	20	109	110	71.2	75.8	0.252315	0.1593
19	6000	0.1	0.03	10	129	79	59.1	56.8	0.298611	0.2067
20	6000	0.1	0.03	15	135	57	58.8	58.6	0.3125	0.222
21	6000	0.1	0.03	20	137	46	47.7	60.3	0.31713	0.229
22	6000	0.1	0.06	10	111	56	42.2	44.3	0.256944	0.2041
23	6000	0.1	0.06	15	123	167	47.6	49.2	0.284722	0.2189
24	6000	0.1	0.06	20	135	38	48.3	51.4	0.3125	0.2391
25	6000	0.1	0.09	10	95	116	45.8	49.3	0.219907	0.1693
26	6000	0.1	0.09	15	100	132	49.2	52.8	0.231481	0.1743
27	6000	0.1	0.09	20	97	52	53.4	56.9	0.224537	0.1827

TABLE NO. 3

Readings for Stainless Steel For 6000 rpm										
Sr.no	Speed	Feed	Depth of Cut	Time	Forces(N)		Temp	simulated temp	stress	Simulated Stress
	(rpm)	(mm/rev)	(mm)	(sec)	Max	Min(-)	(°c)	(°c)	N/mm^2	N/mm^2
1	6000	0.0667	0.03	10	34	12	54.1	56.9	0.118056	0.0239
2	6000	0.0667	0.03	15	59	25	48.1	58.3	0.204861	0.0654
3	6000	0.0667	0.03	20	47	24	58.4	59.2	0.163194	0.0564
4	6000	0.0667	0.06	10	85	46	65.1	70.2	0.295139	0.0918
5	6000	0.0667	0.06	15	96	59	72.1	74.9	0.333333	0.0937
6	6000	0.0667	0.06	20	69	63	74.3	76.1	0.239583	0.0683
7	6000	0.0667	0.09	10	82	78	65.2	63.7	0.284722	0.0961
8	6000	0.0667	0.09	15	91	86	76.8	69.2	0.252778	0.1145
9	6000	0.0667	0.0963	20	84	72	68.1	72.8	0.233333	0.1012
10	6000	0.0833	0.03	10	79	63	41.8	46.9	0.219444	0.08397
11	6000	0.0833	0.03	15	90	89	47.5	50.2	0.25	0.0934
12	6000	0.0833	0.03	20	84	36	48.2	52.6	0.233333	0.0948
13	6000	0.0833	0.06	10	85	43	43.3	47.9	0.236111	0.0997
14	6000	0.0833	0.06	15	95	36	47.4	49.6	0.263889	0.0805
15	6000	0.0833	0.06	20	130	74	48.8	52.7	0.361111	0.1202
16	6000	0.0833	0.09	10	117	88	56.4	60.4	0.325	0.1203
17	6000	0.0833	0.09	15	55	75	68.3	68	0.127315	0.025
18	6000	0.0833	0.09	20	76	59	73.2	74.3	0.175926	0.0187
19	6000	0.1	0.03	10	81	12	49.4	54.3	0.1875	0.1289
20	6000	0.1	0.03	15	82	29	63.1	58.7	0.189815	0.1783
21	6000	0.1	0.03	20	94	63	65.2	66.8	0.217593	0.1847
22	6000	0.1	0.06	10	87	103	52.2	55.7	0.201389	0.2063
23	6000	0.1	0.06	15	98	94	61.3	64.6	0.226852	0.1866
24	6000	0.1	0.06	20	102	181	76.4	76.9	0.236111	0.1887
25	6000	0.1	0.09	10	58	55	71.7	73.8	0.134259	0.0573
26	6000	0.1	0.09	15	65	50	77.8	80.4	0.150463	0.0342
27	6000	0.1	0.09	20	67	52	78.6	85.7	0.155093	0.0402

TABLE NO. 4

Readings for Mild Steel For 4500 rpm										
Sr.no	Speed	Feed	Depth of Cut	Time	Forces(N)		Temp	simulated temp	stress	Simulated stress
	(rpm)	(mm/rev)	(mm)	(sec)	Max	Min(-)	(°c)	(°c)	N/mm^2	N/mm^2
1	4500	0.0667	0.03	10	59	28	41.6	40.7	0.204861	0.0376
2	4500	0.0667	0.03	15	69	38	42.8	44.6	0.239583	0.0472
3	4500	0.0667	0.03	20	75	38	42.6	45.9	0.260417	0.5364
4	4500	0.0667	0.06	10	106	37	45.6	46.1	0.368056	0.2023
5	4500	0.0667	0.06	15	111	43	51.2	55.8	0.385417	0.2662
6	4500	0.0667	0.06	20	126	52	62.3	66.2	0.4375	0.2905
7	4500	0.0667	0.09	10	51	45	48.8	50.3	0.177083	0.0261
8	4500	0.0667	0.09	15	52	45	51.8	54.6	0.144444	0.0245
9	4500	0.0667	0.09	20	67	35	52.9	59.1	0.186111	0.0391
10	4500	0.0833	0.03	10	50	27	44.2	46.8	0.138889	0.0297
11	4500	0.0833	0.03	15	34	31	44.5	48.9	0.094444	0.0173
12	4500	0.0833	0.03	20	62	30	45.3	51.4	0.172222	0.0434
13	4500	0.0833	0.06	10	78	30	45.8	47.3	0.216667	0.0997
14	4500	0.0833	0.06	15	88	38	60.2	55.8	0.244444	0.1202
15	4500	0.0833	0.06	20	85	24	58.9	62.5	0.236111	0.1203
16	4500	0.0833	0.09	10	79	42	55.1	57.1	0.219444	0.0925
17	4500	0.0833	0.09	15	84	35	59.3	58.3	0.194444	0.0987
18	4500	0.0833	0.09	20	75	30	61.4	62.8	0.173611	0.0889
19	4500	0.1	0.03	10	41	19	42.1	43.8	0.094907	0.0278
20	4500	0.1	0.03	15	34	33	43.5	44.6	0.078704	0.0284
21	4500	0.1	0.03	20	50	45	42.8	46.1	0.115741	0.0567
22	4500	0.1	0.06	10	72	21	47.4	48.2	0.166667	0.0786
23	4500	0.1	0.06	15	64	56	52.9	51.8	0.148148	0.0618
24	4500	0.1	0.06	20	61	49	59.4	55.8	0.141204	0.0573
25	4500	0.1	0.09	10	64	35	52.4	57.3	0.148148	0.0642
26	4500	0.1	0.09	15	75	61	54.1	59.3	0.173611	0.0702
27	4500	0.1	0.09	20	68	54	55.6	61.6	0.157407	0.0602

TABLE NO. 5

Readings for High Chromium Steel For 4500 rpm										
Sr.no	Speed	Feed	Depth of Cut	Time	Forces(N)		Temp	simulated temp	stress	Simulated stress
	(rpm)	(mm/rev)	(mm)	(sec)	Max	Min(-)	(°c)	(°c)	N/mm^2	N/mm^2
1	4500	0.0667	0.03	10	62	29	44.5	44.9	0.215278	0.05913
2	4500	0.0667	0.03	15	65	30	43.2	47.1	0.225694	0.06091
3	4500	0.0667	0.03	20	78	29	45.4	49.4	0.270833	0.07763
4	4500	0.0667	0.06	10	65	38	45.8	46.1	0.225694	0.04357
5	4500	0.0667	0.06	15	96	50	48.7	48.2	0.333333	0.09088
6	4500	0.0667	0.06	20	90	59	52.6	50.1	0.3125	0.04765
7	4500	0.0667	0.09	10	36	25	62.1	62.8	0.125	0.19987
8	4500	0.0667	0.09	15	47	38	63.9	65.9	0.130556	0.22869
9	4500	0.0667	0.09	20	56	36	64.2	67.5	0.155556	0.17836
10	4500	0.0833	0.03	10	38	25	45.4	45.2	0.105556	0.017471
11	4500	0.0833	0.03	15	64	39	54.1	53.8	0.177778	0.05806
12	4500	0.0833	0.03	20	75	58	58.4	58.9	0.208333	0.06012
13	4500	0.0833	0.06	10	65	34	46.9	48.1	0.180556	0.05837
14	4500	0.0833	0.06	15	65	39	58.3	57.2	0.180556	0.0534
15	4500	0.0833	0.06	20	84	42	62.3	64.8	0.233333	0.0948
16	4500	0.0833	0.09	10	62	43	71.8	68.1	0.172222	0.0597
17	4500	0.0833	0.09	15	74	62	68.2	69.3	0.171296	0.0705
18	4500	0.0833	0.09	20	48	72	68.8	72.5	0.111111	0.1202
19	4500	0.1	0.03	10	65	40	46.3	47.6	0.150463	0.06203
20	4500	0.1	0.03	15	87	56	52.1	50.3	0.201389	0.0865
21	4500	0.1	0.03	20	91	44	53.1	54.7	0.210648	0.0987
22	4500	0.1	0.06	10	41	46	51.1	52.7	0.094907	0.01289
23	4500	0.1	0.06	15	57	36	54.4	56.8	0.131944	0.0443
24	4500	0.1	0.06	20	76	49	67.7	65.2	0.175926	0.0635
25	4500	0.1	0.09	10	74	38	56.4	58.3	0.171296	0.0645
26	4500	0.1	0.09	15	53	55	54.2	60.8	0.122685	0.0237
27	4500	0.1	0.09	20	69	43	60.3	64.1	0.159722	0.0693

TABLE NO. 6

Reading for Stainless Steel For 4500 rpm										
Sr.no	Speed	Feed	Depth of Cut	Time	Forces(N)		Temp	simulated temp	stress	Simulated stress
	(rpm)	(mm/rev)	(mm)	(sec)	Max	Min(-)	(°c)	(°c)	N/mm^2	N/mm^2
1	4500	0.0667	0.03	10	65	21	43.4	41.5	0.225694	0.06917
2	4500	0.0667	0.03	15	83	50	47.6	45.3	0.288194	0.0915
3	4500	0.0667	0.03	20	78	48	54.1	55.3	0.270833	0.07763
4	4500	0.0667	0.06	10	72	61	48.4	52.4	0.25	0.07357
5	4500	0.0667	0.06	15	79	83	62.6	67.9	0.274306	0.07088
6	4500	0.0667	0.06	20	98	52	74.2	78.7	0.340278	0.09765
7	4500	0.0667	0.09	10	68	42	45.3	45.1	0.236111	0.0899
8	4500	0.0667	0.09	15	83	29	57.2	59.8	0.230556	0.0986
9	4500	0.0667	0.09	20	117	43	81.3	74.5	0.325	0.17836
10	4500	0.0833	0.03	10	54	30	46.6	47.9	0.15	0.08471
11	4500	0.0833	0.03	15	76	28	48.5	49.7	0.211111	0.05806
12	4500	0.0833	0.03	20	143	53	54.3	58.3	0.397222	0.282
13	4500	0.0833	0.06	10	76	49	63.6	67.9	0.211111	0.05837
14	4500	0.0833	0.06	15	90	64	67.4	68.9	0.25	0.0834
15	4500	0.0833	0.06	20	78	60	81.3	78.1	0.216667	0.0948
16	4500	0.0833	0.09	10	75	41	72.1	74.9	0.208333	0.0597
17	4500	0.0833	0.09	15	95	69	73.2	77.2	0.219907	0.0905
18	4500	0.0833	0.09	20	78	61	76.2	82.7	0.180556	0.0602
19	4500	0.1	0.03	10	52	38	45.5	48.3	0.12037	0.06203
20	4500	0.1	0.03	15	62	24	46.8	50.3	0.143519	0.0865
21	4500	0.1	0.03	20	54	39	48.2	52.8	0.125	0.0487
22	4500	0.1	0.06	10	88	46	46.7	47.3	0.203704	0.0928
23	4500	0.1	0.06	15	86	17	68.2	74.8	0.199074	0.0924
24	4500	0.1	0.06	20	98	44	74.3	92.5	0.226852	0.0934
25	4500	0.1	0.09	10	69	47	61.9	82.7	0.159722	0.0645
26	4500	0.1	0.09	15	78	48	84.2	93.7	0.180556	0.0737
27	4500	0.1	0.09	20	62	62	85.6	103	0.143519	0.0793